Individual and collective dynamics of excitable chemical waves:

Chaos and Drift, Synchronization and Chimera

(A thesis submitted for the fulfillment of the degree of Doctor of Philosophy)

Parvej Khan

Supervisor: Prof. Sumana Dutta

Department of Chemistry

Indian Institute of Technology Guwahati

Guwahati-781039, Assam, India

Dedication

To all the love and struggles of them for which I smile, I hope, I dream..

Declaration

I hereby declare that the matter embodied in the thesis entitled **"Individual and collective dynamics of excitable chemical waves: Chaos and Drift, Synchronization and Chimera "** is a result of investigation carried out by me under the supervision of Prof. Sumana Dutta in the Department of Chemistry, Indian Institute of Technology Guwahati, Assam, India.

In keeping with the general practice of reporting scientific observations, due acknowledgments (citations) have been made wherever required.

Parvej Khan

भारतीय प्रौद्दोगिकी संसथान गुवाहाटी
Indian Institute of Technology Guwahati

Sumana Dutta
Professor
Department of Chemistry
Email : sumana@iitg.ac.in
Telephone :+91 361 2582322

To whom it may concern

This is to certify that the thesis submitted by **Parvej Khan (Reg. No. - 196122019)**, entitled **"INDIVIDUAL AND COLLECTIVE DYNAMICS OF EXCITABLE CHEMICAL WAVES: CHAOS AND DRIFT, SYNCHRONIZATION AND CHIMERA"** in fulfilment for the award of Doctor of Philosophy in Chemistry, is a record of original research work carried out by him at IIT Guwahati during the academic year 2019-2024 under my supervision. No part of the thesis has been submitted before for the award of any degree.

26 July, 2024
IIT Guwahati

(Dr. Sumana Dutta)

PhD Supervisor

Acknowledgements

All good things come to an end and now I have reached almost to the destination after a long journey of five years. When I am about to end my PhD journey I would like to express my sincere gratitude to all the individuals for mentoring and supporting me. This section is not enough to name all the people who contributed till date. Therefore, my heartfelt apologies to those whom I might forget to mention.

In the beginning, I would like to thank my supervisor and mentor, Prof. Sumana Dutta, whose constant support and guidance helped me to sustain through this challenging yet beautiful journey. I am also grateful to thank Prof. Aditya Narayan Panda, Prof. Ashish Kumar Gupta, and Prof. Tarak Nath Dey for their valuable suggestions and comments whenever needed.

I feel myself lucky to have Hrishikesh Kalita, my senior in the lab, has been supportive throughout my journey. The four and a half long years, that we spent together in the lab was also a learning experience for me, where we discussed not only subject matter, but also different social and political topic. I also want to thank Sunita Rani and Tejaswini Kalita, younger lab members of our group for their encouragements.

I would like to acknowledge my family member- my parents (Monsur Ali Khan and Hasnuhena Khan), sister (Rumana Khan), uncles (Late Nazrul Ali Khan and Sahidul Ali Khan), my grandparents (Abdul Khaleque Khan, Taslima Bibi, Anowar Alam, Golap Mursheda Begum) and others. It would not have been possible to earn my degree without their struggle and support from my childhood.

It would be an injustice to my feelings if I don't mention Madhumita Saha, whose constant push helped me to rethink my career decision to pursue Ph.D. after spend-

ing four long years as teacher in a school. This section is incomplete without Anasuya Chandra, Subrata Ghosh, Gopal Mondal, Soumendu Barua, Anirban Chakraborty, Mahesh Tekariwal, Ipsita Moitra, and Dhiman Das, with whom I shared good memories and their good wishes contributed a significant capital of my life.

My school teachers played a significant role in shaping of my character from my childhood. Among them, I should name a few, if not all. Swapan Chakraborty, my Bengali teacher in high school built the foundation of my philosophies of life at the early stages. Atanu Chakraborty, who taught me English, always advocated for tolerance and peace in any situation. I might not have learned good English from him, but a socialistic humanistic approach that he inculcated in me is my lifelong learning. Azmine Haque, my Chemistry teacher, taught me the valuable professional ethics that one should maintain for life. Besides this, I want to acknowledge all the other teachers who taught me during my school days. During my graduation and post-graduation, I got the opportunity to have guidance from Dr. Kallol Mukherjee, Dr. Subhajit Ghosh, and other professors. Their teaching helped me to enhance my knowledge and to grow my interest in the subject.

I have always been surrounded by the warmth of many friends throughout my life. The memories I have with them are unforgettable and hold a very special place in my heart. Sihan, Yusuf, Dwipayan, Pankaj, Swapan, Nasib, Javed from my school days, Arindam, Anupam, Debashish, Sovana, Piyali, Udayan, Krishnendu, Manoj, Atiur, Nanda, Debashruti from my college days and here seniors like Subratada, Pradipda, Gourharida, Sayan(Bhattacharjee), Sagnik, Anindya, Anjishnu, Pritam, batchmates like Priyam, Hirak, Shantanu, Eileen, Rabu, Monalisa, Biman, Rahul, Mrinmoy Ujwala, Sayani, Riya, Souryadeep, and juniors like Riddhiman, Sayan(Roy), Hrik, Arnab, Adhiraj, Abhileen, Mouli, Tashmita, Raima, Pracheta are some of them. Certainly, I missed many names, but that is unintentional.

Finally, I want to thank all for what I have learned from all the people named and unnamed in different situations. May it be during discussions over tea, during staging drama and rehearsals, organizing an event, or during any other work. Their involvement and selfless help has been my guiding force in this long journey. I owe my success to them as I believe that there is nothing “individual”; everything is

"collective".

Abstract

Self-organization and the dynamics of rotating spiral waves have captured the interest of numerous researchers within the realm of nonlinear dynamics over recent decades. Various biological systems, such as the human heart and chicken retina, exhibit the presence of spiral waves.

Irregular cardiac rhythm due to spiral wave activity brings great interest in the control and elimination of this kind of spirals from the system. One of the best laboratory model to study the dynamics of cardiac waves is the Belousov-Zhabotinsky (BZ) reaction-diffusion system. In this thesis, we report the experimental and numerical works carried out on individual spirals, as well as on their collective dynamics.

Chapter 1 is a brief introduction of the field of "Nonlinear Dynamics" and pattern formation. The historical development of oscillatory chemical reactions and the Belousov-Zhabotinsky (BZ) reaction has been introduced. The formation of excitable chemical waves as spirals and scrolls and their importance in the context of studying cardiac wave dynamics are outlined. **Chapter 2** briefs about the common methodologies used for our experiments and computer simulation. The main findings of our works are reported from Chapter 3 onwards. In **Chapter 3**, we modified a model developed from the established FKN mechanism of the BZ reaction to study the variation of the spiral wave properties with the explicit concentration of hydrogen ions. We then studied the effect of mild concentration gradients on spiral wave dynamics in our experimental setup in **chapter 4**, we also demonstrated how these results corroborate with our modified model. From Chapter 5 onwards, we began examining collective spiral wave dynamics in our system. In **chapter 5**, we revealed how the counter and corotating pinned spirals synchronize and how they

differ from each other. **Chapter 6** describes the collective phenomena of pinned spirals arranged in a square network, where we report the formation of clusters and chimera of oscillators. **Chapter 7** establishes the importance of communication in the synchronization process in a chemical reaction-diffusion system; the observation being motivated by Huygen's well-known Pendulum sympathy experiment, but new in a chemical system. Lastly, **Chapter 8** concludes with our results, observations, answered and unanswered questions and propose future direction.

Contents

List of Figures

Chapter 1

Introduction

A treasure trove of amazing dynamics and design can be found in nature, including living beings and non-living entities. The globe is diverse and heterogeneous due to an astonishing variety of animals, ecosystems, landscapes, etc. The presence of symmetry and asymmetry, different interactions between individuals, and self-replication processes make the world complex. Science is the methodical investigation that leads to the understanding of the functioning of nature, and each area of the scientific discipline aims to do that from their own perspective.

1.1 Background

1.1.1 Nonlinear dynamics

The term nonlinear dynamics is concerned with the system that changes with time in a nonlinear manner. In dynamics, we often analyze the fate of the system; it might approach equilibrium or exhibit more complex behavior[1]. A key objective of nonlinear dynamics research is to provide an explanation for the emergence of complex structures [2]. The majority of living systems in which we are interested are nonlinear. Almost every area, including chemistry, physics, biology, geology, mathematics, engineering, economics, and even the social sciences, has a footprint in the topic, which makes it very interdisciplinary. Although much of the field's early

progress was theoretical, in recent decades, a number of experimental discoveries have motivated novel computational strategies [3].

1.1.2 Reaction-Diffusion system

Reaction-diffusion systems typically refer to ones in which there is a localized chemical reaction. The chemical species within the system react to form products and are simultaneously transported via diffusion. This, mathematically, can be expressed as follows:

$$\frac{\partial u(x,y,z,t)}{\partial t} = f(u) + D\nabla^2 u(x,y,z,t) \tag{1.1}$$

$$\nabla^2 u = \frac{\partial^2 u}{\partial x^2} + \frac{\partial^2 u}{\partial y^2} + \frac{\partial^2 u}{\partial z^2} \tag{1.2}$$

where $u(x,y,z,t)$ is the system variable, $f(u)$ is kinetic terms describing reaction part, D is diffusion constant, the last term of the right hand side of the equation defines the transfer process or diffusion. ∇^2 is the second order derivative with respect to space coordinates, be it one, two or three dimensional.

1.1.3 Excitable media

An excitable medium is continuous, spatially dispersed media in which perturbation grows. When a perturbation in an excitable system exceeds the threshold value, a macroscopic or observable response occurs. The system goes from an excitable to an excited state, then enters a refractory phase, where the system is not responsive to any more perturbations during this period. The system then eventually reverts to an excitable state and becomes susceptible to perturbation again. The coupling in these systems are local and governed by diffusion-like transport [4].

1.1.4 Self-organization

When a system develops an internal order without any external forcing being imposed, is known as self-organization. As the system grows more structured, its en-

tropy decreases. The second law of thermo-dynamics, on the other hand, stipulates that an isolated system's entropy never decreases. For this reason, self-organizing systems need to be open and exchange mass and/or energy with the surroundings. The interactions between the components lead to this internal organization, which is typically independent of the components' nature. This organization may be spatial, temporal, and spatiotemporal [5].

1.1.5 Patterns and waves

Nature is full with patterns. The stripes and patches on animal coats, symmetry in flowers and leaves, the flashing of fireflies, and in arrangement of flying birds. There are two kinds of patterns: nonstationary and stationary. Patterns that remain constant in space, once they have developed, are called stationary patterns. In contrast, a nonstationary pattern involves a shift in the variable throughout time and space [2], called spatiotemporal patterns.

The presence of reaction along with diffusion or perturbation in the excitable medium mentioned above controls the emergence of a self-organized pattern. One of the most studied pattern is the Turing pattern [6, 7]. The pattern forms in animal coats are examples of the Turing pattern, which is stationary in a short time scale. On the other hand, patterns in the nerve cells and heart muscles are examples of nonstationary ones.

1.1.6 Oscillatory chemical systems and a short history

Fechner's demonstration of an electrochemical cell that generated oscillating current in 1828 was the first documented account of chemical oscillations. In 1894, Ostwald noticed that the rate at which chromium dissolves in acid, is periodic. It was thought at the time that a homogeneous oscillation reaction was impossible since both of the systems were inhomogeneous [8]. Bray discovered the first oscillatory chemical reaction in a homogeneous medium in 1921. A periodic change in the concentration of oxygen and hydrogen was occurring in that reaction which contained iodate, iodine, and hydrogen peroxide. The beginning of modern nonlinear chemical dynamics

started with the accidental reaction of Boris Pavlovich Belousov in his search for a direct conversion of colorless Ce^{3+} from yellow-colored Ce^{4+} from the reaction of the solution containing bromate, citric acid, and ferric ions, where he observed a periodic change. His observation was turned down repeatedly for publishing at that time, and it was not acknowledged by the scientific community. In 1961, Anatol Zhabotinsky, a young doctoral student at Moscow State University, began to examine Belousov's work with minimal alterations to the original reactants. He achieved better results by substituting citric acid by malonic acid. Around ten papers were published in the Russian language before the first paper in English on the Belousov-Zhabotinsky reaction in 1967. Zhabotinsky presented some of his work at a conference on 'biological and biochemical oscillators' held in Prague in 1968. The Prague conference was one of the most effective on this subject, which motivated scientists to consider the Belousov-Zhabotinsky(BZ) reaction. Later, Zhabotinsky used a ferroin indicator, and Zhabotinsky and Zakin showed ferroin could alone catalyze the reaction without cerium. This modified Belousov-Zhabotinsky is now widely used for studying nonlinear chemical dynamics. Many have claimed that the oscillation in the Bray reaction is the result of impurity or the result of bubble formation. The argument was that the response was not a true homogeneous one.

One of the main reason for rejecting Belousov's observation was the belief that it was violating the second law of thermodynamics. It is always challenging to keep track of the entropy of the universe during a chemical reaction, so measuring the change in Gibb's free energy is a way to determine the spontaneity. The main problem was with comparing the chemical oscillations with the oscillations of a pendulum. The oscillations in a pendulum pass through an equilibrium point (Fig. 1.1), but that is not true for an oscillatory chemical reaction. These chemical oscillations are thus called "far from equilibrium" systems. Here, reactants and products do not oscillate. Rather, the concentration of the intermediates (bromide and bromous acid in BZ reaction) oscillates. Though the system's entropy change decreases, the universe's total entropy change does not, so it does not violate thermodynamic laws [8]. Prigogine and his coworkers showed that self-organization in systems 'far from equilibrium' is possible as long as the total change in entropy of the universe is positive. Field,

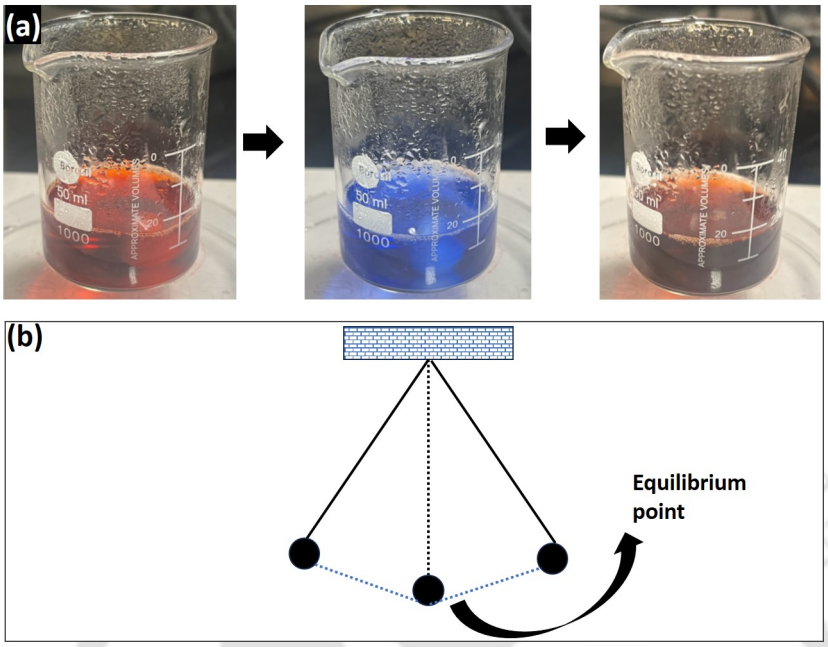

Figure 1.1: Oscillation in BZ reaction and in pendulum.

Körös, and Noyes (FKN) have combined kinetic and thermodynamic approaches and developed a detailed BZ mechanism known as the Oregonator model. These advances in theoretical nonlinear thermodynamics and FKN mechanism have led to the further careful study of oscillating chemical reactions [3], far from equilibrium.

Though the accidental discovery of Belousov's reaction was initially ignored, many chemical oscillators were synthesized afterward. The first systematically designed oscillatory reaction was a chlorite-iodate-arsenite reaction by De Kepper, Kustin, and Epstein [9]. Though the major sources for the development of various chemical oscillators are the Bray and BZ reactions, others include sulfur, phosphorus, cobalt, and manganese chemistry [3]. The following is the overall equation for the conventional BZ reaction:

$$2BrO_3^- + 3CH_2(COOH)_2 + 2H^+ \rightarrow 2BrCH(COOH)_2 + 3CO_2 + 4H_2O \qquad (1.3)$$

Despite the complexity of the reaction's mechanism, three key stages are involved.

Process-1: The reduction of bromate ion and removal of bromide ion.

$$BrO_3^- + 2Br^- + 3H^+ \rightarrow 3HOBr \tag{1.4}$$

Process 2: Oxidation of metal catalyst and autocatalytic generation of bromous acid.

$$BrO_3^- + HBrO_2 + 2M_{red} + 3H^+ \rightarrow 2HBrO_2 + 2M_{ox} + H_2O \tag{1.5}$$

Process 3: The catalyst is reduced and a bromide ion is produced, which restarts the cycle.

$$2M_{ox} + MA + BrMA \rightarrow fBr^- + Others \tag{1.6}$$

Where, $MA = CH_2(COOH)_2$ and M_{ox} and M_{red} are oxidised and reduced state of the Metal catalyst.

An unstirred BZ reaction, which is an excitable system instead of a spontaneously oscillatory one, yields patterns. A growing circular wave can be generated by a point source initiation. Once they have expanded sufficiently, they begin to propagate. A target pattern consisting of blue circles on a red background appears when periodic or continuous stimulation is present. When target waves break, two counterrotating spirals get formed. In an extremely thin reactive layer, a spiral wave is thought to ex-ist, although different shapes in a three-dimensional setting are also possible. This three-dimensional counterpart of the spiral wave is called scrolls [10]. In this thesis, works are carried out with spiral waves.

1.2 Motivation

In the developed world, cardiovascular diseases (CVD) account for over one-third of all deaths [11]. Clinical practices have demonstrated that ventricular tachycardia (VT)/fibrillation (VF) and atrial fibrillation (AF) are the primary causes of morbid-

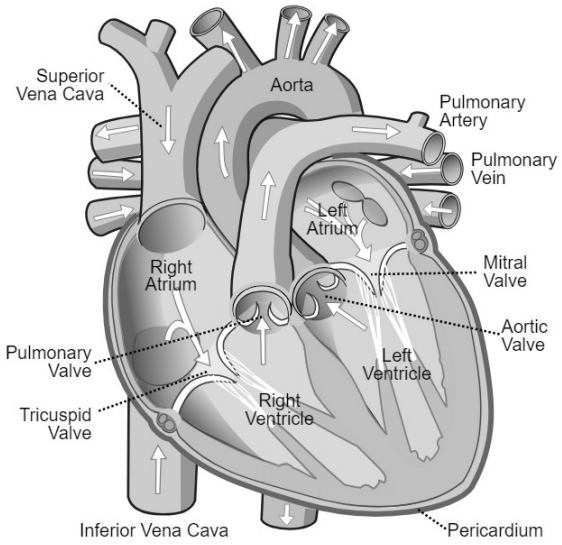

Figure 1.2: Schematic of heart showing the atrial and ventricles. (Downloaded from creative-common-licensed products.)

ity and mortality. AF is the most prevalent prolonged arrhythmia. Heart failure-like diseases are always linked to such sustained arrhythmias [12]. Furthermore, VT or VF serves as a mediator for SCD or sudden cardiac death. Globally, an estimated 4-5 million people face SCD annually [13].

Our heart is located in the chest cavity, halfway between the left and right lungs. Its primary job is to circulate blood throughout the body. The electrical impulse causes a coordinated contraction that results in the pumping of blood. The heart has four chambers and is separated into two parts. The two lower chambers are called ventricles; the higher two are called atria. The blood flow is unidirectional from the atria to the ventricles (Fig. 1.2). The heart is composed of interconnected cells or heart cells known as myocytes, connecting tissues, blood vessels, and nerves. A heart tissue has three layers, namely the internal layer or endocardium, myocardium, and the external layer or epicardium. There is another layer called the subendocardial layer, which is situated between the endocardium and myocardium layer. The Purkinje fibres, or the impulse conducting system, are located at this subendocardial layer

[14, 15].

Myocytes, or heart cells, have a length of 80–100 micrometers and a radius of 5–10 micrometers. A phospholipid bilayer membrane separates each cell from the extracellular environment. Through selective ion channels, only specific ions (Na^+, K^+, Ca^{2+}, etc.) are permitted to pass through this membrane. The transmembrane potential difference that results from the resultant charge difference is regulated by the chemical and electrical gradients present across the cell membrane. For cardiac cells, the resting potential at which the chemical and electrical forces balance each other is approximately -85 mV. If the transmembrane potential crosses a threshold value, it produces an active response. This will occur if a sufficiently large stimulus is given to a cell. The response is known as the action potential. The amplitude of it for a cardiac system is around 130 mV.

In simple terms, an action potential is an alteration in the electrical potential of a cardiac cell that occurs as an electrical impulse passes through it. Figure 1.3 portrays an action potential characteristic of a cardiac myocyte cell. There are five stages to it. Na^+ influx causes depolarization, or the transition from a negative potential to a positive potential, in phase 0. Phase 1 then sees a sharp drop in potential driven on by potassium ion outflow, which is balanced by calcium ion inflow. In phase 3, repolarization is caused by a sluggish outflow of K^+ ions and an inactive Ca^{2+} channel. Phase 4 is when the cell finally reaches its resting potential [15, 16].

The action-potential diagram, which begins at phase 1 and resets at phase 4, exhibits the characteristic of the re-excitation period, also known as the refractory period.

An electrocardiogram (ECG) records the electrical activity of the heart. During an ECG procedure, a person's thorax is covered with many electrodes to capture the voltage differences. Any normal ECG will show the atria and ventricles' depolarization and repolarization. An ECG in Figure 1.4 displays the P-wave, QRS complex, and T-wave. The ventricular depolarization is shown by the QRS complex, the atrial repolarization is indicated by the P wave, and the ventricular repolarization is indicated by the T wave. Since atrial repolarization has a significantly smaller amplitude, it is absent in the diagram [15].

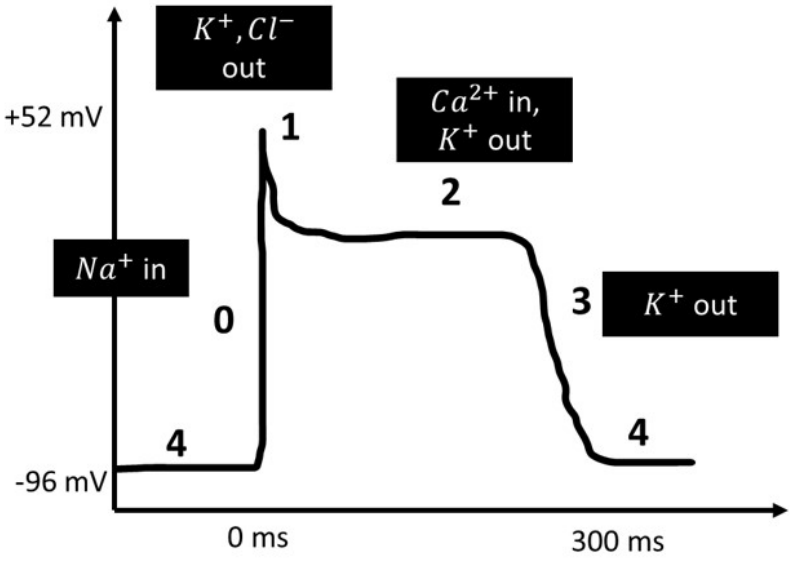

Figure 1.3: Action potential of cardiomyocytes. Depolarization and re-polarization is represented from phase-0 to 3. Phase-4 is demonstrating the resting potential.

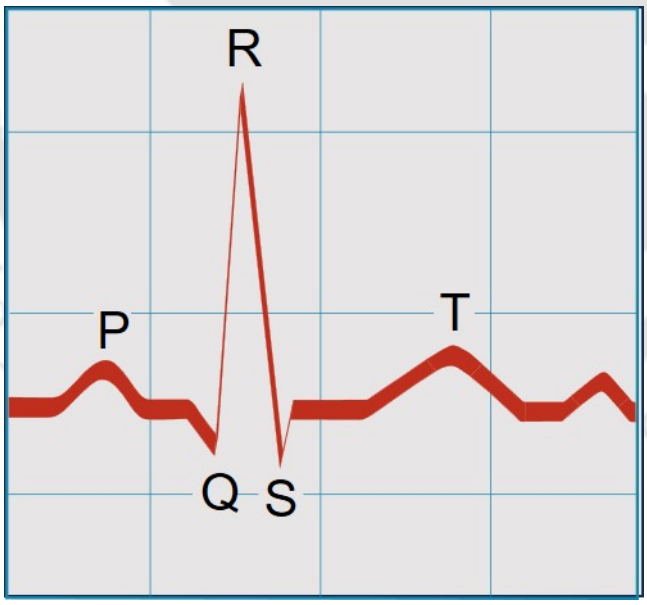

Figure 1.4: A typical heartbeat traced in ECG depicting P-wave, QRS complex and T-wave. (Downloaded from creative-common-licensed products.)

Any abnormalities in cardiac rhythm are possible to be detected by an ECG. A normal rhythm means it originates from the sinoatrial node and is transmitted to the ventricles through atrioventricular nodes with regular conduction velocity in an optimal range. Any deviation causes arrhythmias or irregular beats. Two important arrhythmias are atrial and ventricular fibrillation. Atrial fibrillation is caused by an extremely rapid contraction of the atria and does not originate from the sinoatrial node. Although it does not pose a threat to life, but damages the heart [17]. Ventricular fibrillation is dangerous and can lead to death if not treated immediately with an electric shock defibrillation technique.

A generalized concept of cardiac malfunctions such as tachycardia involves the formation of re-entries or rotors. The term "rotor" bears resemblance to the term "pinwheel," which Winfree utilized to denote the center of the spiral. This region is alternatively referred to as the "core" by physicists. In contemporary medical literature, spiral waves are now frequently equated with rotors [18]. When electrical waves passing through the heart come in contact with any appropriate heterogeneity that can break the traveling wave, the tip of the broken waves curl in to generate the spiral wave in the cardiac system (Fig. 1.5). The critical curvature of the wavefront, excitability, and obstacle size are the major determinants of the spiral creation. Any obstacle greater than 1 mm in size has the potential to generate spiral waves in a normal heart muscle. The core components of VF also include the spiral rotors. Multiple waves travel across the heart during VF. The mother spiral breaks apart, resulting in the presence of multiple rotors(Fig. 1.6) to enhance VF [19].

This discussion about the cardiac system described above introduces the concept of spiral waves and our motivation for their study. Further research on the spiral wave theory of the cardiac system is necessary in order to control the aberrant rhythm. The Belousov-Zhabotinsky reaction system provides an important laboratory model for the study of the spiral and scroll waves (3-D counterpart of the spiral). Researchers have tried to control the waves with various gradients, for example, thermal gradient, electric field gradient, optical feedback, etc. [20, 21, 22]. Moreover, the rotors have never been studied collectively in the context of cardiac rhythm. This research aims to study the spirals in BZ reactions individually and collectively, in the presence of

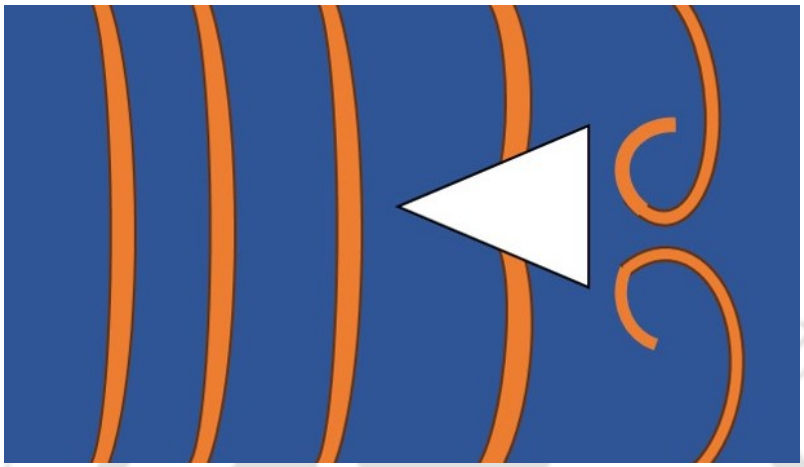

Figure 1.5: Demonstrating the spiral wave formation in presence of appropriate heterogeneity.

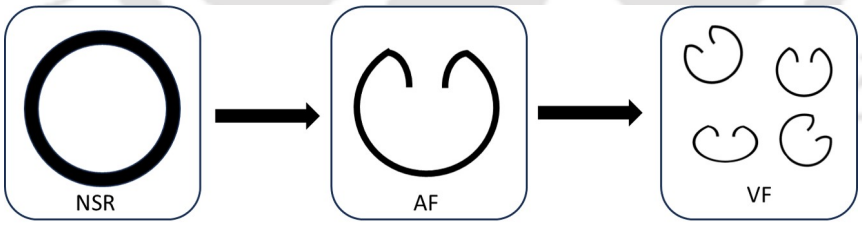

Figure 1.6: Schematic of cardiac rhythms in terms of spiral wave theory. NSR represents the normal sinus rhythm, multiple spiral rotors showing VF condition.

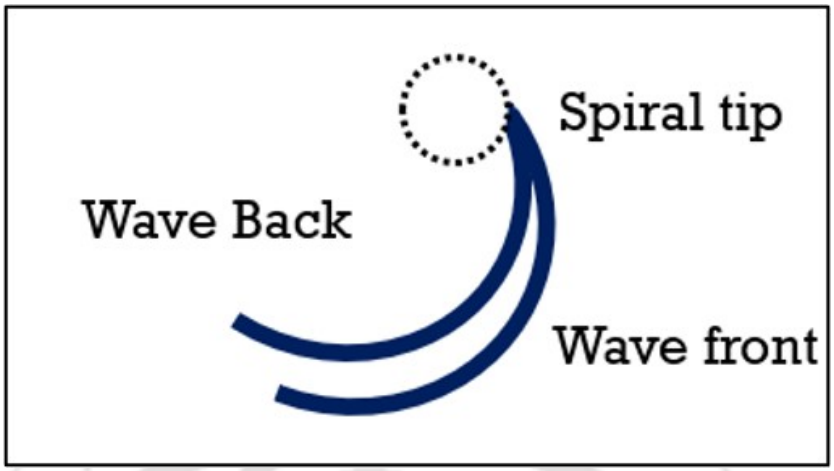

Figure 1.7: A representation of phase singularity or spiral tip. Dashed circle depicts the core of a spiral rotor.

nonlocal coupling.

1.3 Some basic concepts of spirals

1.3.1 Spiral tip and spiral Core

A spiral center, often referred to as a spiral core, is the region that a spiral wave revolves around. The spiral tip is the point where a spiral's wavefront and waveback converge (Fig. 1.7). For either a planar or circular wave, the scenario is not possible. For planar and circular waves, all part of the wave move with same velocity; for spiral waves, this isn't the case, because of the curvature effect. This has been shown in figure 1.8. Curvature plays an important role in temporal evolution of spiral waves. The relation between the normal velocity with curvature is given by the Eikonal equation [23] as,

$$N = c - DK \tag{1.7}$$

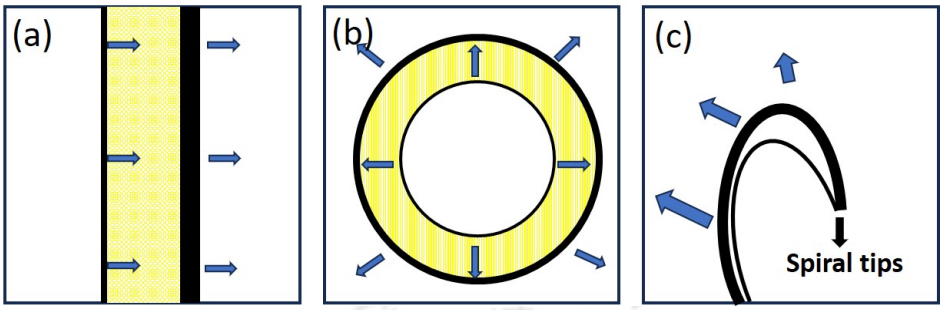

Figure 1.8: Propagation of wave front and wave back for linear (a), circular (b), and spiral(c) waves.

Where, N is the normal velocity, K is curvature, c is velocity of plane wave in the excitable media and D is the diffusion coefficient of the autocatalytic species.

1.3.2 Spiral Trajectories

The path of a spiral tip is called its trajectory. A rigid spiral rotor rotates around a circular path, creating a circular trajectory (Fig. 1.9(a)). The trajectory may be meandering (Fig. 1.9(b)) due to internal instability or external perturbation.

1.3.3 Drift vs Meandering

The drift and the meandering phenomena are not the same. Meandering is the variation of spiral rotation due to internal instability, whereas drift is the directed change of the spiral location with time in the presence of a perturbation [24]. Spiral drifts are of many kinds. A time-dependent force having a period close to the period of the spiral leads to drift called **Resonance drift**. If the properties of the system vary with space, then drift also occurs, known as **inhomogeneity drift**. However, if the properties of the system vary with time, then the drift that occurs is called **anisotropy-induced drift**. For a bounded media, drift may occur if the spiral is close to the boundary, termed **Boundary-induced drift**. Drift may occur due to the interaction of multiple spirals when their cores are near each other, which is called **interaction drift**. Another type of drift is **High-frequency induced drift**,

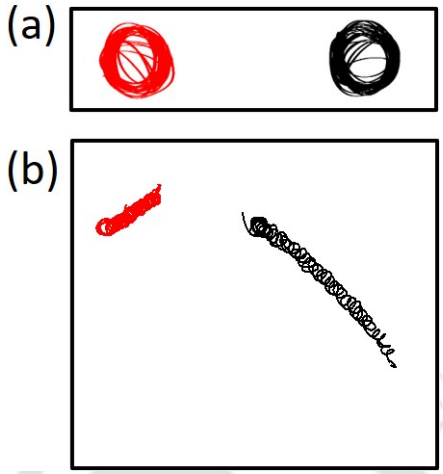

Figure 1.9: Trajectory of two counter-rotating spirals. (a) Rigid rotation and (b) meandering spirals.

which occurs when a spiral wave is overwhelmed by another excitation wave of a higher frequency.

1.3.4 Free and Pinned spirals

Pinned spiral waves are those, in which a normal spiral wave gets attached or anchored to a heterogeneity (Fig. 1.10). The pinned spiral wave has a more extended time period than that of free spirals (Fig. 1.11) [25].

1.4 Concepts on collective dynamics

Till now, we have discussed the concepts of dynamics of individual oscillatory systems. Collective dynamics refers to the study of the coordinated dynamics of those individuals as a collection. An oscillator in a group may behave differently than its behavior as an individual. Synchronization and chimera are two of many interesting phenomena demonstrated in collective dynamics.

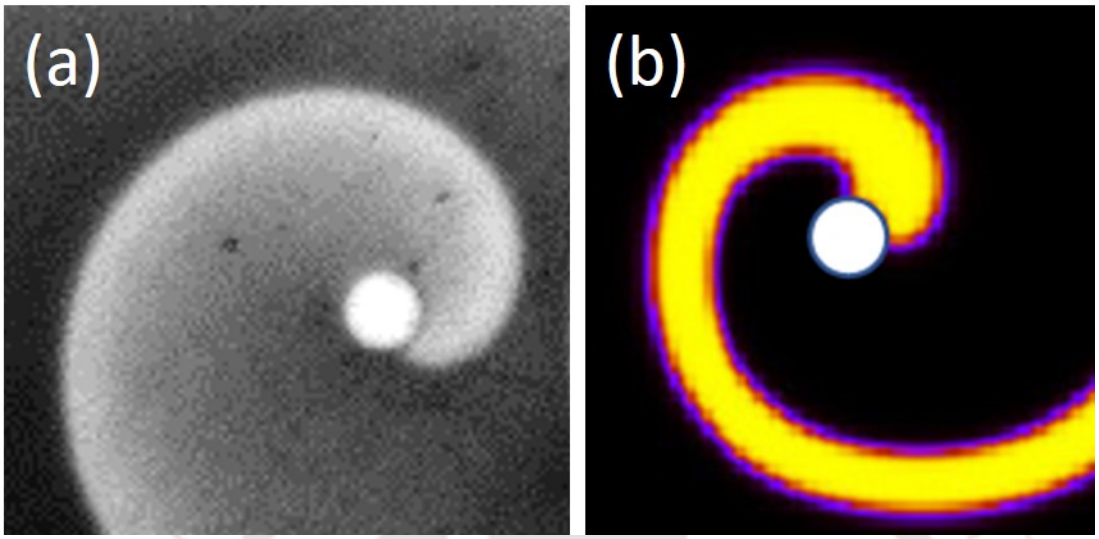

Figure 1.10: Pinned spiral in (a) experimental BZ system and in (b) a numerical simulation.

Obstacle size (mm)	Time period (min)
1.8	12
2.7	18
3.6	24

Figure 1.11: A table to show how the size of pinning obstacle modify the time period of a spiral wave.

1.4.1 Interaction of free spirals

A rigorous study by Kalita *et al.* [26] showed that multiple spirals in a system, interact depending on the distance between the spiral cores and wavelength. The interaction may be attractive, repulsive, etc. If the spirals are far apart, there is no interaction. A critical distance ($d_c = \lambda - d_s$) is defined by the core diameter (d_s) and the wavelength (λ) of the spirals, govern the interaction outcomes. The experiments show if the distance between the spirals is l, then the attraction of spirals leading to annihilation is possible up to $l{=}d_c/2$, then repulsion starts, and no interaction is found if the separation is greater than d_c.

1.4.2 Synchronization

Probably the first scientist to notice and describe the synchronization phenomena was the Dutch researcher Christiaan Huygens, who was well-known for his investigations in optics as early as the seventeenth century. He found that two pendulum clocks suspended from a single support eventually synced, meaning that their oscillations precisely coincided and the pendula consistently moved in opposite directions. Since then, numerous advancements have been made. This phenomenon is now known to exist in several systems like physical, chemical, biological etc. Synchronization can be defined as the adjustment of rhythms of oscillating objects due to their weak interaction. The term "oscillatory system" in physics refers to the" self-sustaining oscillator", which is an active system with an internal energy source that generates oscillations. In mathematics, these are also referred to as autonomous dynamical systems. The term synchronization is not valid for oscillators, which are not self-sustained. The cardiac and BZ systems both exhibit self-sustaining oscillations [27].

1.4.3 Chimera

The term "chimera" describes an intriguing dynamics in which two or more coupled oscillating systems display unique behaviors that coexist. It indicates that while one component of the system exhibits coherent or synchronized oscillation, the other

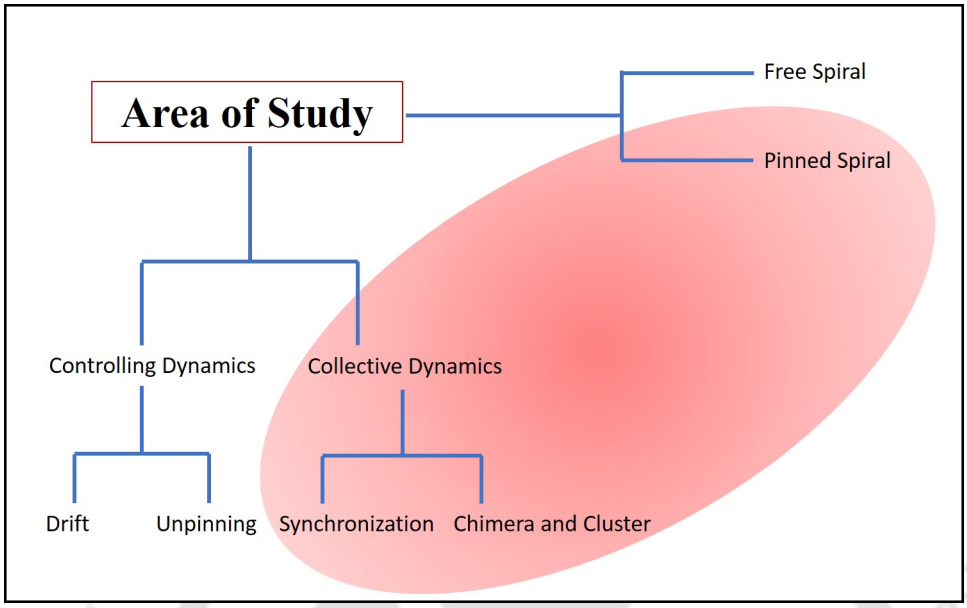

Figure 1.12: The area of study in a flow-chart.

component behaves incoherently or are desynchronized. Numerous chimera types, such as phase, frequency, and amplitude chimeras, have been documented in a variety of research systems [28].

1.5 Problem statements (objectives)

The current research attempts to investigate the spiral wave dynamics in detail in order to comprehend and find possible mechanism to regulate the cardiac wave dynamics. In order to accomplish this, we investigate both pinned and free spirals. We take on the following suggested challenges.

1. To investigate the effect of a mild gradient in controlling the dynamics of spiral waves.
2. To explore the collective nature of two pinned spirals.
3. To understand the behavior of multiple pinned spirals in a defined network.

1.6 Organization of the thesis

The thesis is organized as follows:

Chapter 1 describes the motivation behind the work of this thesis. It briefly discusses key concepts of the field of study.

Chapter 2 briefs about the common methodologies and techniques used for our experiments and computer simulations.

Chapter 3 introduces a modified Oregonator model, which is derived from the established FKN mechanism of the BZ reaction. This chapter shows how the spiral wave properties vary explicitly with the hydrogen ion concentration parameters. Normal outward spiral, meandering spiral, and even spiral breakup phenomena is observed.

Chapter 4 demonstrates an experimental and simulation study to control the spiral wave dynamics with a mild gradient. Here, we used proton exchange resin bead as a source of hydrogen ions in order to produce a mild concentration gradient. The results show controlled drifting of spirals in the presence of a gradient, that increases with increasing number of resin beads.

Chapter 5 displays the observations of synchronization phenomena for pinned spiral rotors. The chapter distinguishes the synchronization phenomena according to the orientation of spiral rotations.

Chapter 6 showcases the collective phenomena of pinned spirals in a square network, where we report the formation of clusters and chimera in our network of coupled rotors. Experimental observations show that the size of the square determines the type of dynamics.

Chapter 7 establishes the importance of communication in the synchronization process in a chemical reaction-diffusion system, the observation is motivated by Huygen's well-known Pendulum experiment, but is newly observed in a chemical system.

Chapter 8 concludes with our results, observations, answered and unanswered questions, as well as proposing a future direction for research.

Chapter 2

Methods and Techniques

2.1 Introduction

Three main techniques have been employed by scientists for a thorough investigation of excitable chemical waves. These three approaches are analytical methods, numerical simulation methods, and experimental methods. Here, like in all the research covered in this thesis, numerical simulation techniques and experiments with unstirred BZ reactions are employed.

2.2 Experimental Methods

2.2.1 Instrumental setup

The instrumental setup for the experiments we performed are as depicted in Fig. 2.1 . Three fundamental components comprise of the instrumental setup: a top-mounted CCD camera for capturing the dynamics; a bottom-mounted light source for illuminating; a Petri dish containing the reaction mixture; and a personal computer for storing the camera-captured snapshots. We alter the system within the Petri dish based on the requirements for a certain experiment.

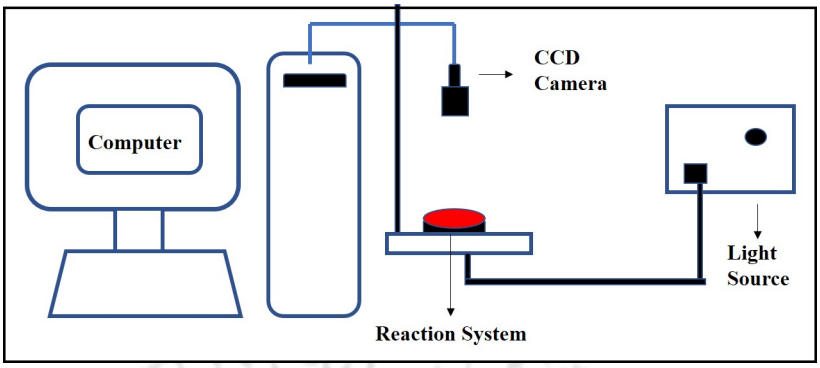

Figure 2.1: An experimental setup showing the reaction system, illuminated with a light source, a CCD camera placed at the top, and a personal computer to record and analyze the captured images.

2.2.2 Preparation of stock solution

We prepared stock solutions of 1 M of sodium bromate, 1 M of malonic acid, and 0.5 M of sulphuric acid. We used a ferroin solution with a concentration of 0.16 mM. For the ferroin-catalyzed BZ reaction, we mixed in a 1:1:10:1 ratio of the said ingredient for our experiments. The final concentrations for our experiments are; 0.04 M sodium bromate, 0.04 M malonic acid, 0.2 M sulphuric acid and 0.006 mM ferroin.

2.2.3 Wave generation

Sustainable waves can be observed for a certain range of concentrations of the components in an unstirred BZ reaction. Waves are produced by placing the mixture in a Petri dish and waiting for it to stabilize until convection ceases. Next, we disturb the excitable system by means of a silver wire. In a thin reaction bed, a two-dimensional circular wave known as target wave forms after a certain induction period. An example of such a target wave is demonstrated in Fig. 2.2(a).

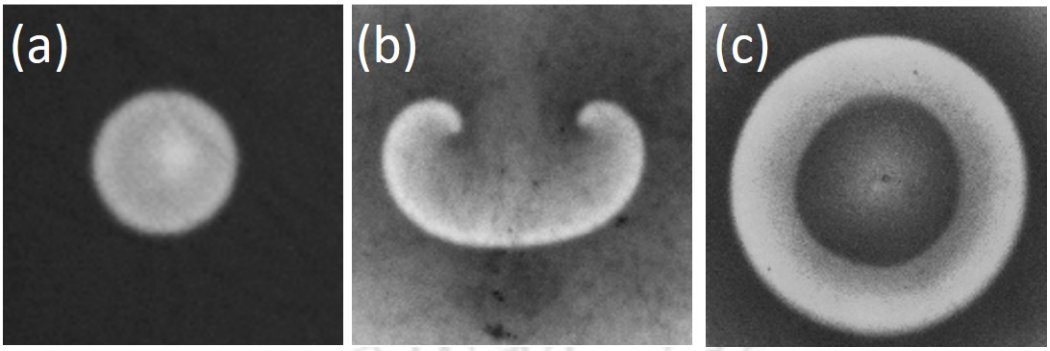

Figure 2.2: Patterns in a BZ reaction-diffusion system. (a) a target pattern (b) a pair of spirals (c) a scroll wave

2.2.4 Spiral and scroll formation

If a target wave is broken because of inhomogeneity, a shift of system excitability, or another physical condition, its two broken ends curl up to produce spirals that rotate counter-clockwise. The broken ends propagate more slowly than the rest of the wave. The frequency of a spiral wave in the same medium is higher than that of the target wave. As a result, the spiral wave will eventually push out all of these trigger waves in a given excitable medium and fill the entire space.

In our case, a pair of spiral waves (Fig. 2.2(b)) are formed by cleaving the target wave. We cleave it with the help of a thin glass slide, as glass is nonreactive with the solution. In comparison, scroll formation occurs in a thicker solution. To prepare a scroll (Fig. 2.2(c)), we generate a target wave in a thin solution, as discussed above; then we pour another layer of the BZ solution over that. A three-dimensional wave evolved with a cylindrical filament.

2.2.5 Pinning of spirals

Spirals and scrolls get pinned or anchored to unexcitable heterogeneities. Cylindrical rubber beads or spherical glass beads are examples of some heterogeneities we use in our experiments. To pin a spiral wave, we carefully place the heterogeneity at the tip of the spiral.

2.2.6 Record and analysis

Recording the experiments is the last stage of the experiment. We capture it from above using a CCD camera and store the images on to a desktop computer. The images are taken at two second intervals. We then use an inhouse MATLAB code to analyze the snapshots.

2.3 Numerical Methods

For the most part, we employed a reaction-diffusion (RD) model to interpret the results of our experiments. The Barkley Model and the Oregonator are the models most utilized to describe spiral dynamics in BZ reactions. These are activator inhibitor RD systems.

2.3.1 RD models

2.3.2 Barkley Model

Barkley Model is the most widely used activator-inhibitor model for explaining the pattern formation in reaction-diffusion systems, expressed as-

$$\epsilon \frac{\partial u}{\partial t} = \left[u\left(1-u\right)\left(u - \frac{v+b}{a}\right)\right] + D_u \nabla^2 u \tag{2.1}$$

$$\frac{\partial v}{\partial t} = u - v + D_v \nabla^2 v \tag{2.2}$$

where u acts as activator and v as inhibitor. D_u and D_v are diffusion coefficients of activator and the inhibitor.

2.3.3 Oregonator Model

The Oregonator model is based on FKN [29] mechanism of the BZ reaction.

The standard Oregonator model considers five irreversible steps, in which the proton concentration is incorporated with the rate constants ($k_1 = k_{R3}H^2$, $k_2 =$

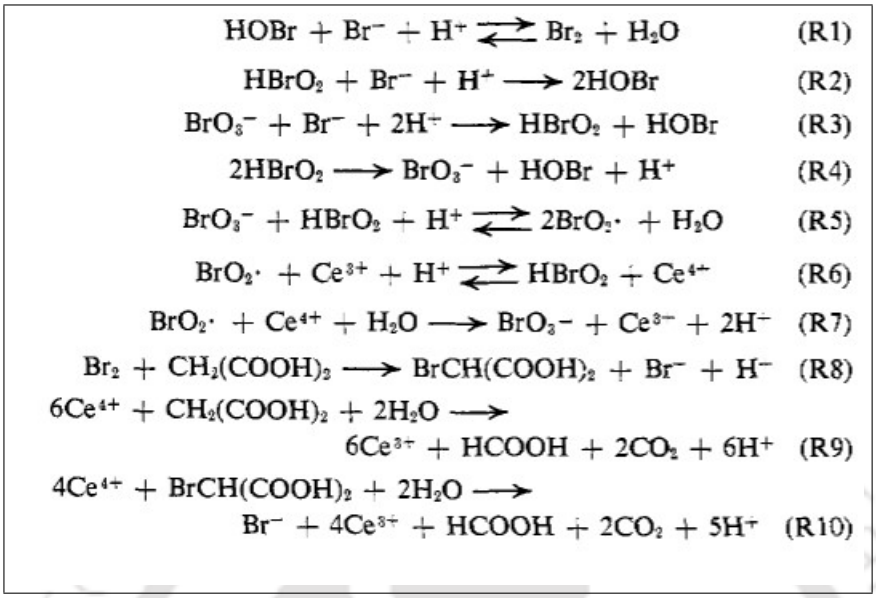

Figure 2.3: FKN mechanism for cerium catalyzed BZ reaction [29].

$k_{R2}H$, $k_3 = k_{R5}H$, $k_4 = k_{R4}$) of each steps. These are given as follows:

$$A + Y \xrightarrow{k_1} X + P \tag{2.3}$$

$$X + Y \xrightarrow{k_2} 2P \tag{2.4}$$

$$A + X \xrightarrow{k_3} 2X + 2Z \tag{2.5}$$

$$2X \xrightarrow{k_4} A + P \tag{2.6}$$

$$B + Z \xrightarrow{k_c} \frac{1}{2} fY \tag{2.7}$$

where A=BrO_3^-; B= Organic species; P=$HOBr$; X=$HBrO_2$; Y=Br^-; Z= Metal in oxidised state, for our study it is Fe^{3+}; f= adjustable parameter. Except X,Y, and Z, the other species (A,B and P) are present in very higher amounts and so their concentration is considered constant. Writing rate equations of X,Y and Z and then making them dimensionless, yields following three equations:

$$\epsilon \frac{\partial x}{\partial t} = qy - xy + x(1-x) \tag{2.8}$$

$$\epsilon^{'} \frac{\partial y}{\partial t} = -qy - xy + fz \tag{2.9}$$

$$\frac{\partial z}{\partial t} = x - z \tag{2.10}$$

where, $x{=}\frac{2k_4X}{k_5A}$; $y{=}\frac{k_2Y}{k_5A}$; $z{=}\frac{k_ck_4BZ}{(k_5A)^2}$; $\epsilon{=}\frac{1}{k_5A}$; $\epsilon^{'}{=}\frac{2k_4}{k_2k_5A}$; $q{=}\frac{2k_3k_4}{k_2k_5}$;
when,

$$\epsilon^{'} \ll \epsilon$$

On applying steady state to y the two variable Oregonator model is obtained which is very similar to the Barkley model. It is given as-

$$\epsilon \frac{\partial x}{\partial t} = x(1-x) + f\frac{q-x}{q+x}z \tag{2.11}$$

$$\frac{\partial z}{\partial t} = x - z \tag{2.12}$$

where x behaves as activator and z as inhibitor.

2.3.4 Modification

In order to get closer to the actual physical system under study, people have updated fundamental models based on requirements of a specific experimental setup. We used a modified form of the Oregonator model for one study. In chapter 3, the redesigned model is discussed in detail.

2.3.5 Solving equations on the computer

We discretized our system in space and used a zero flux boundary condition to solve the equations. To integrate, we used the RK4 and Euler methods in some cases for

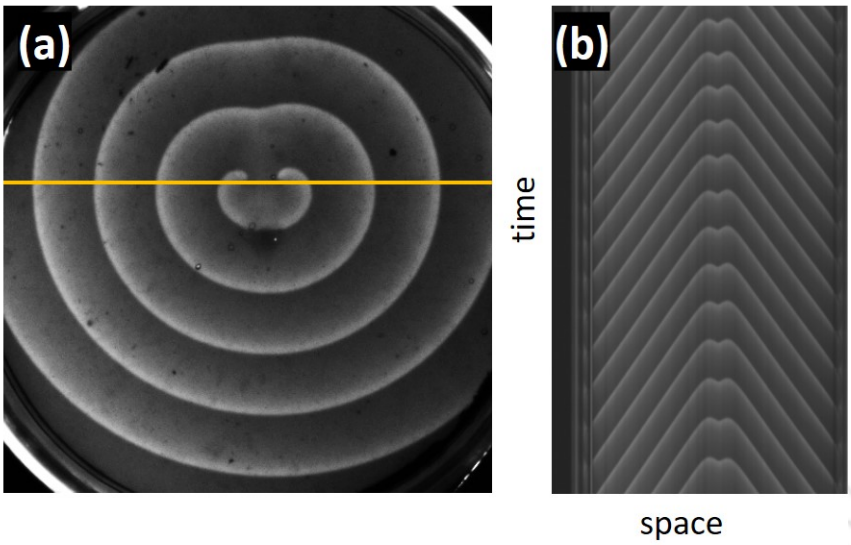

Figure 2.4: A typical experiment. (a) Snapshot 65 min after initiation. (b) Space-time plot along yellow solid line shown in (a).

the models we used. The Euler method is fast and does not lead to considerable variations in the characteristics of the results, compared to the RK4 method. A central difference method is applied to solve the diffusion part of the equations as follows;

$$\nabla^2 u(x,y,t) = \frac{u(x+h,y)+u(x-h,y)+u(x,y+h)+u(x,y-h)-4u(x,y)}{h^2} \tag{2.13}$$

where, h is the step size in a 5-point stencil.

2.4 Analysis

Tip trajectories: To examine the spiral dynamics, a study of the spiral tip movement is necessary. For our studies, we can follow the coordinates of the tips in 2-D space using a self-developed MATLAB code and the captured snapshot images. In

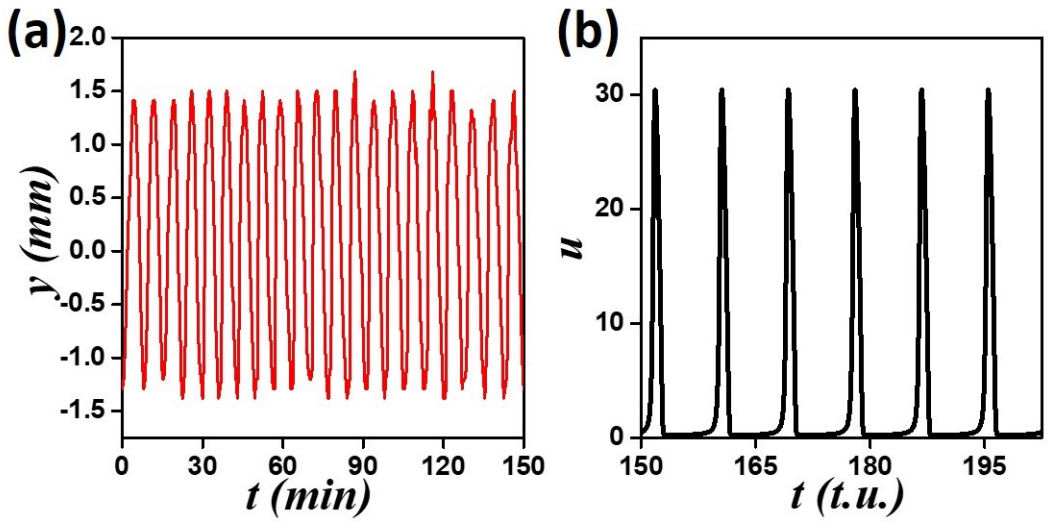

Figure 2.5: Time series plots. (a) y- coordinate is plotted against time for a typical experiment with pinned spirals. (b) Show the variation of activator concentration with time in a numerical simulation.

the case of numerical simulations, we track the tip, which is the intersection of the isoconcentration lines, by setting a specific concentration value for the activator and inhibitor.

Time-space plot: A typical space-time plot shown in figure 2.5 helps to monitor the change in position or characteristics of spiral wave with time.

Time series: A time series, in our case, is the evolution of any of the coordinates with time. We mostly used the time evolution plots to study the collective dynamics.

Chapter 3

Control and dynamics: Modified Oregonator model and spiral properties

3.1 Introduction

Reaction diffusion processes are oftentimes the storehouse of various spatiotemporal patterns. Turing patterns like spots, stripes and labyrinths are abound in the chemical and biological world, and are responsible for the stripes of the zebra or spots on the leopard, inciting awe and admiration amongst the onlooker [30]. Apart from their aesthetic allure, they also have underlying biological significance, which sometimes surpasses the former purpose. Sometimes, the physiological importance is so immense that one needs all the help that can be mustered, to understand the system. One such kind of pattern is the rotating two-dimensional spiral and three-dimensional scroll wave, that is responsible for cardiac arrest, or neuronal transduction, or the only way for tiny microbial colonies to sustain their population when food is scarce [31, 32, 33]. These excitation waves, which could be of electrical nature in the cardiac and neuronal tissues, muscular origin in uterine tissues, and concentration (of microbes) waves in the amoebal population, are self-sustained and share several prop-

erties and follow similar rules of physics [16]. In a chemical reaction-diffusion system, these waves arise out of concentration variations of chemicals, mostly intermediates formed in a reaction. The very first example of such patterns encountered in the chemical laboratory was the Belousov Zhabotinsky (BZ) reaction system [34].

Discovered by Boris P. Belousov in 1951, in his search for an Inorganic analogue of the Krebs cycle, a stirred batch of the BZ reaction in a beaker showed oscillatory behavior, in the change of color of its intermediates [35]. The far-from-equilibrium (thermodynamic) phenomenon was re-verified and modified by some other scientists in the decades to come, most notable amongst whom was Anatol Zhabotinsky, whose name got attached to the reaction [36]. In subsequent years, Winfree and coworkers were able to use a thin [37], unstirred layer of the BZ solution to produce sustainable chemical waves, reminiscent of Turing patterns [38] and more interesting excitation waves, namely target patterns and spiral waves. These waves were similar to the ones found in biological organs and populations, and could be used as a table-top model for their understanding and control.

The mechanism of the BZ reaction was suggested by a group of scientists, Field, Körös and Noyes in 1972 [39]. Popularly known as the FKN mechanism, it led to a better understanding of the kinetics of the complex oscillatory reaction. The most important steps of the reaction were used to set up mathematical models for the further study of the dynamics, leading to the widely accepted Oregonator model [40]. This model, in two dimensions, was an activator-inhibitor model, that was similar to theoretical models of the Turing kind [30], like the Gierer-Meinhardt model [41], which could explain pattern formation and morphogenesis in biological systems. The Oregonator model consisted of two coupled differential equations of concentration variables u and v, that showed oscillations in some finite parameter range. Later, diffusion terms were included in the Oregonator whose numerical simulations could reproduce the spiral wave behavior in the system [42]. Eventually, simplified mathematical models like the Barkley model were also introduced [43] that enabled fast computer simulations of pattern forming reaction-diffusion processes.

The Oregonator model is a well studied system, that has mostly been able to explain many of the actual dynamics observed in experiments with the BZ reaction.

Varying the system parameters, and diffusion coefficients of the two variables, the Oregonator reaction-diffusion equations were able to support traveling wave solutions [44], spiral waves, and Turing patterns [45], the latter amongst which has not yet been observed in an experimental BZ system. However, the current form of the Oregonator model is unable to address the effect of the hydrogen ion concentration explicitly. In a recent study of spiral wave properties in the BZ, the effect of the hydrogen ion was considered to effect only the excitability parameter ϵ [46]. However, in the development of the Oregonator model, $[H^+]$ is also incorporated into other parameters, which is mostly ignored in these studies. The researchers rightly predicted some zones of random oscillations, which may or may not be related to spiral breakup or turbulence. In the cardiac system, sustainable spiral waves are linked with monomorphic ventricular tachycardia [47], and spiral breakup is related to the more lethal ventricular fibrillation [48]. Currently, spiral breakup has being observed in computer simulations of the complex Ginzburg-Landau (CGL) equations [49] and the Fitz Hugh Nagumo (FHN) models [50], or very rarely in modified versions of the BZ [51] having gel-liquid interfaces. However, there has not been any evidence of turbulence in a homogeneous layer of BZ. The existing mathematical models are unable to suggest any control of the experimental parameters so as to capture these elusive phenomena in the BZ reaction. In order to find parameters within the BZ reaction system, where such spiral breakup and turbulence can be encountered and studied, we explore in detail a theoretical model based on the dependable FKN mechanism.

In this study, we develop from the FKN mechanism, an alternative mathematical model, which we christen the modified Oregonator model. Our rate equations are nondimensionalized and the parameters defined, so as to make it suitable for further numerical analysis. The main difference of our model with the existing ones, is the explicit appearance of the hydrogen ion concentration in the final equations. This will enable us to study the system as the initial acid concentrations are varied. Our in-depth numerical simulations by varying the parameter f and concentration variable h, open up new zones of spiral wave activity, including stable and drifting spirals, target patterns, oscillation death, and also spiral breakup leading to turbulence. In previous studies, specific models or modifications were used to describe a particular

phenomena, but here we show a plethora of spiral dynamics with our three-variable reaction-diffusion model, just by tuning some system parameters.

3.2 Model

3.2.1 Mechanism for BZ reaction

The important steps in the mechanism of the BZ reaction proposed by Field-Körös-Noyes(FKN) [34], used for development of most numerical models, is given as−

$$\mathrm{BrO_3^- + Br^- + 2H^+ \xrightarrow{k_1} HBrO_2 + HOBr} \tag{3.1}$$
$$\mathrm{HBrO_2 + Br^- + H^+ \xrightarrow{k_2} 2HOBr} \tag{3.2}$$
$$\mathrm{BrO_3^- + HBrO_2 + H^+ + 2M^{2+} \xrightarrow{k_3} 2HBrO_2 + 2M^{3+} + H_2O} \tag{3.3}$$
$$\mathrm{2HBrO_2 \xrightarrow{k_4} BrO_3^- + HOBr + H^+} \tag{3.4}$$
$$\mathrm{2M^{3+} + MA + BrMA \xrightarrow{k_5} fBr^- + 2M^{2+} + Other\ products.} \tag{3.5}$$

The FKN mechanism involves three main processes: the autocatalysis of $HBrO_2$ (step 3); inhibition by bromide ion (steps 1 and 2), and resetting the cycle (4 and 5). The values of the rate constants are given as k_1= 2 $M^{-3}s^{-1}$, k_2= 1.25 × 10^5 $M^{-2}s^{-1}$, k_3= 45 $M^{-2}s^{-1}$, k_4= 1.4 × 10^3 $M^{-1}s^{-1}$, k_5= 6.5 × 10^{-3} $M^{-1}s^{-1}$ [34].

Expressing the reactions in a more general form gives-

$$\mathbf{A + W + 2H \xrightarrow{k_1} U + P} \tag{3.6}$$
$$\mathbf{U + W + H \xrightarrow{k_2} 2P} \tag{3.7}$$
$$\mathbf{A + U + H \xrightarrow{k_3} 2U + 2V} \tag{3.8}$$
$$\mathbf{2U \xrightarrow{k_4} A + P + H} \tag{3.9}$$
$$\mathbf{V + B \xrightarrow{k_5} \frac{1}{2} f W} \tag{3.10}$$

This system of equations constitute the modified Oregonator (MO) model, where

comparison with the FKN would yield $\mathbf{A} = BrO_3^-$, $\mathbf{W}$= Br^-, $\mathbf{H}$= H^+, $\mathbf{U}$= $HBrO_2$, $\mathbf{P}$ = HOBr, $\mathbf{V}$ = oxidized form of catalyst, and $\mathbf{B}$ = MA+BrMA (malonic acid and its derivatives). This scheme is able to give, by simple linear combination of equations, the overall reaction, $f\mathbf{A} + 4\mathbf{B} + (3f+1)\mathbf{H} \rightarrow (3f+1)\mathbf{P}$, with no net production or destruction of $\mathbf{U}$, $\mathbf{V}$ and $\mathbf{W}$. Hence, they are considered as the intermediates, whose dynamics is of interest to us.

The kinetic behavior of the intermediates can now be written from the above model as-

$$\frac{dU}{d\tau} = k_1AWH^2 - k_2UWH + k_3AUH - 2k_4U^2 \tag{3.11}$$

$$\frac{dV}{d\tau} = 2k_3AUH - k_5BV \tag{3.12}$$

$$\frac{dW}{d\tau} = -k_1AWH^2 - k_2UWH + \frac{1}{2}k_5fBV \tag{3.13}$$

$$\frac{dH}{d\tau} = -2k_1AWH^2 - k_2UWH - k_3AUH + k_4U^2. \tag{3.14}$$

Here U, V, W, and H are the concentrations of the respective variables in units of mol L^{-1} and τ is time in units of s.

3.2.2 Dimensionless form

We further non-dimensionalize the equations in the MO model (11-14), using the following scaling.

$$u = \frac{k_3}{k_5}\frac{a}{b}U, \quad v = \frac{k_1k_3}{k_2k_5}\frac{a^2}{b}V, \quad w = \frac{k_2}{k_3}\frac{1}{a}W, \quad h = \frac{2k_1k_3}{k_2k_5}\frac{a^2}{b},$$

where u, v, w, and h, are the dimensionless variables, giving us the set of non-dimensional kinetic equations

$$\epsilon \frac{du}{dt} = \frac{1}{2}wh^2 - uwh + uh - qu^2 \tag{3.15}$$

$$\frac{dv}{dt} = uh - v \tag{3.16}$$

$$\epsilon' \frac{dw}{dt} = -qwh^2 - 2quwh + 2qfv \tag{3.17}$$

$$\frac{dh}{dt} = -wh^2 - uwh - uh + qu^2 \tag{3.18}$$

a and b being the concentrations of A and B. In the above set of equations, the parameters are given by,

$$\epsilon = \frac{1}{h_0}\frac{k_5}{k_3}\frac{b}{a}, \quad \epsilon' = \frac{1}{h_0^2}\frac{2k_4k_5}{k_2k_3}\frac{b}{a}, \quad q = \frac{2k_1k_4}{k_2k_3},$$
$$\text{and} \quad t = k_5 b\tau, \quad \text{where} \quad h_0 = \frac{k_2k_5b}{2k_1k_3a^2}.$$

The values of a and b are considered to meet usual experimental conditions [42], and can be varied to give different values of the parameters.

As the reactions are carried out in an acidic environment, the amount of hydrogen ions can be considered to be in excess. Hence, h in the above equations can be considered as a constant parameter, and we have a modified version of the three-variable Oregonator model as equations (3.15-3.17).

Numerical Methods

In order to study spiral wave activity in a spatially extended system, the BZ reaction is often carried out in an unstirred gel medium where diffusion plays a major role in modifying the dynamics of the system. The gel however, rules out any convection in

the medium. For such a system, the reaction-diffusion equations are given as:

$$\frac{du}{dt} = \frac{1}{\epsilon}\left[\frac{1}{2}wh^2 - uwh + uh - qu^2\right] + D_u\nabla^2 u \tag{3.19}$$

$$\frac{dv}{dt} = [uh - v] + D_v\nabla^2 v \tag{3.20}$$

$$\frac{dw}{dt} = \frac{1}{\epsilon'}\left[-qwh^2 - 2quwh + 2qfv\right] + D_w\nabla^2 w \tag{3.21}$$

where, D_u, D_v, D_w are the diffusion coefficients of u, v and w, respectively.

In order to numerically integrate the equations (19-21), zero flux boundary conditions are applied across all four boundaries. The system parameters are chosen as $\epsilon = 0.035$, $\epsilon' = 0.008$, $f = 0.9$, $q = 0.01$. The time-step and space-step were chosen as $\Delta t = 0.012$ t.u. and $\Delta x = 0.35$ s.u., respectively, which translates to 0.651 ms, and 3.16 μm. These values of Δt and Δx are convergent and yield best resolution of patterns in our parameter range, and also can be varied by around 20%, without causing any major changes to the nature of the waves, or the time period and wavelength of the corresponding spirals. Simulations were carried out in a 300×300 (105 s.u. $\times$ 105 s.u.) grid. Eulers method is used for the integration, and a central difference method helped to calculate the diffusion term. Stable rotating spirals, with non-meandering circular cores are observed in a range of parameters. For our analysis, we vary the parameters from a base condition, at which the system supports an outwardly rotating spiral. The base condition has diffusion constants of $D_u = 0.1$, $D_v = 0.057$, $D_w = 0.11$, with $h = 0.3$. The values of the diffusion coefficients are taken in a ratio so as to match their actual expected values depending on their molecular weights (molecular weight of u or $HBrO_2$ is 113 g mol^{-1}, of v or ferroin is 596 g mol^{-1} and that of w or bromide is 80 g mol^{-1}.). The initial values of u, v and w are taken to be zero across the entire space, as they are intermediates of the BZ reaction, except for a thin area signifying the initial wave-front. A plane wave is initiated in the middle of the square area, by taking three stripes of width $2\Delta x$ and length $60\Delta x$ having non-zero values of the variables, emulating the front and back of the wave. The straight plane wave initiated, curled up to form a pair of counter-rotating spirals.

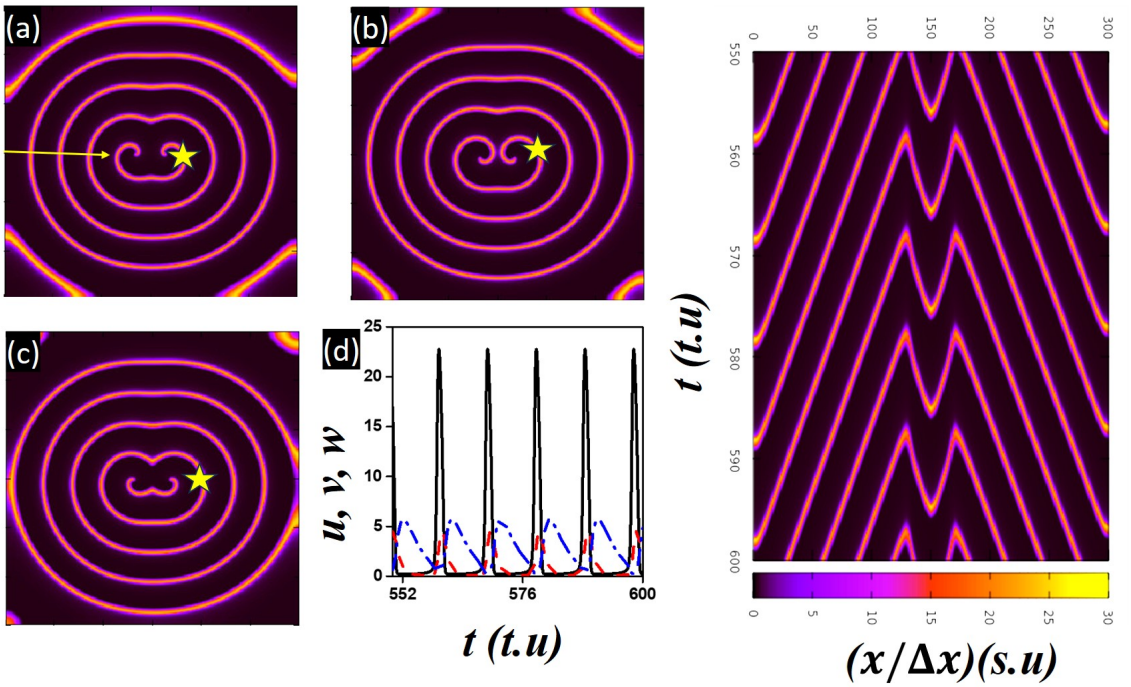

Figure 3.1: Stable spiral. All parameters are same as the base condition. (a)-(c) Snapshots at 552 t.u.,555 t.u., and 558 t.u., respectively. The star marks on the spiral wave-arm show the outwardly movement of the wave. (d) Time variation of the three variables u as solid black curve, v the dashed red curve and w is the dash dotted blue curve (same curve types are used across the images) (e) Time space plot between 550 to 600 t.u. along yellow arrow shown in (a). Color key for the snapshots and timespace plots is depicted between (a) and (b), and is similar across the figures.

3.3 Results

3.3.1 Variation with f

Spirals

In our model, we found sustained oscillations in the range of $0.6 < f < 1.5$, and $0.1 < h < 0.55$. Beyond this zone we get oscillation death, or fixed points. In this range, stable spirals are obtained for $0.6 < f < 1.2$ for $0.28 < h < 0.5$. These spirals were outwardly rotating, meaning that the tip rotates towards its own wave-arm,

and the wave emanated from a single rotation of the spiral moves outward. Fig. 3.1 show the snapshots of one such counter rotating pair of spirals at the base condition. Fig. 3.1(a-c) are snapshots at three instants during a single rotation at intervals of $T/3 = 3.0$ t.u. A color bar shows the variation of the values of variable u, which has been plotted here. Light golden colors, seen in the centre of the spiral wave-arm corresponds to high values of the activator u. Dark colors are areas with low u. A star mark on the spiral wave-arm keeps track of the position of the wave-arm with time, hence depicting the outwardly movement of the wave. The concentrations of the three variables u, v and w oscillate in time at every point in space, and data for one such point $u(150,70)$, which is at an appreciable distance from the spiral tips, is shown in Fig. 3.1(d). The sustainable, stable spiral wave pair has a time period of $T = 9.5$ t.u. and wavelength $\lambda = 11.7$ s.u. that can be easily calculated from the time-series and time-space plot [Fig. 3.1(d) and (e)].

Core defect and Oscillation death

We then varied the system parameter f. Reducing the value of f, while keeping all other values same as the base condition, continues to give us stable spirals, until $f = 0.62$, when we observe core defect, leading to spiral breakup, and finally turbulence. Fig. 3.2(a) shows the generation of the defects during the initial stage of the spiral formation, which leads to a chaotic stage with multiple fragments of spiral waves [Fig. 3.2(b)], which is reminiscent of atrial fibrillation in the cardiac system. The time space plot also shows the break-up of the spiral wave-pair after 30 t.u. into the initiation.

Further lowering of the $f-$ value leads to oscillation death, as seen in Fig. 3.3.

Now, increasing the value of f from the base condition, we obtain drifting spirals at around 1.0, and then target patterns beyond that.

More phenomenon could be obtained by varying the values of ϵ and $\epsilon^{'}$. A variation of the diffusion coefficients to $D_u = 0.9$, $D_v = 0.05$, $D_w = 0.01$ did not change the variation in the nature of the wave-behavior. Only the values of f for which the wave nature transformed from one kind to another, shifted by a meagre amount. However,

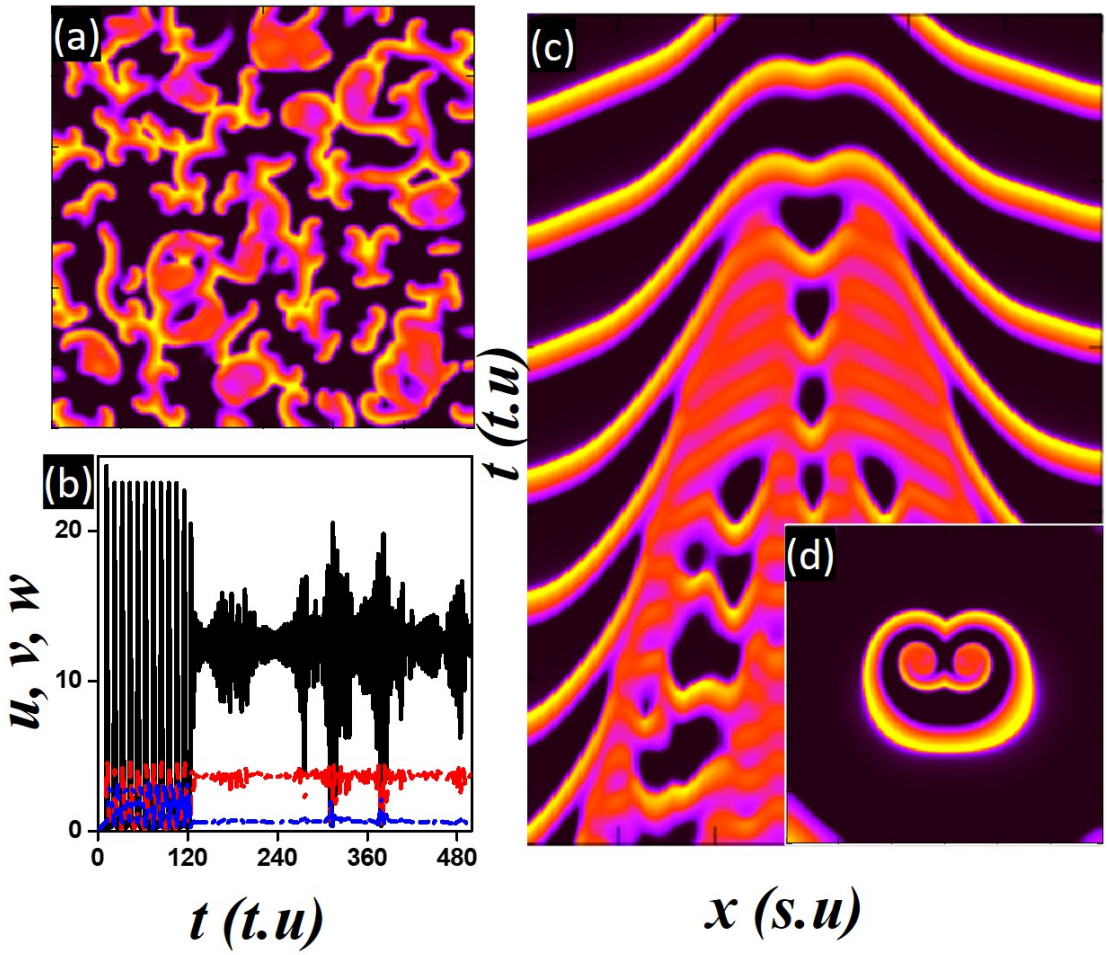

Figure 3.2: Core-defect leading to spiral wave-break. All parameters are same as the base condition, except $f = 0.57$. (a) Snapshot at 32 t.u., (b) snapshot at 500 t.u., (c) time space plot between 30 to 80 t.u.

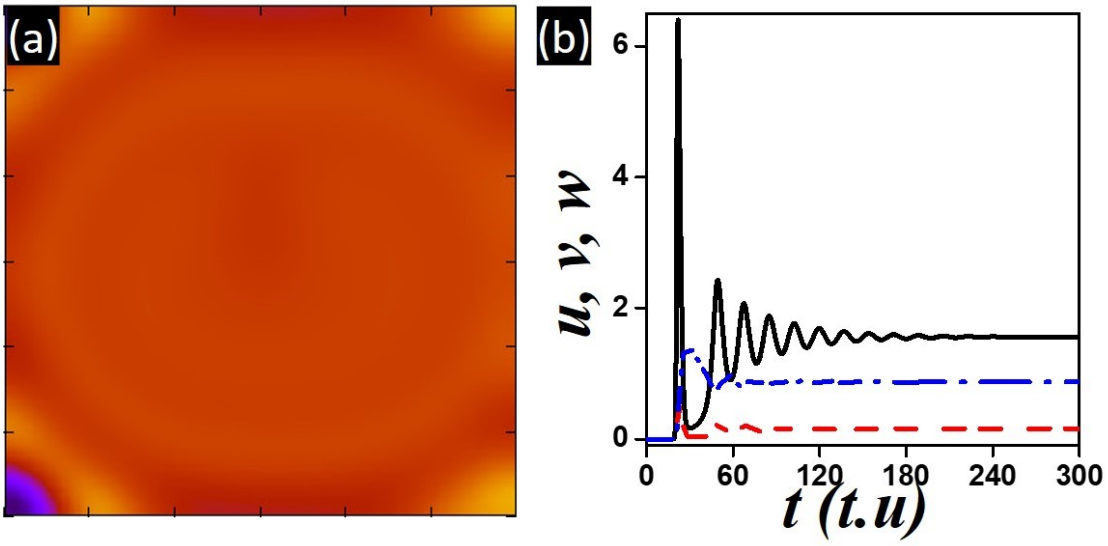

Figure 3.3: Oscillation death. (a) Snapshot at 432 t.u., (b) time-series of the three variables showing the decay of oscillation. $f = 0.55$, all other parameters same as the base condition. This oscillation death is also observed with lowering h for f=0.9.

we wanted to see if the change in the values of h had any effect on the wave nature.

3.3.2 Effect of hydrogen ion concentration

Earlier studies on the BZ system and the Oregonator model had shown that changing hydrogen ion concentration had a major effect on the excitability of the system, and hence modified the wave nature [46]. However, in those studies, the effect of the H^+-ion concentration could only be considered implicitly as a modification of the system parameter, ϵ, or an added acidity factor [52]. Our modified Oregonator model enables us to explicitly vary the initial hydrogen ion concentration to predict the effect of the same on the nature of the system.

In order to explore the effect of h, we start with the base condition, and vary the value of h. While increasing the value of h upto 0.55, stable spirals are obtained, beyond which the system has no solution. Decreasing the value of h however yields interesting results.

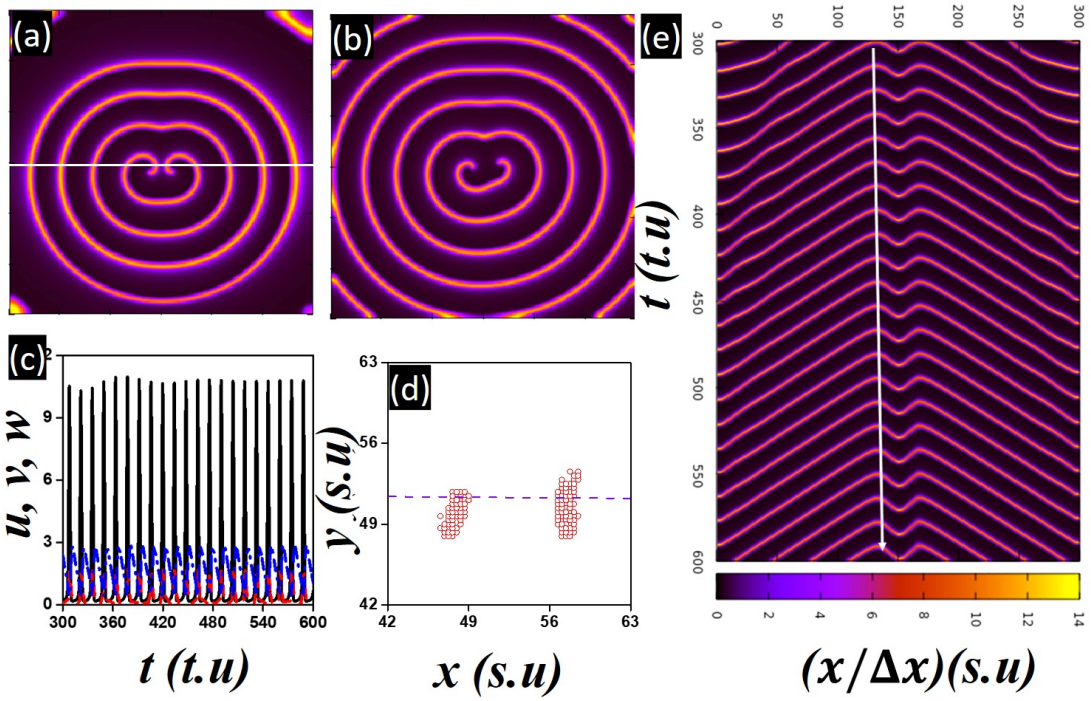

Figure 3.4: Drifting spirals. Snapshots at (a) 360 t.u. and (b) 900 t.u. (c) Time series (d) is tip trajectory and (e) time space plot (along white line in panel (a))for the duration of 300 t.u. − 600 t.u. $h = 0.22$, all other parameters same as the base condition.

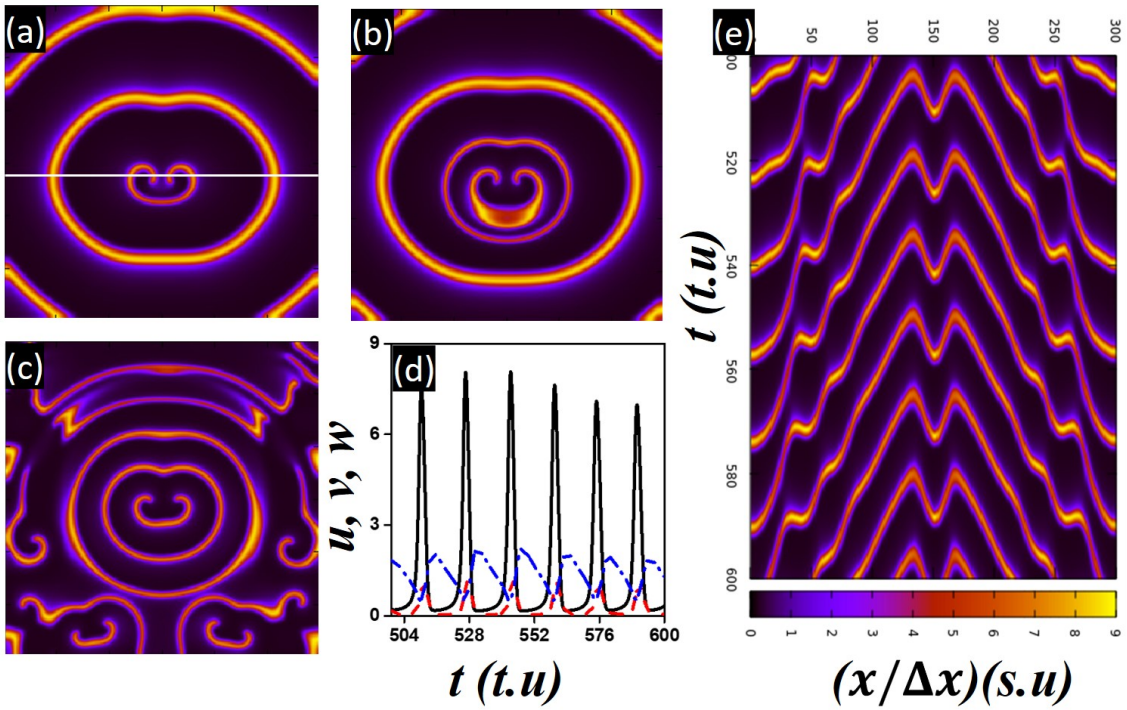

Figure 3.5: Spiral breakup. Snapshots at (a) 72 t.u., (b) 180 t.u., and (b) 612 t.u. (d) Time series of the variables, showing envelope kind of variation of the oscillation-maxima. (e) Time space plot for the duration of 500 t.u. – 600 t.u. All parameters same as the base condition, except h which is equal to 0.18.

As h is decreased below 0.3, the spiral starts to get unstable. At $h = 0.22$, one of the spiral tips become anisotropic, and starts drifting away from its initial position. The same can be observed in Fig. 3.4. The white arrow in the time-space plot points to the time when anisotropy seeps into the system. The tip trajectory also explains the drifting nature of the unstable spiral.

At lower h values, one of the drifting tip starts to undergo wave-break, leading to a wide-spread spiral break. Fig. 3.5 shows wavebreak for $h = 0.18$. Although the final picture [3.5(c)] may seem to have similarities with that of the core defect leading to wavebreak [Fig. 3.2(b)], the propagation of the wave-break and the nature of the time-space plots differ much. Here, the spiral starts to break at one site, and

that propagates, whereas in the former case, the perturbations began as defects near the spiral cores.

At $h \leq 0.2$, there is no more formation of spiral. The straight plane wave that we initiate does curl up at its ends, but before they turn further to form a pair of counter-rotating spirals, the two ends touch and form target waves. The snapshot, oscillations and time-space plot of target waves for $h = 0.16$ can be seen in Fig. 3.6. Time period calculated from Fig. 3.6(b) and (c) give values around 18.3 t.u.

Before we reach oscillation death, at values of $h < 0.1$, it passes through a fleeting region of chaotic oscillations, that is distinct from the spiral breakup regions (similar to Fig. 3.7). This chaotic regime has also been witnessed for some more pairs of (f, h) values. (depicted by red open circles in Fig. 3.8). This is different from both kinds of spiral wave-break, as there are no singularities present in the system at any given time. However, the low-amplitude oscillations are irregular and chaotic, as seen in Fig. 3.7.

We varied f and h systematically, over the entire range of values, where the system undergoes sustainable oscillations, while keeping all other parameter values constant. We were able to generate the phase-diagram Fig. 3.8(a), where all seven kinds of phenomena discussed above were observed.

We also varied the diffusion coefficients to consider a fast diffusing activator, and slow inhibitor. Such kind of modifications in diffusion values in computational studies of FHN model has been previously carried out [50], to explore spiral breakup in excitable systems. A parallel analysis of our modified model, considering that the activator u diffuses 20 times faster than the inhibitor v (instead of $\sim$1.7 times as is dictated by its molecular formula), we generate a phase diagram of wave behaviors, as depicted in Fig. 3.8(b). We can see a similar Hopf bifurcation along the horizontal or vertical directions, as we vary h or f. A comparison of Fig. 3.8(a) and (b) shows that the exact values at which the wave nature changes has been shifted. Also, the occurrence of the spiral breakup leading to turbulent states are more frequent in the latter case of fast activator and slow inhibitor, in keeping with earlier studies. However, we did not come across any new phenomenon by modifying the diffusion coefficients in this way. Hence, our modified model is robust enough to generate the

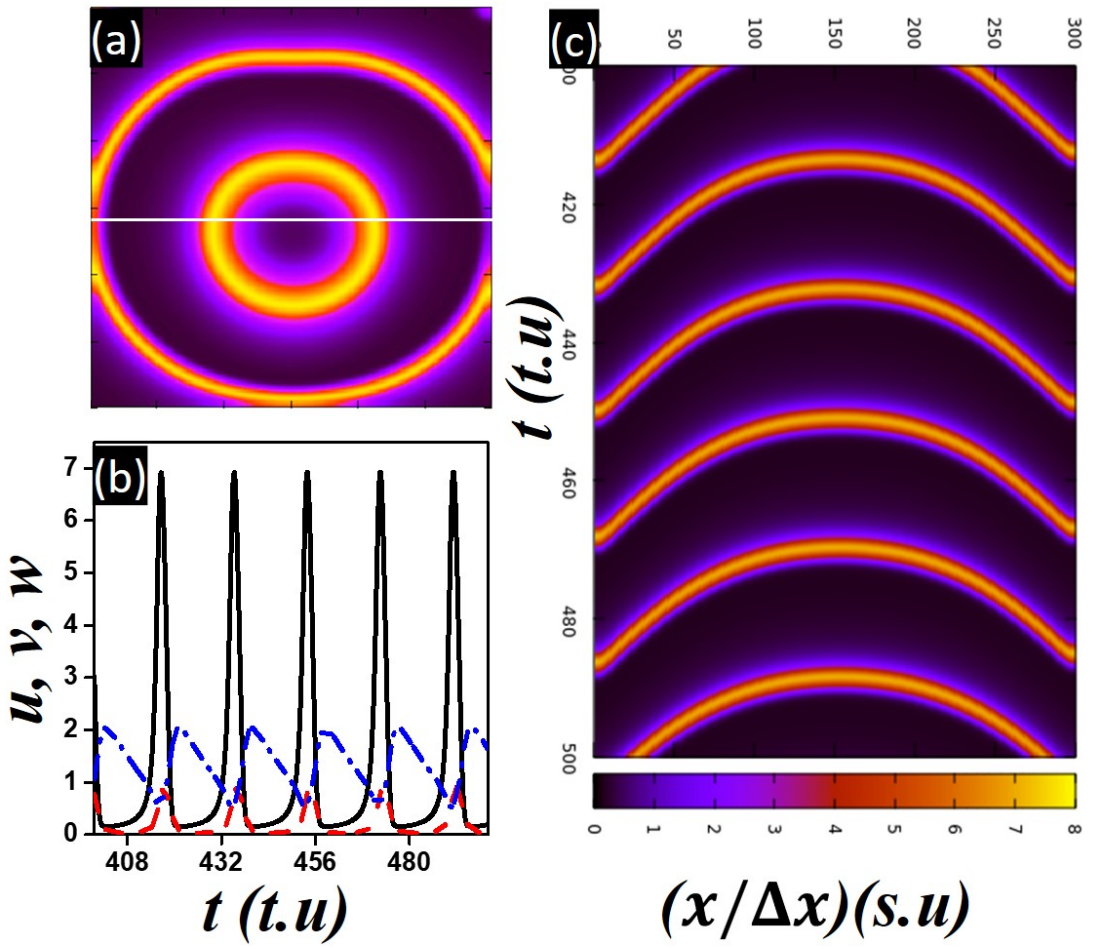

Figure 3.6: Target patterns. Snapshot at (a) 360 t.u., (b) time series showing oscillations, and (c) Time space plot for the duration of 400 t.u. − 500 t.u. $h = 0.16$, while all other parameters are same as the base condition.

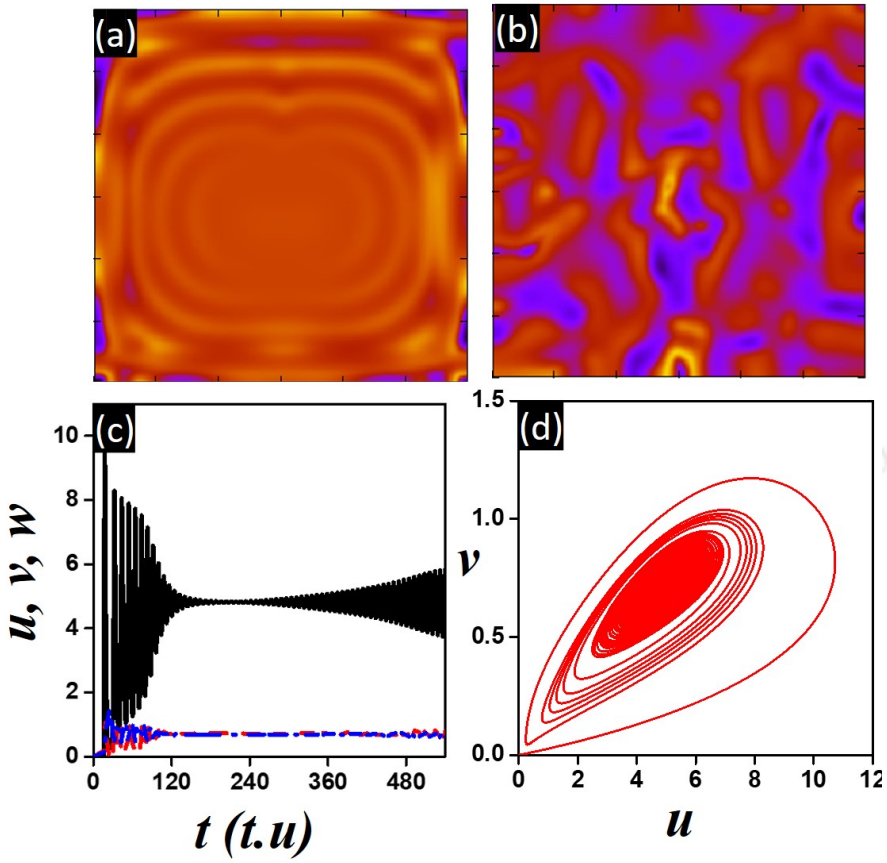

Figure 3.7: Low-amplitude chaotic oscillations. Snapshots at (a) 180 t.u. and (b) 900 t.u.; (c) time series and (d) phase diagram of the propagating variables for $f = 0.7$ and $h = 0.15$, and all other parameters same as the base condition.

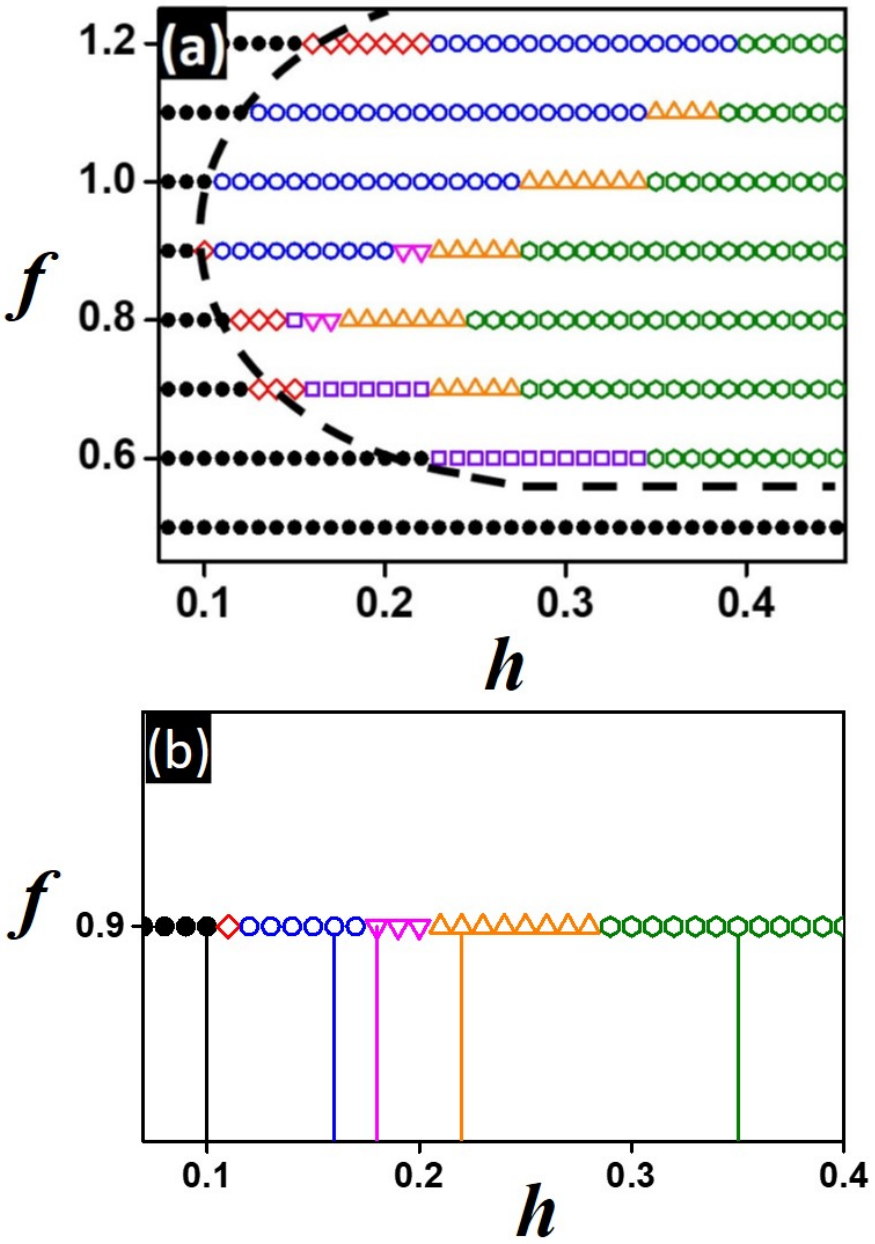

Figure 3.8: Variation in wave property with f and h variation. Black full circles depict oscillation death, while blue open circles designate Target pattern. Red diamonds stand for chaotic oscillations and magenta upturned triangles denote spiral break-up.The orange triangles are for drifting spirals while olive hexagons are the regular stable spiral waves. The violet squares are for the turbulent dynamics emanating from core defect. (a) for $D_u = 0.3$, $D_v = 0.17$, $D_w = 0.34$, (Ratio of D_u:D_v:D_w is kept same) $\Delta t = 0.015$ t.u. and $\Delta x = 0.45$ s.u. (b) for the figures used in this chapter for different phenomena described above. Vertical lines are representing the data points for corresponding phenomena described in details from Fig. 3.1 to 3.7, here, $D_u = 0.1$, $D_v = 0.057$, $D_w = 0.11$, $\Delta t = 0.012$ t.u. and $\Delta x = 0.35$ s.u. $\epsilon = 0.035$, $\epsilon' = 0.008$, and $q = 0.01$ are kept constant.

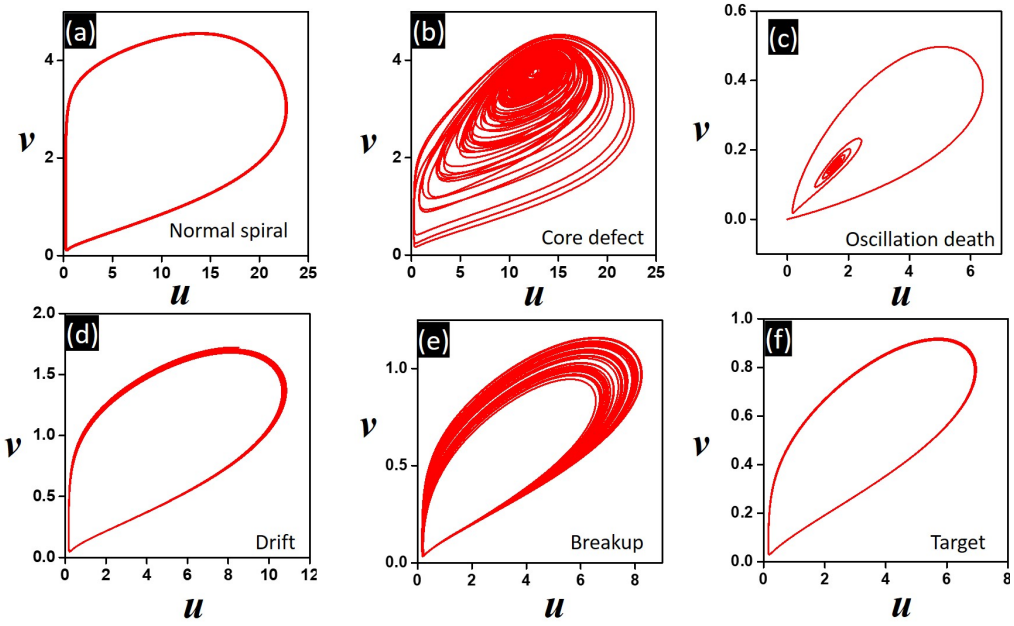

Figure 3.9: Phase diagrams for varied wave nature. (a)limit cycle for sustainable steady spirals, (b) core defect leading to turbulence, (c) Fixed points in oscillation death , (d) drifting spirals, (e) spiral breakup, and finally (f) Limit cycle in target patterns.

entire range of excitation waves, considering natural diffusion coefficients.

The Fig. 3.8 can also be called a Bifurcation diagram, as the change in the wave nature with variation of the system parameters are portrayed here. This is supported by the activator-inhibitor (or $u - v$) phase diagrams for every case, as shown in Fig. 3.9. A Hopf bifurcation can be observed when the $f = 0.9$ line passes from fixed points (black closed circles) to limit cycles (blue open circles), as h value increases, in its lower limits. The black curve traced on the figure [Fig. 3.8(a)] shows the zone of Hopf Bifurcation for the system, with increase in hydrogen ion concentration.

3.4 Discussion and Conclusion

In this work, we have proposed a modified version of the Oregonator model, with an explicit hydrogen ion parameter. Starting from the well established FKN mechanism of the BZ, we have developed the model with necessary non-dimenionalization and redefined the parameters in the process. The hydrogen ion concentration was previously incorporated within the rate constants and parameters of the Oregonator model. Our modified Oregonator model allows for an independent treatment of the H^+-ion concentration, and hence enables us to ascertain the possible effects of this ingredient in the recipe of the BZ. It has been observed that the nature of the pattern formation in a spatially extended BZ system, under the influence of diffusion, can vary widely, with changing initial acid concentrations, depicted as h.

We began with a base condition where the system could sustain stable spiral waves. At first we explore the change in the dynamics of the excitation waves, with variation of f. We observed that spirals were formed in the range $0.6 < f < 1.6$; increasing value of f beyond this, yielded no spirals. Decreasing the $f-$ value below 0.6 first gave core defect leading to turbulence ($f = 0.57$), before quickly transforming into a steady state, signifying oscillation death ($f \leq 0.55$). Next we varied the $h-$value. The trajectory of spiral tips as a function of H^+-ion concentration had been studied in detail in an earlier study [46]. Here, we try to explore the change in the overall nature of the waves. It was seen that with decrease in the value of h, the oscillations and the entire dynamics of the system slows down. This is reflected in the increase of the time period of oscillations, and a corresponding decrease in the amplitude. For the target patterns where the values of h are quite low ($h = 0.16$), the time period is around 18.5 t.u., which is almost twice than that of the stable spiral formed in the base condition ($h = 0.3$), when all other parameters are held constant. Such a trend in time periods was also observed in earlier experiments with the BZ, where decrease in time period of spirals was observed by increasing the H^+-ion concentration [46]. In the same study, while the numerical solution of the reaction-diffusion process did not yield any turbulent state, simulations with the original two variable Oregonator model (sans diffusion) had predicted that spiral

waves will give way to random oscillations, followed by stable oscillations without spiral formation, with increase in the excitability parameter ϵ. This ϵ is considered inversely proportional to $[H^+]$, so the trend we have observed in our wave characteristics is supportive of the earlier findings too. However, with the two-variable model of the Oregonator, the spatial patterns were not well explained in the predicted range of ϵ values depicting "random oscillations". In our current model, by explicitly considering the H^+-ion concentration, our simulations enable us to observe the spatiotemporal dynamics of the concentration waves, as h is varied. With decreasing $h-$value, we have observed stable spirals ($h = 0.3$) giving way to spiral breakup with chaotic oscillations ($h = 0.22$) leading to turbulence. The system then generates target patterns with stable oscillations ($h = 0.16$, stable limit cycle), and finally oscillation death ($h < 0.1$, stable fixed points), as $h-$value is further lowered, reminiscent of the Hopf bifurcation diagram with increase in excitability parameter ϵ, in the two-variable Oregonator model.

Spiral breakup was observed in some earlier numerical studies of the generic Barkley model or the modified versions of the FHN model [53], mostly with some modifications, such as delay in the production of inhibitor [50], external or internal gradients (like concentration, electric current) [54, 55], or multiple reaction layers [51]. The current work is different in the sense that it uses a model derived from the original FKN mechanism, and all dynamical behavior can be obtained by only changing the parameters. Here we explored mainly the role of parameter f and the effect of hydrogen ion concentration, h, on the system dynamics. Unlike the previous studies, we did not neglect the diffusion of the inhibitors, viz. v or Fe^{3+} and w or Br^-.

In experiments with the BZ, the effect of substrate concentration, $[BrO_3^-]$, [MA] and $[H_2SO_4]$, has been carried out in earlier studies [46, 56]. The change in initial substrate concentration of these three species does change the excitability of the medium. However, the excitability depends on various factors other than hydrogen. So, in order to observe the sole effect of the hydrogen ion concentration, our modification of the Oregonator model was required. The current three variable model was able to support the formation of stable spirals, target patterns, and finally os-

cillation death. It was also successful in demonstrating other elusive phenomena like spiral breakup and defect-mediated wave-break, through a systematic parametric investigation of the model. Further study can be carried out to observe changes in system dynamics with changes in ϵ and $q-$ values. A reduced two variable model of our modified Oregonator is also successful in sustaining spiral waves, and can be explored further as a more simplified model. Again, for more involved calculations, one may carry out numerical studies with all the four variables, including the fast-diffusing $h-$variable. In case there is a local variation in hydrogen ion concentration or diffusion, the four-variable model will enable one to study the same in intricate details.

Summary

- In this chapter we introduced a modified Oregonator model dervied from the FKN mechanism.
- Spiral wave properties are observed with explicit hydrogen ion concentration change.
- Phenomena like spiral break-up is observed by varying the hydrogen ion concentration in different ranges of diffusion.
- Oscillation death, target pattern, spiral drift are other phenomena observed with our model.
- This model can be used to explain the effect of a gradient of hydrogen ions on the spiral wave dynamics in a BZ reaction, as will be described in the next chapter.

Chapter 4

Control and dynamics: Drift of spiral waves in presence of a mild gradient

4.1 Introduction

Certain chemical and biological systems are able to sustain excitation waves like target waves, two dimensional (2D) spiral waves and three-dimensional (3D) scroll waves. These waves are selfsustained and are ruled by laws of curvature dynamics [57]. A concave wavefront is faster than a plane one, and hence, once a spiral is formed in the media, its frequency will surpass those of any regular plane waves in the system [58]. This is why when such rotating waves are created in the cardiac system, it becomes an independent pace maker in the heart, leading to tachycardia, or faster heart beats. A further break-up of spiral and scroll waves leading to the formation of many such rotors will result in lethal conditions of atrial and ventricular fibrillation, that can reflect as cardiac arrest [59]. Hence, the study and control of these waves is of paramount importance to physicians and scientists alike. However, it has always been challenging to control the complex spatiotemporal dynamics appearing in such excitable media. Sudden cardiac arrest is often treated with a defibrillator that

involves the administering of strong, fast electric shocks. While this may remove the unwanted electrical rotors from the heart, it may sow the seeds of future cardiac arrest. So scientists are on the lookout for milder techniques to control such waves of electrical activity in the heart [60, 19].

Other than the cardiac system, biological systems such as the social ameoba, Dictyostelium discoidium [61], neuronal [62], uterine [63] and retinal [64] tissues, and some other nonlinear chemical systems like the Belousov-Zhabotinsky reaction system [65] and the catalytic oxidation of CO on Pt [66], also sustain spiral and scroll waves. The BZ system, which constitutes the oxidation of an organic acid by sodium bromate, in the presence of sulphuric acid and a metal catalyst with variable oxidation states, is a well known laboratory model for the study of these excitation waves [67]. Its chemical kinetics, established by Field, Koros, and Noyes, known as the FKN mechanism, has been able to explain the oscillatory behavior of the system [29]. Considering the most important steps in the kinetics of the complicated reaction, the group from Oregon established the mathematical Oregonator model for the BZ system [68]. Considering a diffusive coupled-process to emulate an unstirred layer of the BZ, the Oregonator model was able to show the formation of excitation waves, viz. 2D spirals waves and 3D scroll waves [10]. Both the BZ and its mathematical model have been extensively used for the study of the control and dynamics of these spiral and scroll waves [69, 70].

Previous experimental and theoretical studies have shown that different kinds of external and internal perturbation, like light, noise, electrical potential, electromagnetic field, and thermal gradient, can affect the excitability of a reaction diffusion system [71, 72, 73, 74]. This can lead to a change in the dynamics of its sustained excitable waves. Spiral waves drift away from their initial position under the influence of electrical and thermal gradients [20, 21, 22], while scroll waves align themselves perpendicular to the direction of the gradient [75, 76]. A vertical CO2 gradient in a closed container of BZ reaction has shown to induce a twist in 3D-scroll waves [77], while spiral rotors drifted under the influence of other high frequency excitation waves [78].

In this work, we try to control the dynamics of a spiral wave in the BZ reac-

tion system, by applying a concentration gradient of hydrogen ions. Here, we use ion exchange resin beads to produce a concentration gradient of H^+ions in our two-dimensional reaction system. Increasing H^+ion concentration is known to increase the excitability of the BZ-medium. A homogeneous increase in the concentration of sulphuric acid, and hence [H^+], is known to result in a linear increase in the frequency of the spiral, and an exponential decay of the wavelength [79], [80]. Hence, we expected that a gradient of H^+ions would effect the dynamics of the spiral tips in some way. It remained to be seen if the concentration gradient acted like the external gradients that had already been studied, or the effect was somewhat different. Compared to the strong external gradients used earlier to control spiral and scroll waves, like electric fields and thermal gradients, the concentration gradient applied in our study is much weaker and can be internally applied within the system. We find that our spiral drifts under the influence of a gradient of hydrogen ions. If the spiral wave pair is placed along the gradient, resulting in the two tips experiencing different strengths of the gradient, the spiral tips move in different directions. The amount of drift depends upon the strength of the gradient and the position of the spiral. The usual form of the Oregonator model cannot be used to precisely describe our experimental system. Hence, we use a modified kinetic model, that we derive from the FKN mechanism. The numerical simulations carried out on this modified Oregonator model corroborates well our experimental results.

4.2 Experimental methods

We carried out experiments using the BZ reaction system. The reaction mixture was composed of a solution of 0.04 M sodium bromate, 0.04 M malonic acid, 0.2 M sulphuric acid, 0.6 mM ferroin indicator, and agarose (0.8 wt/vol %), in millipore water. The mixture was heated upto the melting temperature of the gel, after which it was allowed to cool for about 6 minutes with continuous stirring. Then it was poured into a Petri dish so as to form a layer of 3 mm height. The gel matrix was used in order to avoid convection. A circular wave was generated dipping the tip of a silver wire for a few seconds at the centre of the dish. This wave was then

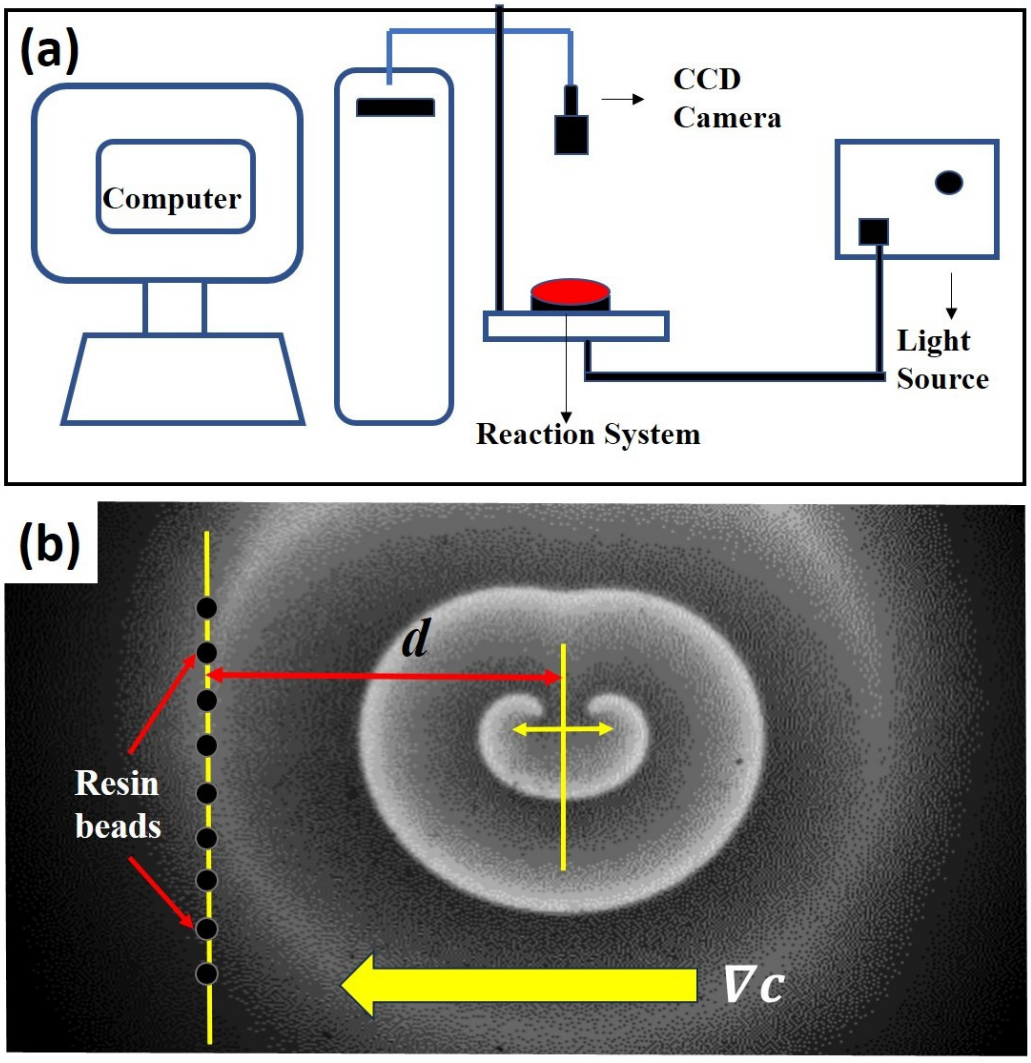

Figure 4.1: Experimental set up: (a) describes a full set-up of our experimental system, and (b) illustrates the initial snapshot of a typical experiment, in the presence of a concentration gradient introduced in the form of a column of ion-exchange resin beads (black circles on the left). Area of the snapshot is 6.40 cm $\times$ 3.75 cm and d is the distance between the column of beads and the center of the line joining the spiral tips. The direction of concentration gradient (∇c) is shown by an arrow.

allowed to expand before it was cleaved manually, to form a pair of counter-rotating spiral waves. The reaction system was monitored with a charged coupled device (CCD) camera (mvBlueFOX 220a) through a blue filter, while it was illuminated from below with a diffused white light. A schematic diagram of the set-up has been given in Fig. 4.1(a). The images were recorded onto a personal computer at an interval of 2 seconds. The data was analysed with inhouse MATLAB codes. All the experiments were performed at room temperature (22±1 °C).

To study the effect of a concentration gradient, we introduced hydrogen exchange resin beads, Amberlyst 15 hydrogen form, into the system. This is expected to act as a source of H^+- ions. A typical experiment is shown Fig. 4.1(b). After the initiation of the spiral pair, we allowed it to rotate atleast three times before introducing the resin beads, in the form of a straight line, thus creating a gradient of hydrogen ions, that decreases as we move away from the column. All the beads were kept equidistant from each other within a length (column height) of 3.0 cm. The distance (d) between the line joining the tips of the spirals (before introduction of the beads) and the column of beads was varied to change the gradient strength experienced by the spiral pair.

4.3 Experimental results

Ion exchange resins appear as solid, insoluble beads, which contain weakly bound ions. They are capable of exchanging these ions when they are in contact with other solutions. Normally, ion exchange resins consist of a matrix of cross-linked polymers with uniformly distributed ion active sites. In our case, we used a cation exchange resin (Amberlyst 15 hydrogen form), which means its matrix is negatively charged and capable of losing or exchanging positive ions (hydrogen ions). In our reaction system, the cations present are Na^+ and $Fe^{2+/3+}$. Soaking the beads overnight in a solution of the Ferroin catalyst did not change their color. We decanted the liquid solution and carried out UVspectrophotometric analysis of the same (fig. 4.2). There was no change in absorption intensity, which proves that neither did the Ferroin bind to the resin, nor was the H^+ion exchanged by the $Fe^{2+/3+}$ of the catalyst.

Our column of resin beads on one side of the spiral would create a gradient of hydrogen ion concentration in the medium. Increasing the number of resin beads would also increase the strength of the gradient.

Fig. 4.3(a and b) show the snapshots from one of our experiments. A visual comparison of the initial (Fig. 4.3(a)) and final (Fig. 4.3(b))snapshots clearly shows the drift of the tips. We trace the spiral tips with time and see that the left tip moves upward while the right tip moves downward (Fig. 4.3(c)). It is notable that the distance separating the two tips also increases with time. Here, one of the tips starts rotating a little faster than its counterpart, leading to an asymmetric meeting of the spiral tips as is seen in Fig. 4.3(b) (area encircled in red). This can also be verified by generating the time-space plot, and calculating the time periods of the two tips at a later stage of the experiment. The time space plot (Fig. 4.3(d)) is constructed from the cross section of the snapshots of the experiments along the yellow line shown in Fig. 4.3(a). It spans a time interval of 32 min. We see that the left spiral has a time period of 380 s, while for the right one it is 390 s. So the spiral tip nearer to the beads is rotating slightly faster than its counterpart.

To get a quantitative measure of the drift of the spirals we calculated the distances traveled by the tips for 120 minutes after addition of the resin beads. We calculate the final displacement of the tip from its initial position as the path length, L and the actual distance covered by the tip at every instant along its hypocycloid trajectory 29, as the traversed distance s. We report here the L and svalues for the tip close to the column of resin beads, the left tip in our case. As the number of beads (n) is increased, the drift of the tip increases (Figs. 4.4(a) and Fig. 4.4(c)), suggesting a linear dependence of the drift on n. Results for nine experiments with varying d values show that the trend is same for any separation distance. Hence, more the number of beads, more is the gradient strength. Figs. 3b and 3d depict the change in path length (L) and traversed length (s) as functions of d. As the initial separation of the resin beads from the center of the tips increases, the drift of the tip decreases. This means that the net effect of the gradient applied due to a fixed number of beads (n) on the spiral tip decreases, as we move it away from the resin column. When n = 4, the decreasing trend of s is no longer linear (Fig. 3d), may be because the

gradient strength is a bit weak, and increasing distance renders it even weaker. This is also reflected in the path length (L) for higher d values

Fig. 4.5 show a comparison between left and right tip. The path length, L and the traverse length, s travelled by both the tip is measured with increasing gradient strenght (increasing n) for d= 1.5 cm is shown in Fig. 4.5(a and c). Both show that the right tip travels more than the left one, and s, and L increases with gradient strength. Fig. 4.5(b and d) depicts the effect of separation distance, d for n=6. A nonlinear decrease of the travelled distance (s and L), occured with increment of the separation.

4.4 Model

The BZ-system is traditionally studied by the Oregonator model which is derived from the FKN (Field Koros Noyes) mechanism [29] of the reaction. The Oregonator model is a three-variable system, that is often simplified to a two-variable activator inhibitor model, where bromous acid ($HBrO_2$) is the activator, u, and the oxidized form of the catalyst,(Fe^{3+}) is the inhibitor, v [40].

$$\frac{\partial u}{\partial t} = \frac{1}{\varepsilon}\left(u(1-u) - \frac{fv(u-q)}{(q+u)}\right) \tag{4.1}$$

$$\frac{\partial v}{\partial t} = u - v \tag{4.2}$$

However, the hydrogen ion concentration does not appear in either the two- or three-variable models of the Oregonator, as it gets embedded in the kinetic parameters f, q and ϵ. In order to model our reaction system with a source of hydrogen ions in a particular area, we had to modify the Oregonator model. In previous chapter we reported in the details of our modification of the Oregonator model to include the explicit concentration of the hydrogen ions. The modified Oregonator is given as a four variable model.

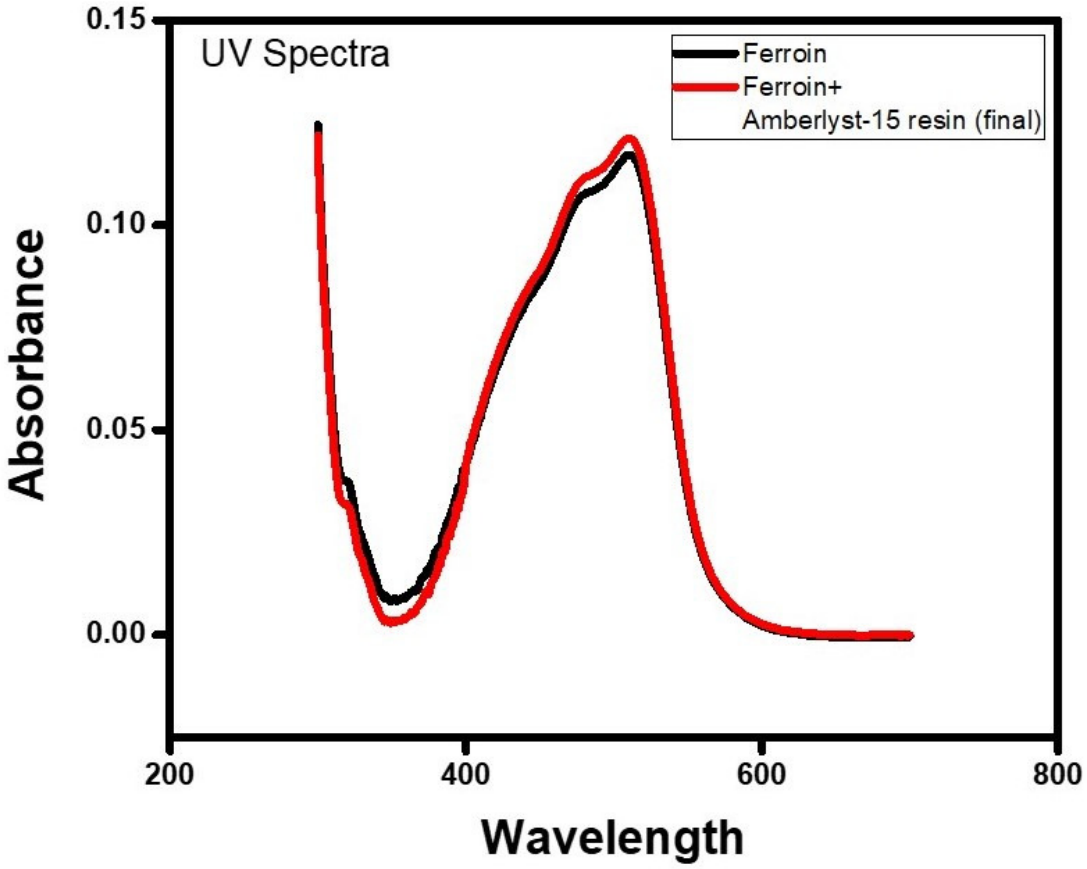

Figure 4.2: Result from a UV spectrometric analysis of only ferroin solution (black) and of resin-soaked ferroin solution showing that the ferroin is not being loaded in the resin matrix.

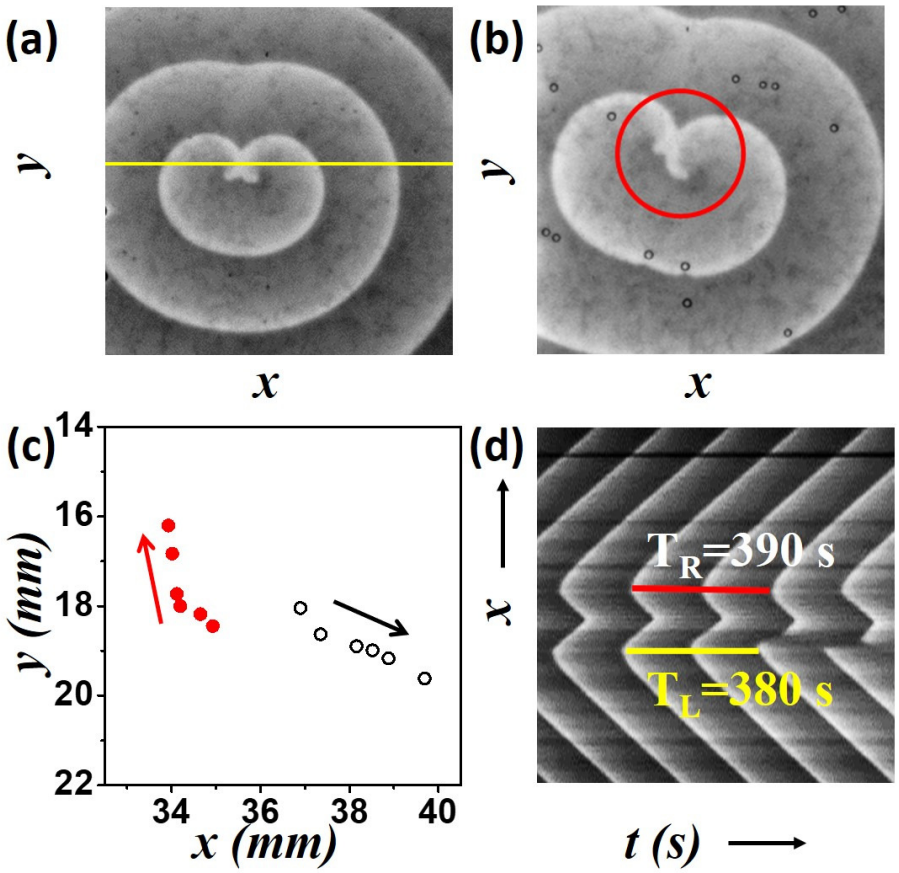

Figure 4.3: Drift of the spiral tips for an experiment, with 6 beads, at a distance of d = 1.0 cm. (a) Initial snapshot of the experiment just after the addition of the resin beads, (b) snapshot 94 min after the addition of beads. Area of the snapshots are 2.15 cm $\times$ 2.15 cm. (c) Position of spiral tips (red, left and black, right) at intervals of 24 min. (d) Timespace plot of the experiment showing time periods of the two tips around 13-18 rotations (78-110 min).

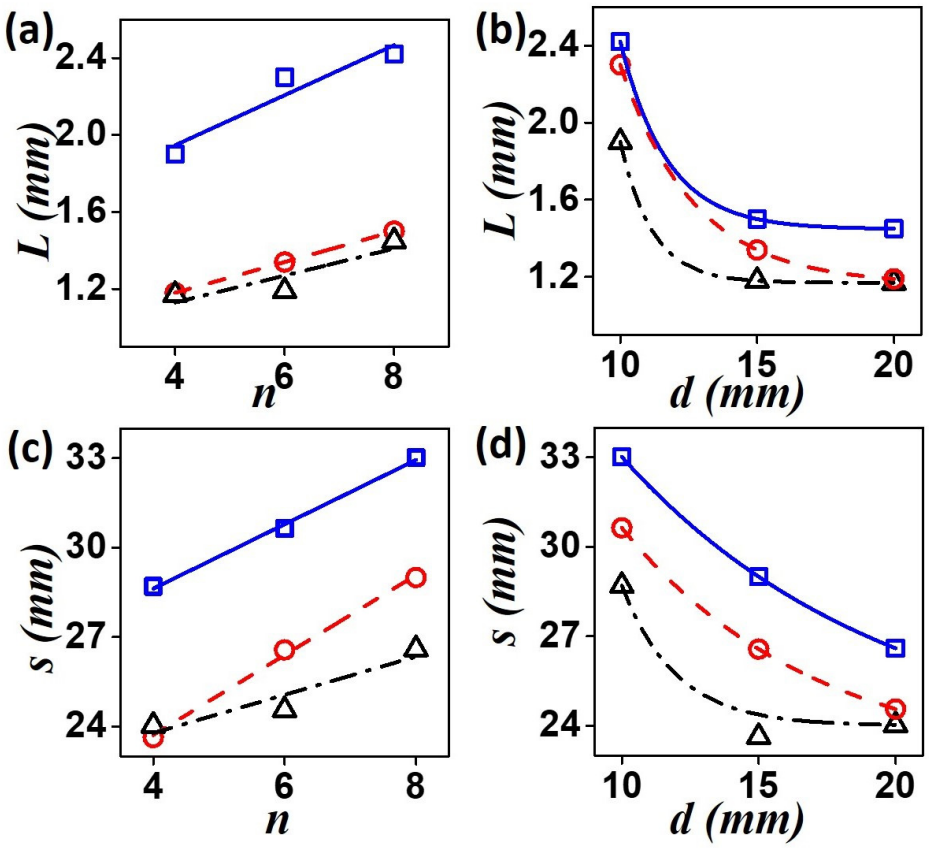

Figure 4.4: Experimental results. (a,b) Path length, L and (c,d) traversed length, s of the left tip during 120 min of the reaction. (a) and (c) Variation of L and s with number of beads, n. Blue squares (solid line) are for $d = 1.0$ cm, red circles (dashed line) are for $d = 1.5$ cm and black triangles (dashed dotted line) represent values for $d = 2.0$ cm. (b) and (d) Trend of changing lengths with increasing distance d. Black triangles (dashed dotted line), red circles (dashed line) and blue squares (solid line)are for n = 4, 6, and 8, respectively.

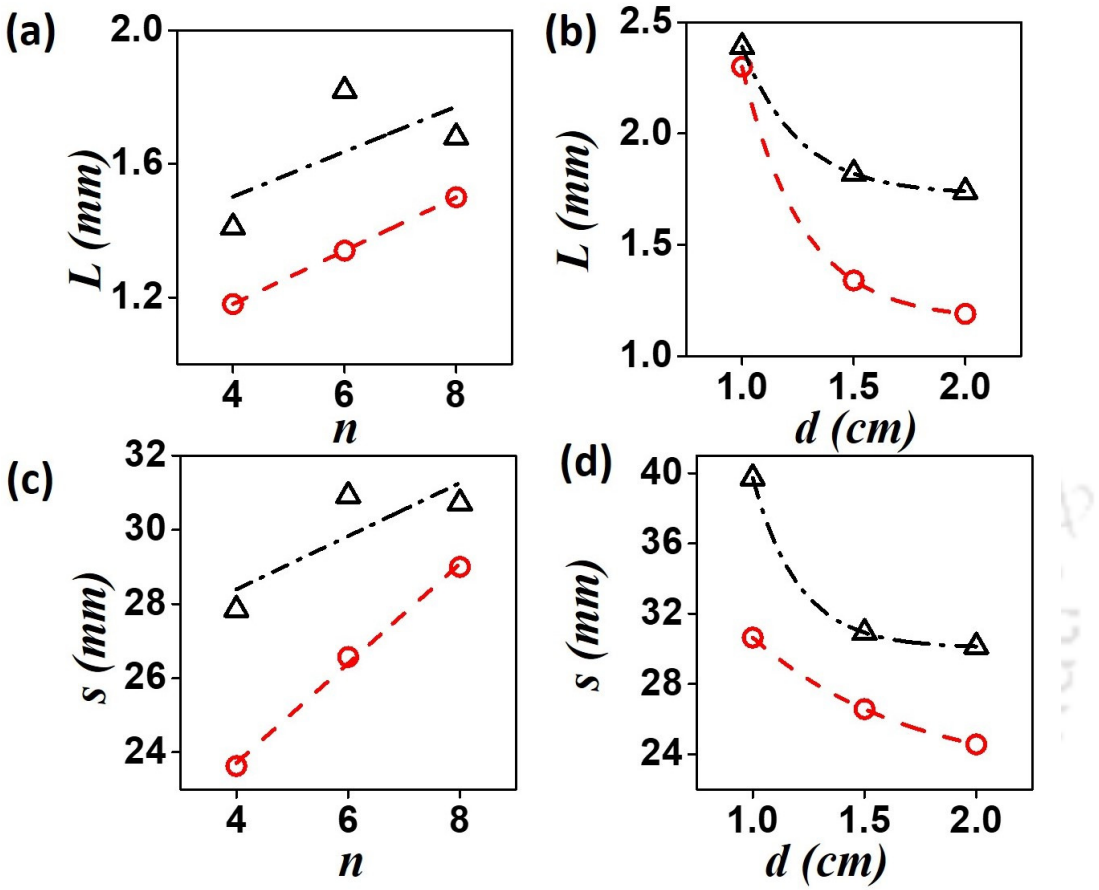

Figure 4.5: Depicts the plot of path length(L) and traverse length(s) with respect to the number of beads and separation distance in our experimental study.(a) Show the path traveled and (c) show the traverse length by left(red) and the right(black) tip with respect to number of resin beads(d=1.5 cm). (b) and (d) show the change in L and s for different separation distances(n=6).

$$\epsilon \frac{du}{dt} = \frac{1}{2}wh^2 - uwh + uh - qu^2 \quad (4.3)$$

$$\frac{dv}{dt} = uh - v \quad (4.4)$$

$$\epsilon' \frac{dw}{dt} = -qwh^2 - 2quwh + 2qfv \quad (4.5)$$

$$\frac{dh}{dt} = -wh^2 - uwh - uh + qu^2 \quad (4.6)$$

where u, is the concentration of the activator $HBrO_2$, and v, that of the inhibitor Fe^{3+}, w is $[Br^-]$, and h is the concentration of hydrogen ions.

As, $\epsilon' << \epsilon$, steady state approximation can be employed on w [40], giving us

$$w = \frac{2fv}{h(h+2u)}$$

Substituting this value of W in the above equations [3-6], we have

$$\epsilon \frac{du}{dt} = fv\frac{h-2u}{h+2u} + u(h-qu) \quad (4.7)$$

$$\frac{dv}{dt} = uh - v \quad (4.8)$$

$$\frac{dh}{dt} = -2fv\frac{h+u}{h+2u} - u(h-qu) \quad (4.9)$$

This can be further simplified by considering that excess h is initially present in the system, so that the hydrogen ion can be considered as a parameter. We thus obtain a two variable model with the following equations

$$\epsilon \frac{du}{dt} = fv\frac{h-2u}{h+2u} + u(h-qu) \quad (4.10)$$

$$\frac{dv}{dt} = uh - v \quad (4.11)$$

In the presence of diffusion, the modified Oregonator model takes the following

form.

$$\epsilon \frac{du}{dt} = fv\frac{h-2u}{h+2u} + u(h-qu) + D_u\nabla^2 u \quad (4.12)$$

$$\frac{dv}{dt} = uh - v + D_v\nabla^2 v \quad (4.13)$$

where D_u and D_v are the diffusion coefficients of u and v respectively.

4.5 Numerical methods

We integrate the equations [4.12-4.13] by discretizing the space over 300 $\times$ 300 grid points (105 s.u. $\times$ 105 s.u.), with the grid spacing kept at 0.35 space units. Euler integration method with time steps of 0.01 time units was employed. The system parameters f=1.0 , q=0.01, ϵ=0.09 are kept constant throughout the simulations. D_U and D_V are taken as 0.7 and 0.3 respectively. The initial value of H is taken as $H_0 = 0.5$. This set of parameter values can sustain spiral waves which undergo rigid rotation. We have maintained no flux boundary conditions for our simulations.

A target wave is initiated by choosing the wave front and back as isoconcentration areas ($u = 0.09$, $v = 0.0$) and ($u = 0.0$, $v = 0.0002$), respectively. We allow the wave to expand and at $t = 3.0$ time units, we cleave it at the middle like we did in our experiments, by setting zero concentration values as ($u = 0.0$, $v = 0.0$).

To create a gradient of hydrogen ions similar to our experiments, we varied H systematically as per the following equation:

$$H(x,t) = H_0 + a(105 - x)^2 + bt \quad (4.14)$$

where, the parameters a and b were varied to emulate the slow release of the H^+-ions from the column of resin beads. For ease of presentation, we express the gradient strength in our results and discussions, in terms of the value calculated at the far left after 1000 time units, $\Delta h = a \times 105^2 + b \times 1000$.

The direction of the gradient and the change in hydrogen ion concentration in space with time can be understood in figure 4.6. It also shows how the gradient

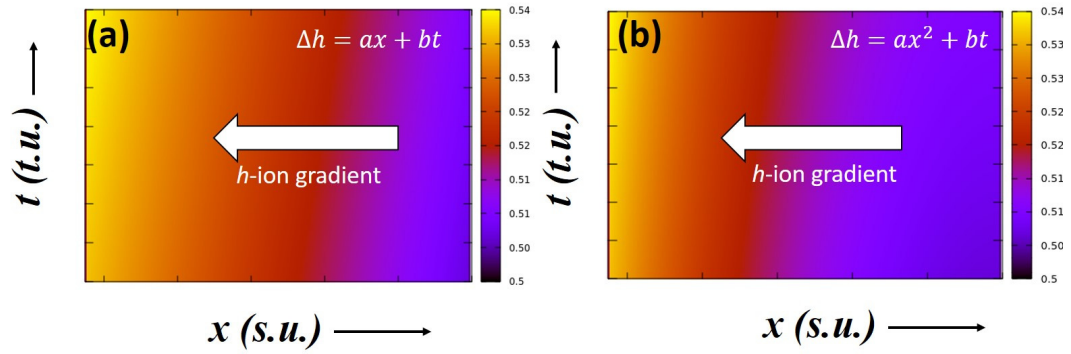

Figure 4.6: Space-Time plot of hydrogen ions. (a) demonstrate the gradient in space with time for a linear gradient. (b) depicts for a nonlinear gradient. White arrow show the direction of the gradient.

works if the variation of H^+-ions in linear fashion as well as in nonlinear mode. Comparison between figure 4.6(a and b) tells us that the achivement of maximum limit of hydrogen ion concentartion is faster in case of linear gradient compared to that of nonlinear variation. We chose the nonlinear one, which replicates our experimental observations.

4.6 Numerical results

We carried out simulations for three different gradient strengths, $\Delta h = 0.04$, 0.06 and 0.08. A visual observation of the experiments revealed a drift of the spiral tips when a gradient in the concentration of H-ions was introduced into the system, which was absent earlier. The snapshots from two cases, one with zero gradient (Fig. 4.7(a and b)) and another with $\Delta h = 0.04$ (Fig. 4.7(c and d)) at two different times are shown in Fig. 4.7. The later image is after over 200 rotations. It clearly shows that, in the presence of the gradient, there is an appreciable drift of both the tips.

By our definition of the concentration gradient [equation (14)], the value of $H(x,t)$ experienced by the two tips are different, the left tip enduring a larger value of $H(x,t)$ at any given time than its right counterpart. This accounts for the faster rotation of the left spiral as compared to the right one, its expanding wave arm causing a greater

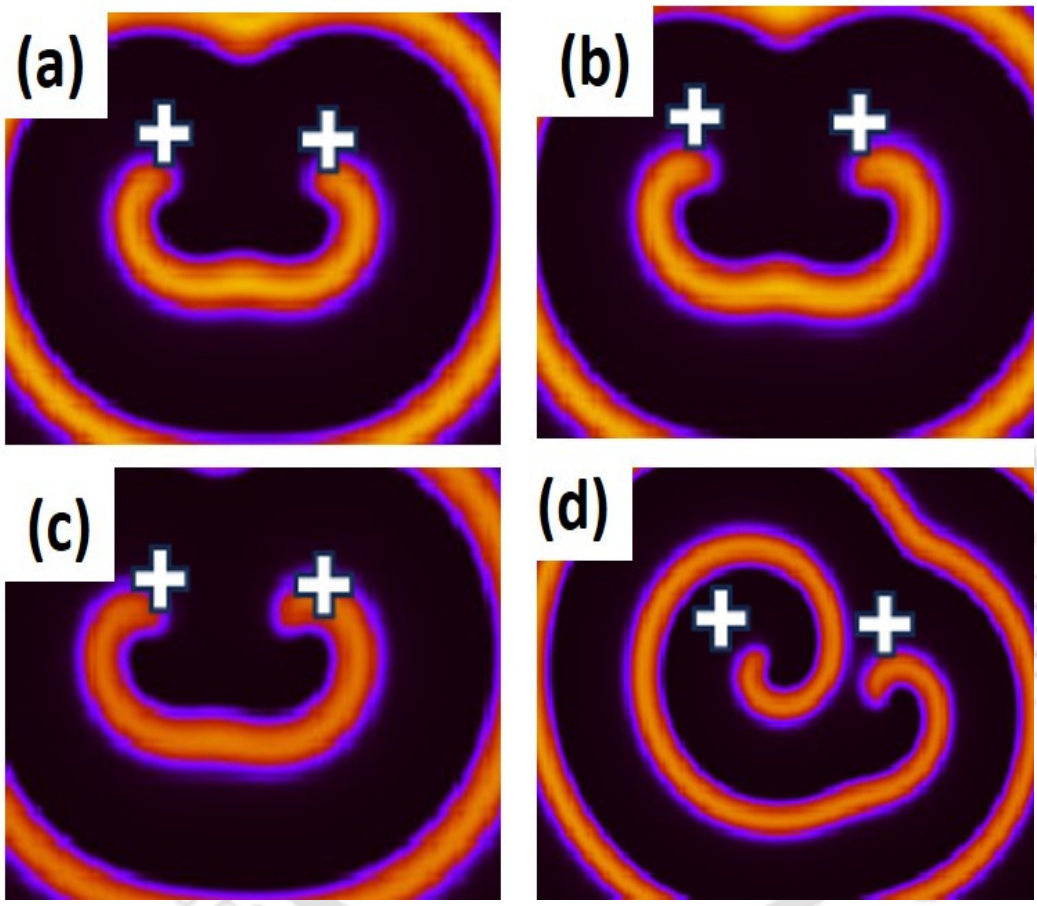

Figure 4.7: Results of numerical simulations. Snapshots showing the difference between two cases (a-b) zero gradient, (c-d) Δh=0.04. (a) and (c) are initial snapshots at 150 t.u. and (b) and (d) are snapshots at 1000 t.u.

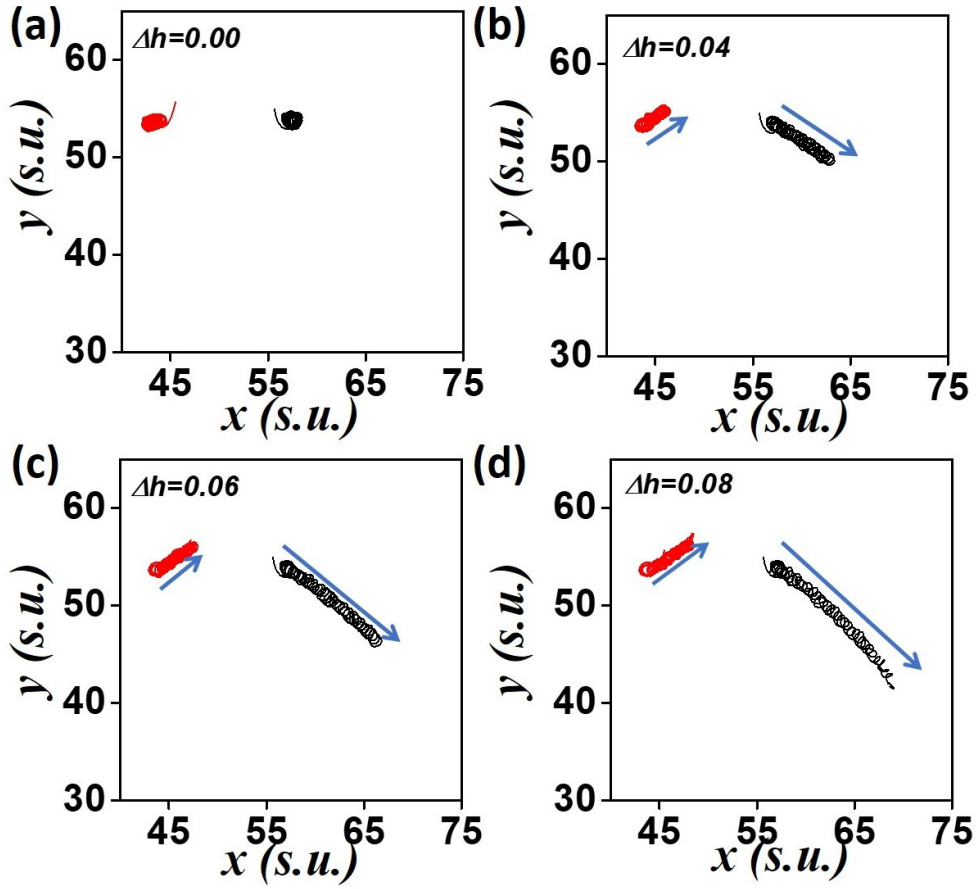

Figure 4.8: Movement of spiral tips under a concentration gradient. Trajectories of the spiral pair for 1000 t.u. at different gradient strengths (a) Δh=0.0 (b) Δh=0.04 (c) Δh=0.06, and (d) Δh=0.08.

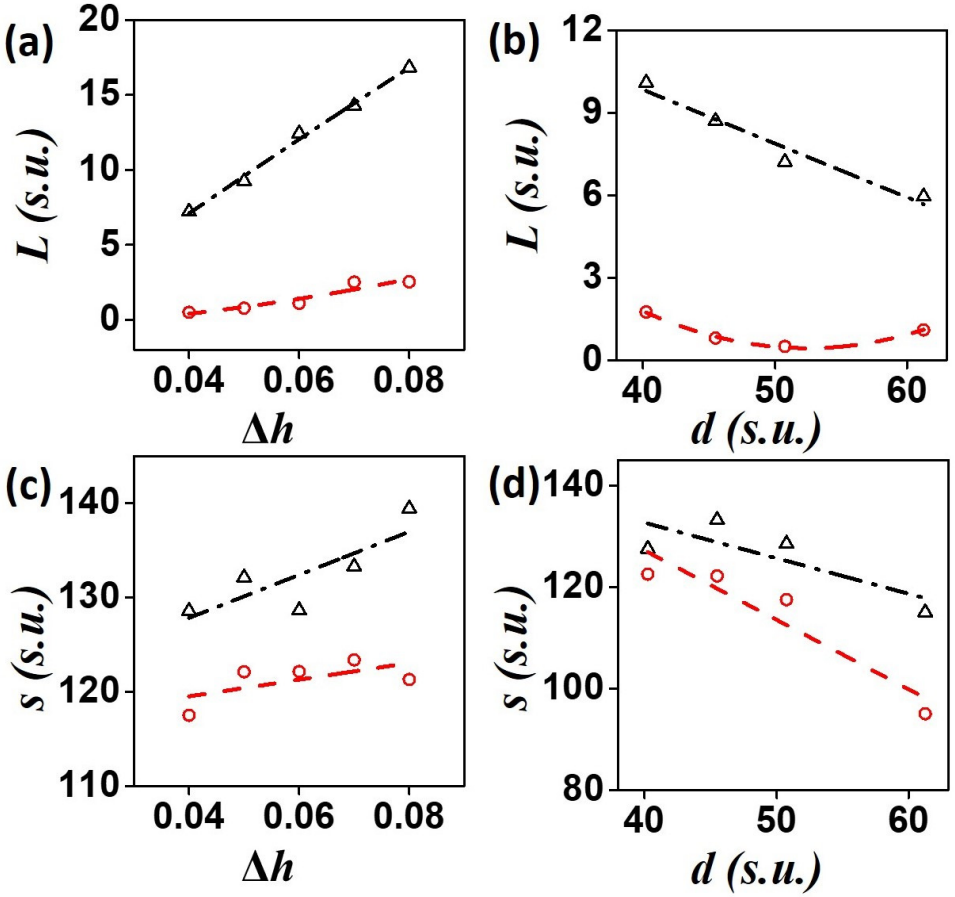

Figure 4.9: Influence of gradient strength on drift of spiral tips. (a) and (c) show the trend of path length, L and traversed length, s on varying values of Δh. (b) and (d) are plots for the L and s with changing spiral position, d. Distances covered at 900 time units by the left tip are depicted as red circles (dashed) that by the right tip as black triangles (dash-dot). In (a) and (c) $d = 50.75$ s.u. and in (b) and (d) $\Delta h = 0.04$.

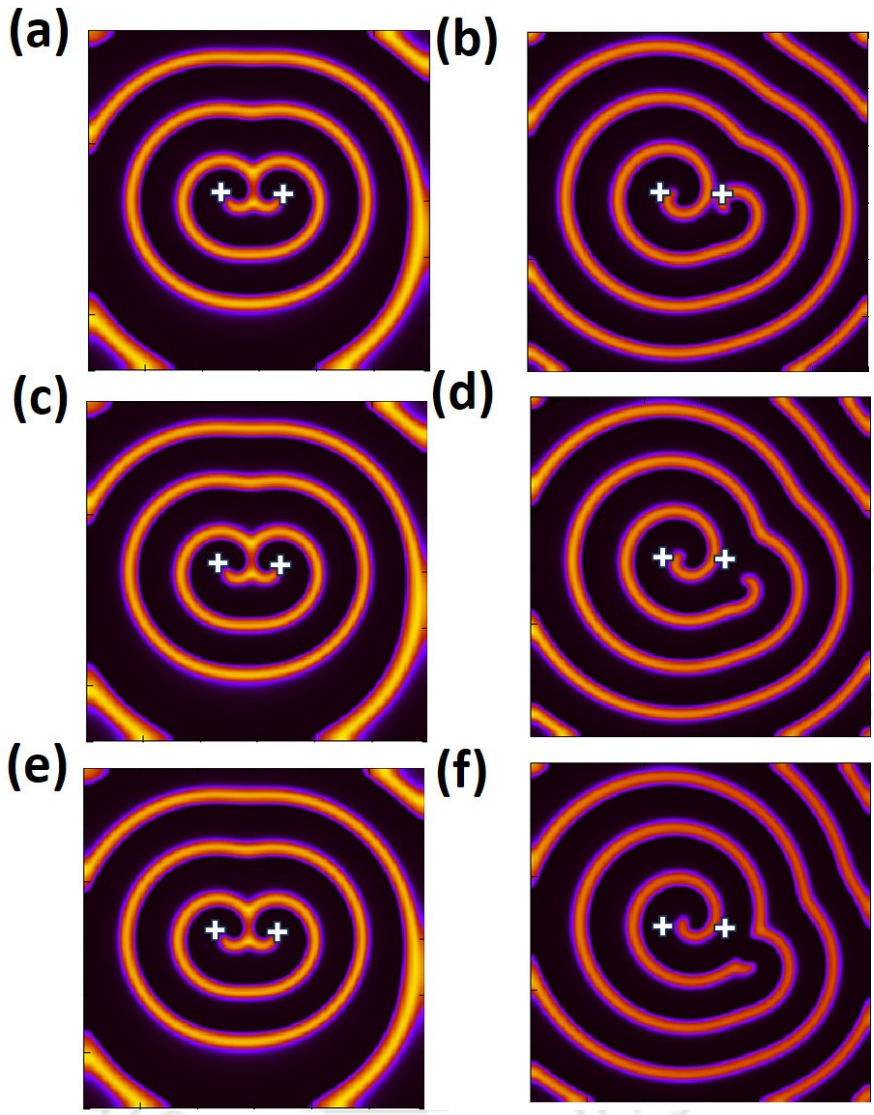

Figure 4.10: Snapshots (105 s.u × 105 s.u) from the numerical simulations at different gradient strengths at d=50.75 s.u. (a,c,e) show the initial position of the spiral tips(at 100 t.u.) and (b,d,f) show the tip positions at 900 t.u. for gradient strengths of - (b)0.04, (d)0.06, (f)0.08

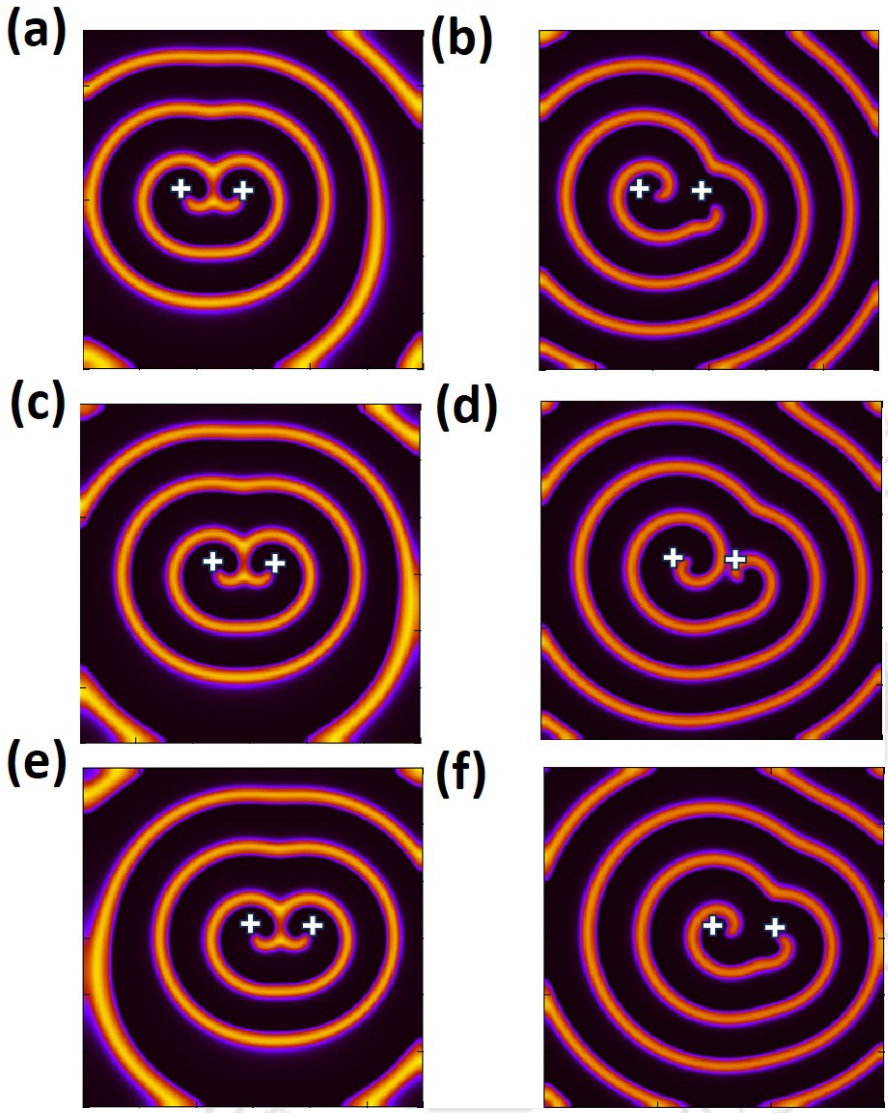

Figure 4.11: Snapshots (105 s.u × 105 s.u) from the numerical simulations at different positions of the spirals at a gradient strength of 0.04.(a,c,e) are the initial snapshots at 100 t.u. for d=40.25,50.75,61.25 s.u. respectively. (b,d,f) represents the same at 900 t.u.

drift of the right tip (Fig. 4.7d). This is clearly reflected in the tip trajectories of the two spiral tips. Trajectories from four numerical experiments, with varying hvalues are depicted in Fig. 4.8. With time the two tips are moving away from each other, the left tip moving in an upwardly fashion, while the right tip moves downward. The distance moved in the case of higher gradient is observably larger.

The distance traversed by both the spiral tips are plotted in Fig. 4.9(a and c) as functions of Δh. The path length (final displacement of the tip), L, and traversed length (actual distance covered by a tip), s, are seen to linearly vary with gradient strength. Next we varied the initial position of the spiral, with respect to the left boundary, where the concentration is the highest (Fig. 4.9(b and d)). With increasing dvalues, the net drift decreases. The path length of the left tip (black triangles in the figures) is smaller than the right one (red circles in figure), in a given time, except when d is very large, or the spiral pair very far from the left boundary. This was also evident from the plots of the trajectories (Fig. 4.8). However, there is no appreciable difference in the traversed length, s, for the two tips, with increasing gradient strength. On the other hand, with increasing d, the traversed length for the left tip supersedes the right one, for higher dvalues. This could be because the left tip rotates faster causing the greater drift of the right spiral, leading to comparable and sometimes greater traversed lengths of the former. This causes a nonlinear trend in the change of s with d.

All these drifting analysis and observations can also be read in more simpler way, with the snapshots. Fig. 4.10 show the drift of spiral tips with increasing gradient strength, while Fig. 4.11 describes the effectiveness of a particular gradient strength. Snapshots reveal that the higher gradient strength causing more drift and effectiveness decreases with separation distance, as we analyzed in terms of traverse distance and path length.

4.7 Discussions and conclusions

By introducing a source of protons into an otherwise homogenous layer of BZ solution (gel), we have successfully employed a chemical gradient in the system. When spiral

waves are subjected to this gradient of protons released from the ion exchange resin beads, their motion is affected by the resulting inhomogeneity. We have observed that the tip lying close to the column of beads starts rotating faster than its counterpart, albeit with only a slight increase in frequency. Both spiral tips start reorienting themselves, and the left tip moves towards the top of the medium, while the right one moves downward. Such a kind of reorientation of spiral tips, and subsequent breaking of the symmetry of the two counterrotating tips, leading to deformation of spiral shape, was also seen in earlier studies with stronger gradients like electric field [21]. Here they observed that the two spiral tips separated from each other as they moved towards the anode. In yet another study, it was observed that the distance between the two spiral tips would decrease with time [20]. In our case, we observed that the distance between the two counter-rotating spiral tips kept on increasing over time.

In our numerical simulations, we carried out studies considering the gradient strength as a function of distance. Initially, we considered it a linear function of the distance (from the column of resin beads), as $H(x,t) = H_0 + a(105 - x) + bt$. However, the trends obtained from our computational studies did not exactly match that of our experiments. Figure 4.6 displays a comparison of hydrogen ion mobility in both linear and nonlinear gradients. Hence, we considered the nonlinear variation of the gradient strength (as in Eq. 4.14). The results now matched the experimental observation more closely. This points to a non-linear variation of the gradient in space. This is markedly different from any external gradient that one may employ, like electromagnetic fields or thermal gradients. The movement of the hydrogen ions in the 2D space as ion exchange takes place, leading to a gradient in the concentration of protons, will be an interesting study by itself, and may be carried out in the future. Furthermore, our numerical simulations allow us to study the effects of a stronger concentration gradient across larger distances.

In conclusion, we can summarize that a concentration gradient can influence the dynamics of spiral waves. Proton-exchange resin beads that do not bind to the metal catalyst is an able candidate to introduce a concentration gradient within the homogeneous BZ media. In our experiments we observed that drift of the spiral

tips were higher with more number of beads and decreased as we moved the spiral away from the column of beads (increased d). In our numerical simulations with the modified Oregonator model that we developed to include the explicit effect of the H^+ion concentration at every point, we observed similar changes in the spiral dynamics with a nonlinear form of gradient. As the spiral was shifted away from the left boundary (high concentration), the drift decreased. One may wonder if there is a critical distance beyond which the effect of the concentration gradient is negligible. Future work can be carried out with this aim. The conclusions drawn from this work improves our understanding of the effect of ionic gradient on these excitation waves, and may help us in their control in biological systems, such as cardiac tissues.

Summary

- This chapter describes how mild gradient is able to drift spiral waves.
- Experimental observations are corroborated by numerical simulations with our modified model.
- Drift of the spiral tip is controllable with gradient strength/number of resin beads.
- We could not unpin a pinned spiral with this mild gradient.

Chapter 5

Collective dynamics: Synchronization phenomena of pinned spiral rotors

5.1 Introduction

Synchronization of biological oscillators are highly *typical* [81], and examples can be found in the flashing of fireflies [82], neuronal network [83], Cryptocurrency network [84], etc. In the mercury beating heart (MBH) experiments [85], the presence of synchronization phenomena is also observed in a chemical system. Theoretical experiments on arrays of coupled rotors have been carried out where phenomena like synchronization and chimera were observed, which often depended on the coupling strength [86, 87, 88]. Synchronization phenomena in a network are also effective in explaining the difficulties in the recognition of facial emotions of an ADHD individual [89].

Here we study the interaction of spiral waves and their synchronization. Spirals and scroll patterns are often encountered in nature [90, 91, 92, 93]. These excitable waves are also well-studied phenomena in self-organized systems. Understanding the dynamic behaviors of these waves is vital to explain many physiological activities

like cardiac arrhythmia [94]. The study of the control these waves has been carried out using various gradients like thermal [95], electric field, or cross fields [96]. The study of synchronization of spiral waves in experimental systems in the BZ reaction, without photosensitization, is one of the latest additions to the field. A recent study on the interaction of multiple spiral waves reveals different kinds of dynamics like attraction and repulsion, depending upon the separation of the spiral-cores [97].

Steinbock and others numerically explored the synchronization phenomena of pinned spiral rotors depend on their wavelength and the separation of the two rotors [98]. Rotational synchronization in phase and frequency of counterrotating pinned spirals were also shown in simulation as well as in experiments with BZ reaction where the spirals have been pinned to obstacles of different diameters [25]. Recent experiments with camphor boats have shown synchronization phenomena [99]. Pinning locks the frequency of spiral rotors and arrests any kind of drift. This situation is very much comparable to the case when rotating singularities formed in cardiac waves get attached to scar tissues. In this manuscript, we look into the phase synchronization phenomena of pinned spirals having the same sense of rotation.

Structures beyond pairwise interactions are widespread in various fields like neurology, ecology, biology, sociology, etc. [100, 101]. Practical phenomena are more prominently higher order than pairwise interaction and so more complex. The abrupt dynamical shift is standard in HOI [102]. The most straightforward higher-order interaction is a 2-simplexes system. The correlation in the neuronal activity in the brain is often described by the interaction in 2-simplexes [103]. Achieving a synchronization state in such a complex system was always a challenge and becomes more complex in an experimental study [104, 105].

Synchronization of spiral wave patterns was observed in a nonlocally coupled two-layer network of discrete oscillators [106]. One of the very recent studies showed the mixed synchronization of oscillators in a network containing three nodes[107]. Though most of the connections or interactions present in nature are complex and of higher order, they are still less studied in experimental systems. A motif of a higher order can have a wide range of geometry and interconnections between the nodes[108]. Here we explored a system with three nodes, where each node are indi-

vidual spirals rotating in the same reaction medium, and thus one may consider the involvement of a higher order interaction. Towards achieving these means, we extend our system to a network of three oscillators in a triangular geometry in a BZ reaction-diffusion system. Till date, no such studies are reported in literature. Through our experiments and numerical simulations, we show that two corotating pinned spirals may behave differently than counter-rotating ones. Also, three co-rotating pinned spirals in a triangular network can reach a state of lag-synchronization, with respect to the initial condition.

5.2 Experimental Methods

We performed our experiments with the Belousov-Zhabotinsky reaction system. The BZ reaction is a redox reaction, in which the bromate ion oxidizes the organic acid to carbon dioxide and reduces it to bromide ion. The reaction is a multistep reaction and a possible mechanism is the FKN mechanism. Intermediates formed during the reaction are responsible for the chemical oscillations. BZ reaction can produce sustainable oscillation for up to a long time. The stock solutions for our experiments are prepared using millipore water. The concentration of the ingredients in the final solution were: 0.04 M sodium bromate, 0.04 M malonic acid, 0.16 M sulphuric acid, and 0.001 M ferroin. 0.8 wt./vol % of agar gel is used to embed the reaction ingredients. The experiments were carried out in a petri dish with a diameter of 6 cm. The temperature was maintained at 23±1°C, at normal atmospheric pressure throughout the experimental observations. The layer of the reaction mixture is 2 mm in depth. We initiated a circular wave by inserting a silver wire at the center of the dish for a little while. Spirals are created by physically cleaving the spontaneous circular waves using a thin glass slide. A glass slide is non-reactive with the BZ solution and can thus be used to create two pairs of spirals. Spherical glass beads of 1.4 mm diameters are put near the tips of the spirals, in order to anchor them. We pinned the two co-rotating spirals, and the other two are allowed to drift apart to near the boundary so that the free counterparts of the spirals do not affect the pinning site. We pinned three spirals in the same way to examine a higher order network.

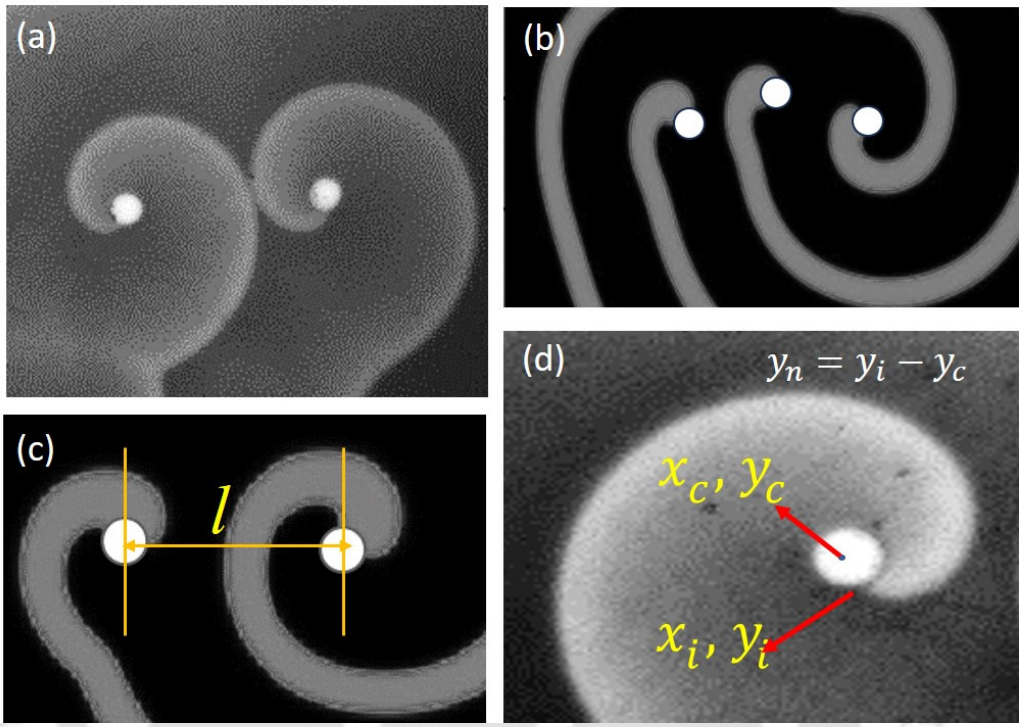

Figure 5.1: Snapshots and the details of the experimental and numerical system studied. (a) is the snapshot of a typical experiment (2 cm $\times$ 2.5 cm) with two corotating pinned spirals. (b) and (c) are the snapshots from numerical simulations. (b) describes the system with three pinned rotors arranged in a triangular geometry, (c) depicts the numerical snapshot of two corotating spirals pinned to heterogeneities. l is center to center distance between the two rotors arranged in a line. (d) shows a zoomed view of one pining site with the positions marked. (x_i, y_i) is the instantaneous position of the i^{th} spiral tip and (x_c, y_c) is the center of the spiral core in the global coordinate system. (x_n, y_n) is the tip-position in local coordinate system (taking the centre of the circular obstacle as origin).

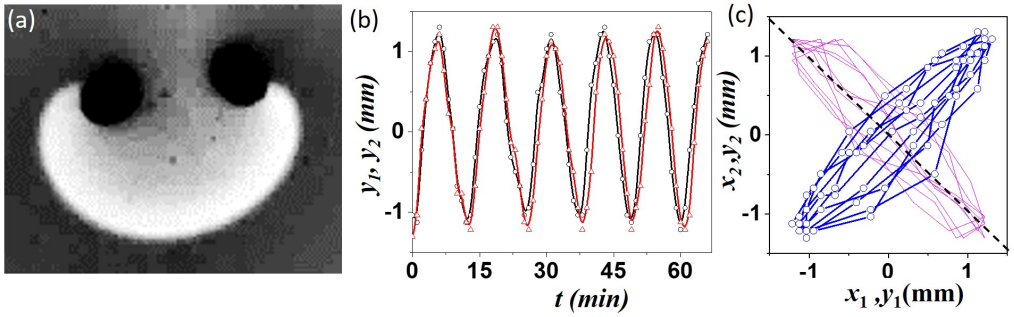

Figure 5.2: Experiment with two counter-rotating spirals pinned to similar heterogeneity. (a) Snapshot of the experimental system (b) depicts the time evolution plots of the $y-$coordinates of both the counterrotating spirals, (c) demonstrate the phase plots of x and y- coordinates show the complete synchronization.

We monitored the experiment under a CCD camera, recorded the snapshots on a personal computer at 2-second intervals, and analyzed the images using a MATLAB code.

5.3 Experimental Results

5.3.1 Complete synchronization of counterrotating pinned spirals

Before starting experiments with corotating spirals we checked the phenomena for counterrotating spirals. We pin both the counterrotating spirals with rubber baeds of same diameter (1.8 mm) and observed the attainment of complete synchronization from very early. This can be seen in Fig-5.2. The time-series plot at Fig-5.2(b) show the simultaneous increase and decrease of the $y-$ coordinates with time, and the phase plot at Fig-5.2(c) confirms the conserveness of the rotation in a particular space due to complete synchronization.

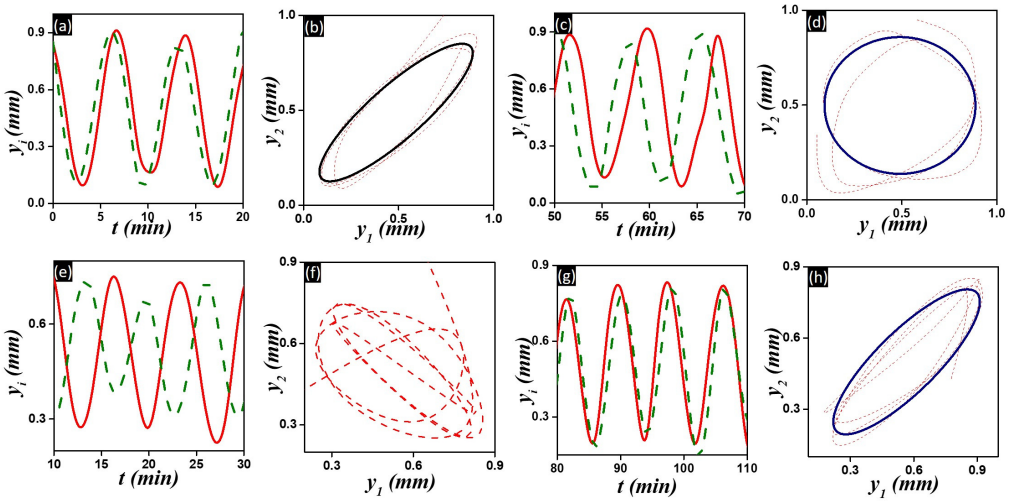

Figure 5.3: Experiments with two corotating pinned spirals with a variation of the center-to-center distance, l. (a) and (c) show the time evolution plots of the y-coordinates of both the spiral rotors at initial and final stages for l=9.5 mm. (b) and (d) show phase plots corresponding to (a) and (c). (e) and (g) show the time evolution plots of the y coordinates of the spiral rotors at the initial and final stages of experiment for l=14.9 mm. (f) and (h) show the corresponding phase plots for (e) and (g). The time evolution plot and the phase plots clearly show the increment of lag for l=9.5 mm in (a-d), and a transition to a synchronized state for l=14.9 mm (e-h).

5.3.2 Lag formation in corotating pinned spirals

Fig-5.1 demonstrates the experimental system as well as the numerical system under study. A snapshot from a typical experiment is shown in Fig-5.1(a), while similar snapshots from the numerical simulations for two and three co-rotating pinned spirals are shown in Fig-5.1(b) and (c). Initially, two or three pairs of spirals are created by the method described earlier. We took a chemically unreactive object and pushed the counterpart of each pair to the boundary physically with great care. The main difference between a free spiral and a pinned spiral is that they differ in their frequency and they mostly do not meander. The frequency of the free spiral is greater than a pinned one. We pinned all the spirals with glass beads of the same diameter to make the natural frequency of the rotors identical. We then study the phase synchronization of the pinned rotors. Though it should be noted that the counterpart of each pinned spiral is free and so certainly moving faster, we can neglect the effect of these waves for a certain time frame (120 mins in our situation), as the free counterpart is far away from our area of observation. All our observations were made within that time period. Fig-5.1(d) shows the coordinates of the center of a spiral core (x_c , y_c) and the positions of the spiral tip (x_i , y_i).

To analyze the system, we looked at the y-coordinates of all the rotors. The positions of both the tips (in local coordinates) are taken as follows:

$$y_n = y_i - y_c$$

The y-cordinate of spiral the tips in the local coordinate system has been taken by considering the spiral core as origin. We normalized the y_i's of all the spiral rotors obtained from their tip position and then plotted against time to get the time evolution plot.

In the phase plots, the coordinates (y_2 or y_2 and y_3) are plotted with respect to y_1 for the initial and final time series with a dashed line. The black and navy solid curve on the phase plots over the dashed curve is added externally to represent the synchronized dynamics more evidently, except for the cases of asynchrony, where one may observe the phase plot of the asynchronous rotor covering the entire phase

space.

Fig-5.3(a-d) represent the experimental observations and results of two corotating spirals for l = 9.5 mm. We can observe that the initial phases are in complete synchronization (5.3(a)) but there is a phase lag, that increases (5.3(c)) with the evolution of time. The increment of this phase lag can be easily understood from the phase plots. The initial phase plot in Fig-5.3(b) shows an almost fully synchronized state, whereas the final state in Fig-5.3(d) describes the lag formation.

We further varied the l distance. Fig-5.3(e-h) shows an experimental result with l = 14.9 mm. Here, the separation is 1.6 times more than the earlier case. Here, we observed that the two rotors attained complete phase-synchronization, which is evident from Fig- 5.3(g), which shows the time evolution plot for the final 25 minutes of the reaction. The phase plot at Fig-5.3(h) also points towards the increase in phase synchronization.

5.3.3 Lag synchronization in a triangular network

For pairwise interaction, we observed a transition from one synchronized state to another. Does it behave in the same way as a higher-order network system? To answer this, we investigated the simplest higher-order network with three spiral rotors pinned to heterogeneities and arranged in a triangular geometry. Fig-4 describes such a situation in an experiment. Fig-5.4(a) is the snapshot describing the placement of the rotors. The snapshot is the zoomed and stretched view of an area of 1.1 $\times$ 2.8 cm^2, where the black, red and green circles represent the trajectories of the rotors. Fig-5.4(b,c) show the time evolution of the y-coordinates of the rotors. Fig-5.4(e,f) are the phase-plots showing the dynamical behavior at initial(5.4(d)) and final (5.4(e)) stages. It can be seen from the phase plots that y_1 and y_3 were in lag sync from the beginning but there exists a little asynchrony between y_1 and y_2. Final phase plot shows that all the rotors are in lag synchronization with each other.

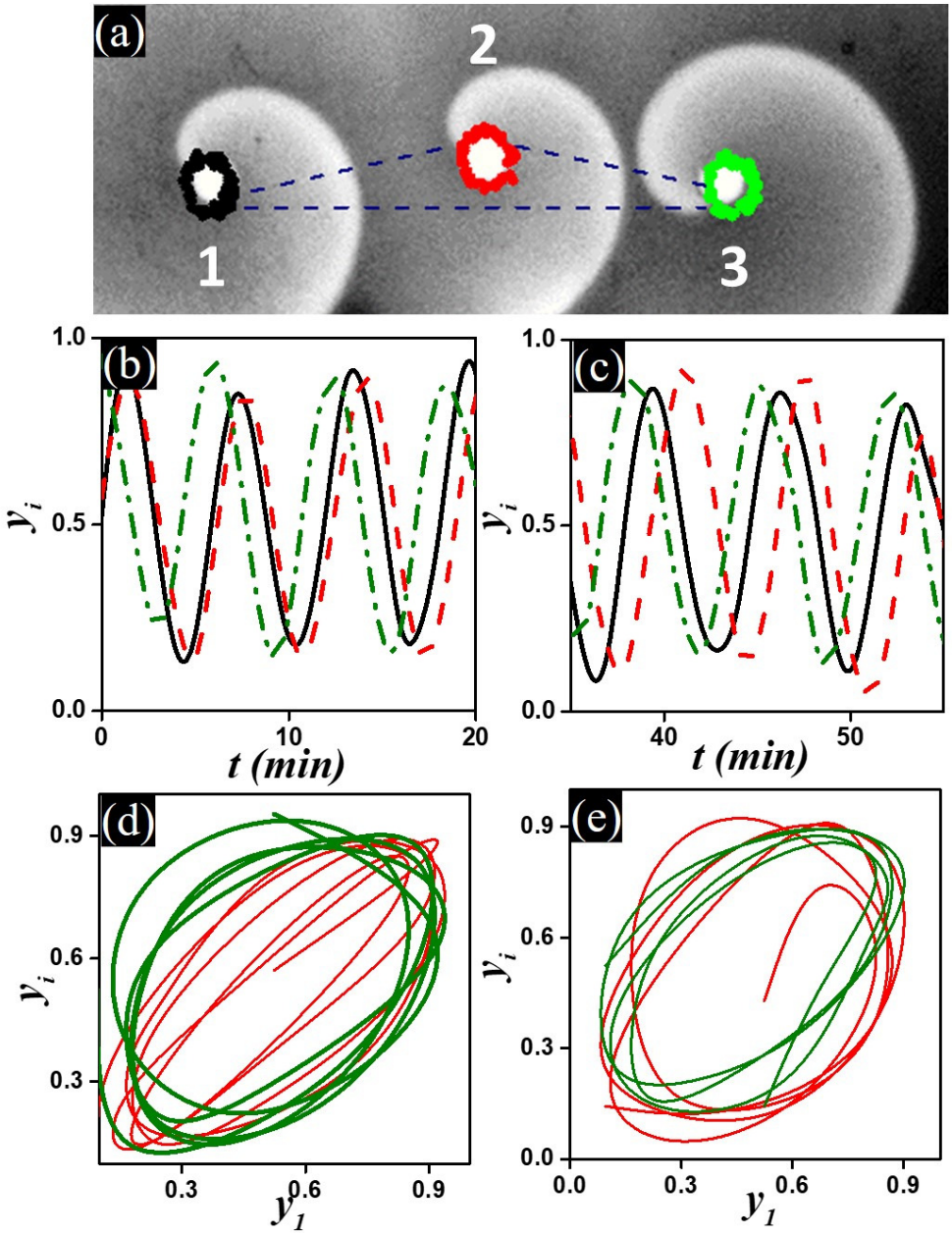

Figure 5.4: Experimental results of three corotating pinned spirals in a triangular network. (a) illustrates the experimental description with the three rotors pinned to circular heterogeneities. Black, red, and green circles over the heterogeneous obstacles represent the tip trajectories of the spirals attached to them. (b) and (c) show the time series at initial and final times. (d) and (e) are the phase plots at the initial and later time. The time series as well as the phase plots describe the transition to lag synchronized state of all the rotors. The figures have been color coordinated, as time series and phase plots for y_2 are given in red, and y_3 given in green.

5.4 Numerical Methods

We used Barkley's Reaction-Diffusion model to simulate our experimental system, as the model incorporates an activator and an inhibitor dynamics, like our experimental one [109]. Hence, it is widely used to describe the BZ reaction system [110].

$$\epsilon \frac{\partial u}{\partial t} = \left[u(1-u)(u - \frac{v+b}{a}) \right] + D_u \nabla^2 u \tag{5.1}$$

$$\frac{\partial v}{\partial t} = u - v + D_v \nabla^2 v \tag{5.2}$$

where,

$$\nabla^2 u = \frac{\partial^2 u}{\partial x^2} + \frac{\partial^2 u}{\partial y^2}$$

$$\nabla^2 v = \frac{\partial^2 v}{\partial x^2} + \frac{\partial^2 v}{\partial y^2}$$

Here, u is the activator, and v an inhibitor. Spiral patterns were generated with a specific set of parameter values, $a = 0.85$, $b = 0.07$, $\epsilon = 0.02$. Diffusion coefficient values D_u and D_v are considered equal (1.0). This set of parameter values generated sustainable spirals in our 300×300 space grid system when we solved the numerical integration using Euler's method. The time step is taken as 0.01, and the space step size is taken as 0.35. For choosing the space-step and time-step, we checked for different values and selected the best out of that, which produces good numerical accuracy and yields a stable pair of spirals in our system with counter-rotating spirals. For the corotating spirals we used the same step-size. The maximum time step limit for solving the said model using Euler's method can also be found in the article of D. Barkley [109] for generating stable spirals. Circular regions of the diameter of 7 space units are modelled as heterogeneous obstacles to pin the spirals, by maintaining the magnitudes of u and v as zero inside this region.

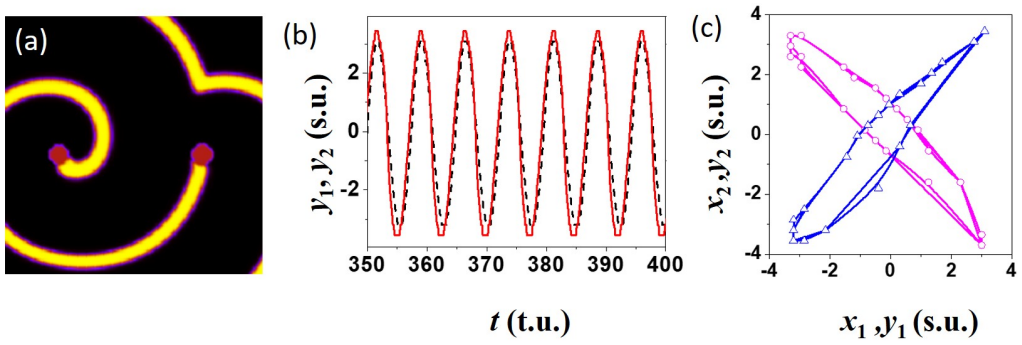

Figure 5.5: Numerical simulation with two counter-rotating spirals pinned to similar heterogeneity. (a) Numerical snapshot of the system, (b) depicts the time evolution plots of the $y-$coordinates of both the counterrotating spirals, (c) demonstrate the phase plots of x and y- coordinates show the complete synchronization.

5.5 Numerical Results

5.5.1 Complete synchronization of counterrotating pinned spirals

Like our experiments, we performed numerical simulation for a system with two counterrotating pinned spirals before we move towards the corotating one. Fig-5.5 demonstrate the result of such system where the disk diameters are 5.25 s.u. The time-series plot in Fig-5.5(b) show the simultaneous increase and decrease of the $y-$coordinates with time and phase-plot in Fig-5.5(c) of both $x, y-$ coordinates confirms the complete synchronization behavior.

5.5.2 Lag formation in corotating pinned spirals

To mimic our experiments, we varied l in our numerical simulations. Fig-5.6 demonstrates the numerical results where l is 17.5 s.u. and 21.0 s.u., respectively. We noticed the formation of a lag in each case. The generation of lag is significantly less if the value of l is very high as 24.0 s.u. or 28.0 s.u. In these scenarios, the initial and final states remain in almost the same condition, which means they maintain the

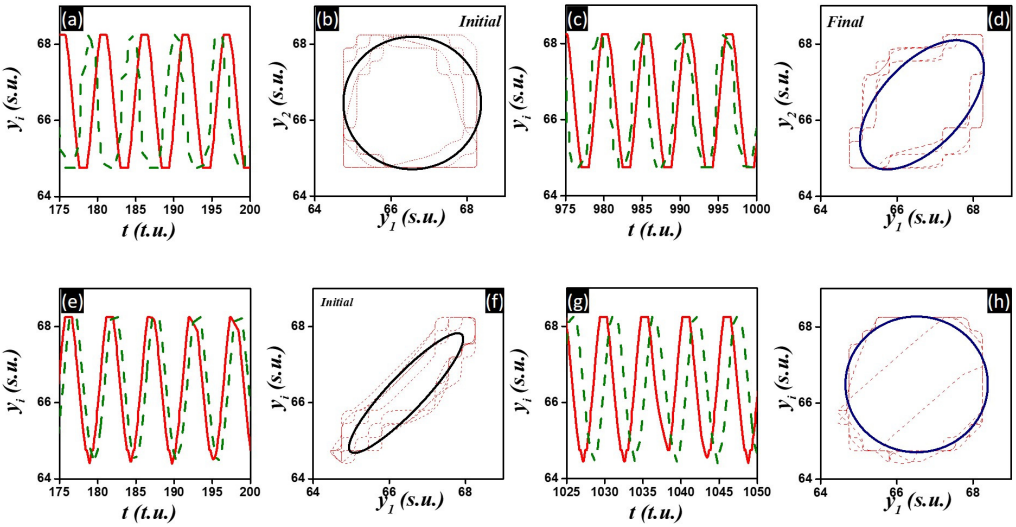

Figure 5.6: Results of numerical simulations for two corotating pinned spirals with a variation of l. (a) and (c) show the time evolution plots of the y-coordinates of the spiral rotors at initial and final stages for l=17.5 s.u. Here final stage is after synchronization has been achieved. (b) and (d) show the corresponding phase plots for (a) and (c). (e) and (g) show the time evolution plots of the y-coordinates of corresponding phase plots of (f) and (h) for l=21.0 s.u. (a-d) illustrates the transition from a more lag-synchronized state to a lesser lag, (e-h) describes a situation of increasing lag for a system with two corotating pinned spirals.

complete synchronization behavior if they were initially in complete synchronization. This can be explained on the basis of coupling strength. The more the l value, the coupling decreases and so the less transition from the initial behavior is observed.

The features of the experimental results can be compared with the numerical findings demonstrated in Fig-5.6(a-h). Fig-5.6(a-d), where l is 17.5 s.u., the behavior is similar to that observed in Fig-5.3(e-h) for the experiments. In both the cases, we notice a transition to complete synchronization behavior. The initial and final time series plots and the respective phase plots represent the transition.

Fig-5.6(e-h), in the same way, demonstrates the situation observed in Fig-5.3(a-d) for the experiment. The increase of phase lag and transition to a lag-synchronized state from an almost completely synchronized state is obsered from the time series and the phase plots.

5.5.3 Lag synchronization in a triangular network

This behavior can also be observed in Fig-5.7, which explains the results of the numerical simulation where three rotors are placed in a similar network. A description of the system is given in Fig-5.7(a). Fig-5.7(b,d) shows the initial time evolution and the phase plots. Both show that y_1 and y_3 are in little asychrony but y_1 and y_2 are in lag synchrony. Fig-5.7(c,e) depicts final dynamics in time series and phase plots. It can be seen that both y_2 and y_3 are in a synchronized state with respect to y_1, with some amount of lag.

5.6 Discussion and conclusion

Counter-rotating spirals attached to heterogeneities of the same diameter remain in a synchronized state, or if there is any phase difference in the beginning, it overcomes that [25]. Previously, we showed synchronization is evident even if the heterogeneity is of different diameters for counterrotating spirals in the work of Kalita *et al.* [97]. So, it was an obvious question: what happens if the rotors were co-rotating? Here in this article, we show experimentally that a pair of co-rotating pinned spirals may

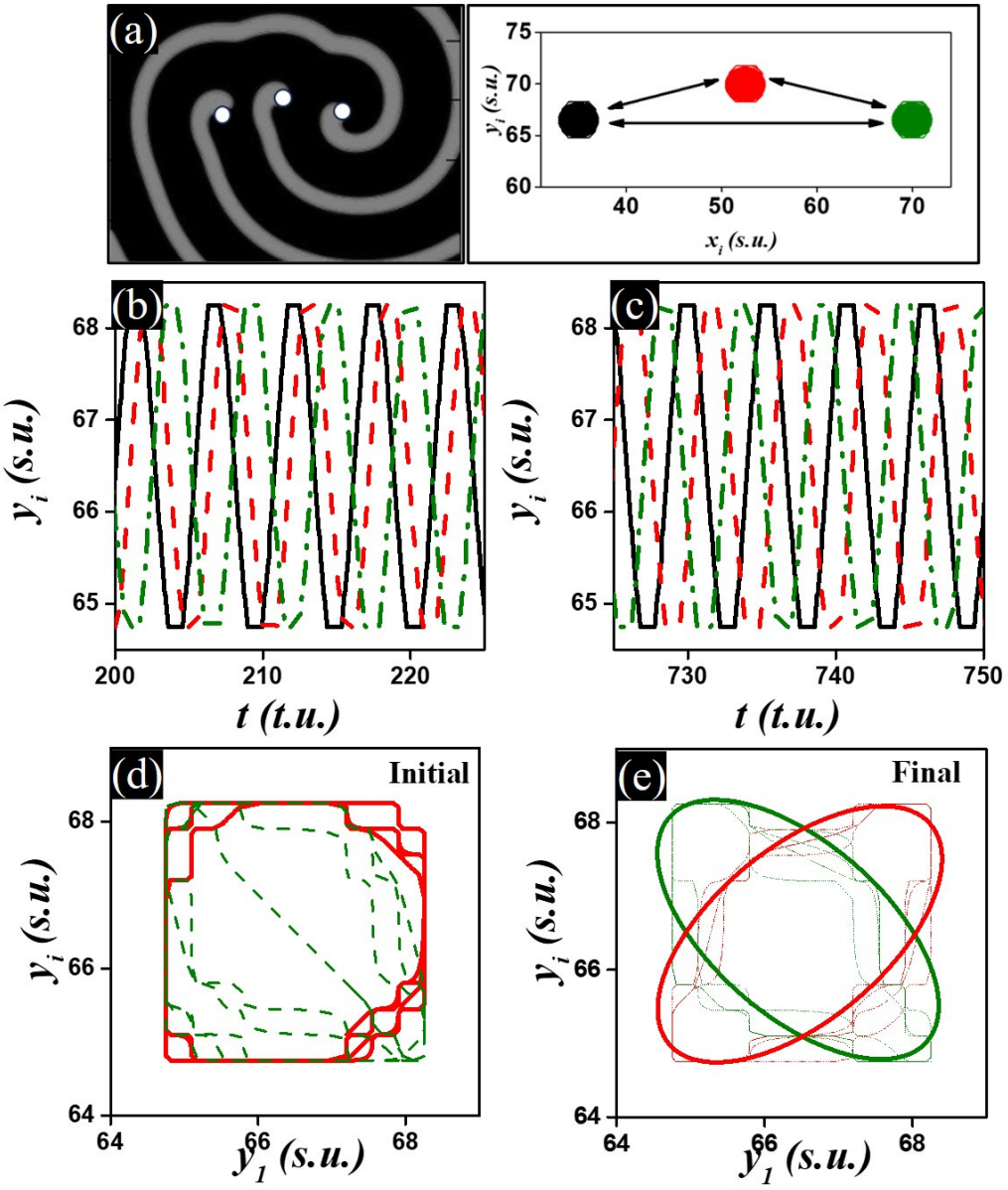

Figure 5.7: Numerical results of three corotating pinned spirals in a triangular network. (a) illustrates the description of the system. (b) and (c) show the time series at the initial and final state. (d) and (e) depicts the phase plots corresponding to the initial and final time series. A comparison of the time series and the phase plots of the initial and the final states illustrate the formation of lag-synchronized states of all the rotors at the final state. Figures have been color coordinated as in Fig-5.4.

behave differently, starting from a phase synchronized state it can reach to another state through a lag.

In our experiments, we could not remove the counterparts of the corotating spirals entirely from the system. As a pair of counter-rotating spirals are formed when we cleave the circular wave, we has to push the unpinned counterpart to such an extent that it barely effects the pinned spirals, which are under our active investigation. However, a limitation of our setup is that we could not run our experiments for a very long time without the influence of the free counterpart. Hence our system was not perfect, as our experiments had a time-restriction. Making a perfect network of corotating spirals in an experimental system still remains a challenge. The simulation results on the other hand are free from these experimental barriers. In our numerical simulations, we found that the fate of the network of two and three spirals is the same as that of or experiments, that is, there is a change in synchronization behavior from the initial state through a lag. For a pairwise system, if the separation is higher, in our case at 35.5 or 45.5 space units, we found that the complete phase synchronization remains unchanged with time. If the separation (17.5 or 21.0 space units) is less, a shifting of one rotor is very obvious, which means a lag is formed. The development of lag with the progression of time was noticed in our experiment, too.

For three corotating spirals in triangular network, the phases of all the rotors finally reached a synchronized state, though they were not in synchrony at the beginning. We observed the same phenomena of reaching a synchronized state through mutual interaction in both our experiments as well as in our numerical simulations. We did not check the observations varying the separation(l) for our network, which can be a scope of further study.

Synchronization in a complex system depends on the coupling strength among the oscillators. In our case, the distance seprating the rotors determines the coupling strength. The effect of the simplicial complex on synchronization has been shown using Rulkov-map neurons connected pairwise and in higher-order chemical interaction [111]. Gallo *et al.* [112] showed that directed higher-order interaction brings in synchronization. The common abrupt transition between incoherent and synchronized states is also known [113]. The test with a chemical network was first

carried out by Showalter *et al.* [114] using a photochemical BZ reaction in a star network. The novelty of our work lies in the fact that the higher-order network of rotating spirals in a BZ solution has not been studied before. The rotation directions of all the oscillators are made unidirectional. The pinning obstacles are of the same diameter, and so are the frequencies of the spiral waves. The spiral rotors are globally coupled. The coupling strength for these or more spirals could have been varied with the separation(l), making it more asymmetric. This could open up a new direction in the study of the system. A recent work reported the uncertain delay in the neuronal network leading to turbulence, through a synchronization transmission [115]. Whether this could happen in our experiments with the BZ system, is a scope of future research.

Though most of the work in the higher dimensional network is motivated by a neuronal network system, we propose that it can help in the understanding of even the cardiac system, where the electrical activity of our heart gives rise to cardiac waves. Pinning of spiral waves to heterogeneities in the BZ, may be compared with the cardiac waves pinned to scar tissues. More pinning may produce different kinds of interaction. So, for better understanding of pinned cardiac waves in a network, we need to study similar kind of situations.

Summary

- Synchronization of biological oscillators are found everywhere.
- In this chapter we report the synchronization of spiral rotors in the BZ reaction-diffusion system.
- Counter-rotating pinned spiral rotors show complete synchronization when they are pinned with similar heterogeneity.
- Corotating pinned spirals demonstrate a lag synchronization.

- Corotating pinned spirals arranged in triangular geometry also show a lag synchronization.

Chapter 6

Collective dynamics: Cluster and chimera states in a network of pinned rotors

6.1 Introduction

Synchronization and related complex dynamics in lattices of coupled oscillators has been a topic of general interest in the field of nonlinear sciences. It has its applications in the understanding of natural phenomena and designing engineering marvels, and is widely studied across biology, physics and chemistry [116, 117, 118, 119]. While the first documented study of synchronization can be said to be the Huygens' pendulum in the 17th century [120], we have since come a long way, through the systematic study of coupled oscillators by Winfree in 1967 [121], to the studies of Kuramoto [122], Strogatz [123], and Crawford [124]. The concept of collective synchronization [125] paved the way for the discovery of more exquisite phenomenon like partial synchrony and cluster formation [126]. The icing on the cake came with the discovery of chimera states, the simultaneous coexistence of coherent and incoherent behavior, in a network of non-locally coupled oscillators [127, 128]. The first experimental evidences of the phenomenon were found almost simultaneously, in two

different systems, an array of coupled maps realized optically [129] and a network of photosensitive chemical oscillators [130]. Ever since, several systems have been discovered that show the emergence of chimera states. In nature, the observation of partial synchronization patterns can be used to explain unihemispheric sleep in some mammals, first-night effect and collective social behavior in humans, and even epileptic seizures [131, 132]. The existing experimental and theoretical studies on chimera and cluster states have tried to achieve a better understanding of these intriguing phenomena. However, these studies were unable to provide an explanation of processes such as arrhythmia and fibrillation in heart tissues that results in sudden cardiac death [133]. The role of synchronization in the working of the cardiac system is well established. The cells of the heart synchronize, and their collective dynamics results in the beating of the heart [134]. The fibrillation of the heart is accompanied by the presence of several rotating singularities; two-dimensional spiral and three-dimensional scroll waves, causing different parts of the heart to beat out of sync [58]. Such a rotating singularity is also known to attach itself to heterogeneities in the cardiac muscle (phenomenon of pinning), like scar tissues [19]. Other than cardiac tissues, these spiral waves are also responsible for intricate physiological phenomena in neuronal and uterine tissues and colonies of living matter [62, 63, 61]. Hence, the interaction of such excitable rotors, and their synchronization behavior, is of great fundamental interest. In this letter we study the synchronization of a network of identical spiral rotors in an experimental system. We choose a minimal network of four identical spirals, in a chemical reaction-diffusion system. The question of the minimal number to demonstrate the phenomenon of chimera was solved in recent years, as four oscillators could constitute two subsets of population, one synchronized and the other asynchronized [135, 136]. Chemical oscillators were one of the first experimental systems used to demonstrate the existence of a chimera state [130]. However, that study and corresponding work in the field considered a large population of discrete chemical oscillators, either locally coupled by diffusion [137] or globally coupled by light [[118], [138]]; or non-locally coupled electrochemically [139]. The novelty of the present work lies in considering a network of globally coupled spiral rotors, pinned to circular unexcitable heterogeneities, in an otherwise

homogeneous reaction-diffsuion system. Spiral waves have an intrinsic frequency of rotation, which can be modified when these singularities are pinned to unexcitable osbtacles of varying sizes and shapes [140]. We also develop a mathematical model of Kuramoto oscillators, coupled by complex potentials, to better understand the dynamics of these interacting spiral rotors. We successfully demonstrate, for the first time, the existence of chimera and cluster states in arrays of pinned spiral rotors. Such a system can be further explored to study larger and more complicated networks of rotors in natural processes. We believe, the study of the mutual dynamics of these waves in a confined space, will shed light on the role of partial synchronization of spiral waves in the advent of cardiac arrest.

6.2 Experimental Methods

Our experiments are carried out using a Belousov-Zhabotinsky (BZ) reaction system. It comprises of a solution of 0.16 M sulfuric acid, 0.04 M sodium bromate, 0.04 M malonic acid, and 0.001 M ferroin, embedded in a 0.8 % w/v agar gel matrix. The solutions are prepared in Millipore water. All experiments are carried out in Petri-dishes of 8 cm diameter, at room temperature (23±1 °C). The thickness of the reaction gel is maintained at around 2 mm. Two plane waves are initiated, side by side, in the center of the circular dish, far from the system boundaries, by inserting the tip of two silver wires into the reaction mixture for a few seconds. When a circular wave reaches the desired dimension, we cleave it with the help of a thin glass slide. The free ends of the wave now curl in to form a pair of counterrotating spiral waves. Subsequently, four identical, chemically-inert, rubber cylinders, with a height equal to the thickness of the reaction layer, are placed in a square lattice, so as to allow the tips of the four spirals to anchor onto them, as shown in Fig. 6.1. The system is illuminated from below with a diffused, cold white light source, and is observed by a charge-coupled device camera (mvBlueFOX 220a) mounted over it. A blue dichroic filter is used on the camera for better imaging. The images are recorded onto a personal computer every 2 seconds and are later analyzed by using interactive, inhouse MATLAB codes. The spiral tip position is recognized as the

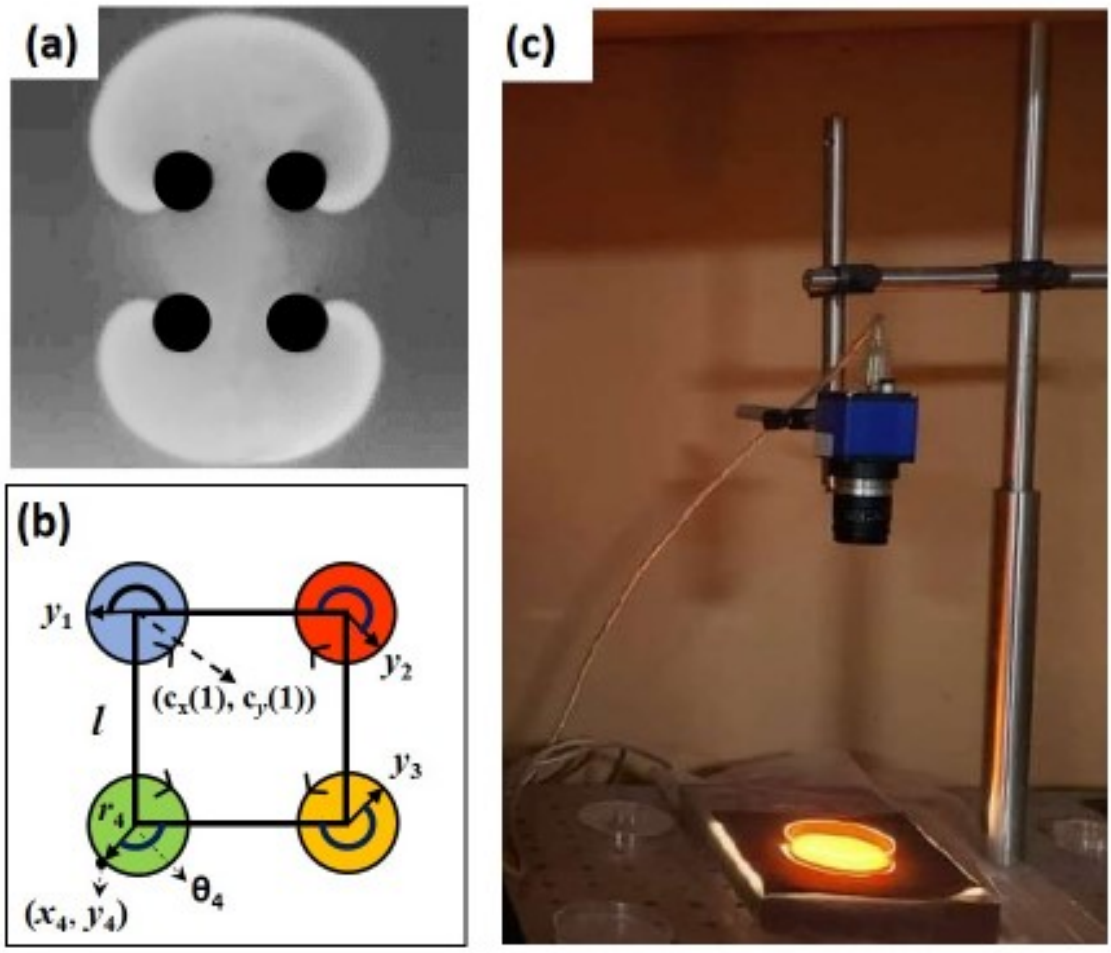

Figure 6.1: Experiments to study synchronization of a globally coupled network of four spiral rotors pinned to identical obstacles. (a) Snapshot of a typical experiment with light-colored spiral waves anchored to black rubber disks. Area of the snapshot is 31.7 × 31.7 mm^2. (b) Illustration defining the parameters of the pinned rotors: instantaneous position (x_i, y_i), phase angle (θ_i), radius of the rotor (r_i). r_{ij} is the distance between two rotors at any instant. (c) depicts an image of the experimental setup, showing the camera placed over the reaction-containing petri-dish, which has been illuminated from below with a white light source.

point of highest curvature touching the unexcitable disk.

6.3 Experimental Results

Figure 6.1(a) shows the snapshot of a typical experiment, where each of the four spirals are anchored to a rubber disk of radii 1.8 mm. The centres of the circular disks are placed on the vertices of a square of dimension l = 10 mm. An illustrative sketch of this network of four identical rotors, is shown in Fig. 6.1(b), with all important parameters marked therein. The tips of the spirals are located at (x_i,y_i), measured in reference to the local-coordinate frame. The positions and phases of the rotors can be monitored by noting the values of (x_i,y_i) and θ_i respectively, at any given time. In all our subsequent figures, we report only the y_i coordinates of the rotors, as θ_i and x_i values can easily be calculated for aknown value of y_i [141].

Choosing identical cylindrical disks as pinning heterogeneities ensures that the frequency of all the rotors is initially the same. Also, every rotor will experience the exact same force, if they were fully synchronized. Hence, we can call the system globally synchronized. Across our experiments, we vary the dimension of the square, keeping the radii of the pinning heterogeneities unchanged.

6.3.1 Cluster states

Figure 6.2 shows examples of two experiments where the formation of cluster states has been observed. When $l = 10$ mm, the spiral rotors are arranged into groups of two kinds: rotors 1 and 3 move in sync, while rotors 2 and 4 are lag synchronized with respect to them. This is evident from the time-series [Fig. 6.2(d)] and phase-plot [Fig. 6.2(e)] of the experiment. This kind of behavior can be called a doublet-singlet-singlet cluster. We consider the rotors that are synced in-phase to constitute a group. The upper panel in the figure is representative of a triplet-singlet kind of cluster formation, where rotors 1, 2 and 4 are in-phase synchronized, as is observed from the temporal evolution of the rotors [Fig. 6.2(a)] and their phase portrait [Fig. 6.2(b)]. Rotor-3 is in lag synchrony to this triplet. Here, $l = 7$ mm.

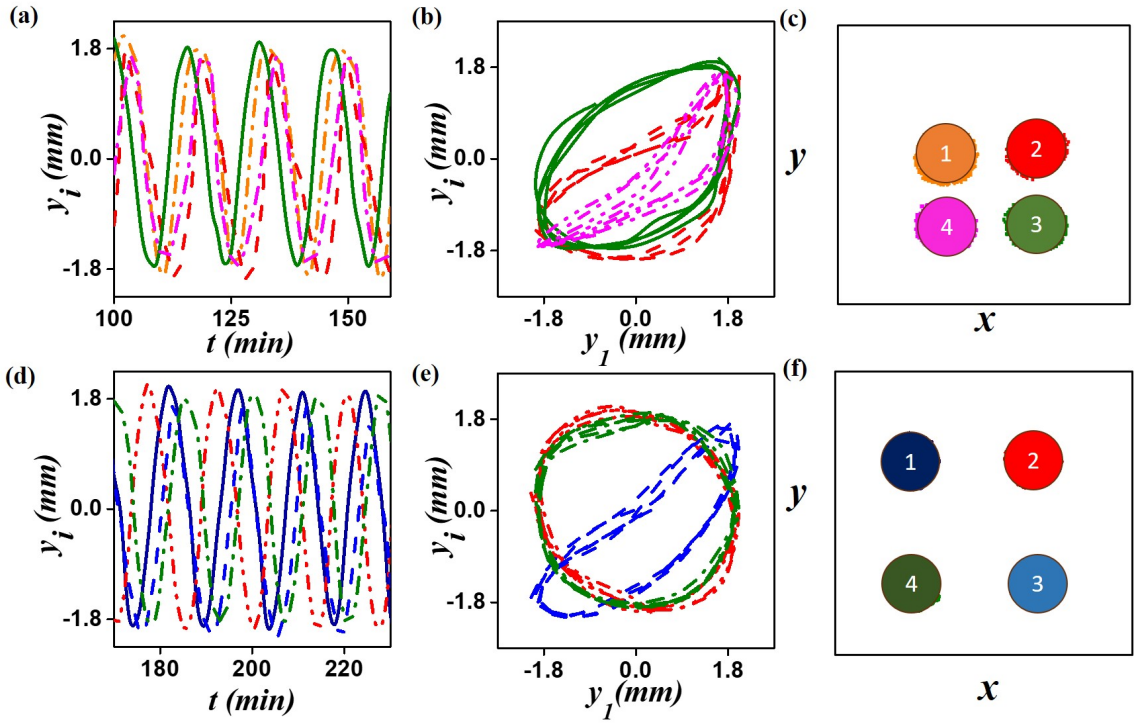

Figure 6.2: Phase-cluster formation of four identical rotors. (a)-(c) Triplet-singlet synchrony for $l = 7$ mm, (d)-(f) Doublet-singlet-singlet cluster for $l = 10$ mm. (a) and (d) depict the experimental time-series of the four rotors after synchronization has been reached. (b) and (e) show phase diagrams of the experiments with respect to y_1, during this later period of time. (c) and (f) are illustrations of the final synchronization of the rotors, color coordinated and showing all the connections between them. Colors used in corresponding time series and phase diagrams are same as the color of the rotors depicted in the illustrations. (a)-(c) Rotors 1,2 and 4 and in sync, while 3 in a lag synchronized. (d)-(f) Rotors 1 and 3 are in sync, forming a doublet, while rotor 2 and 4 maintains a lag.

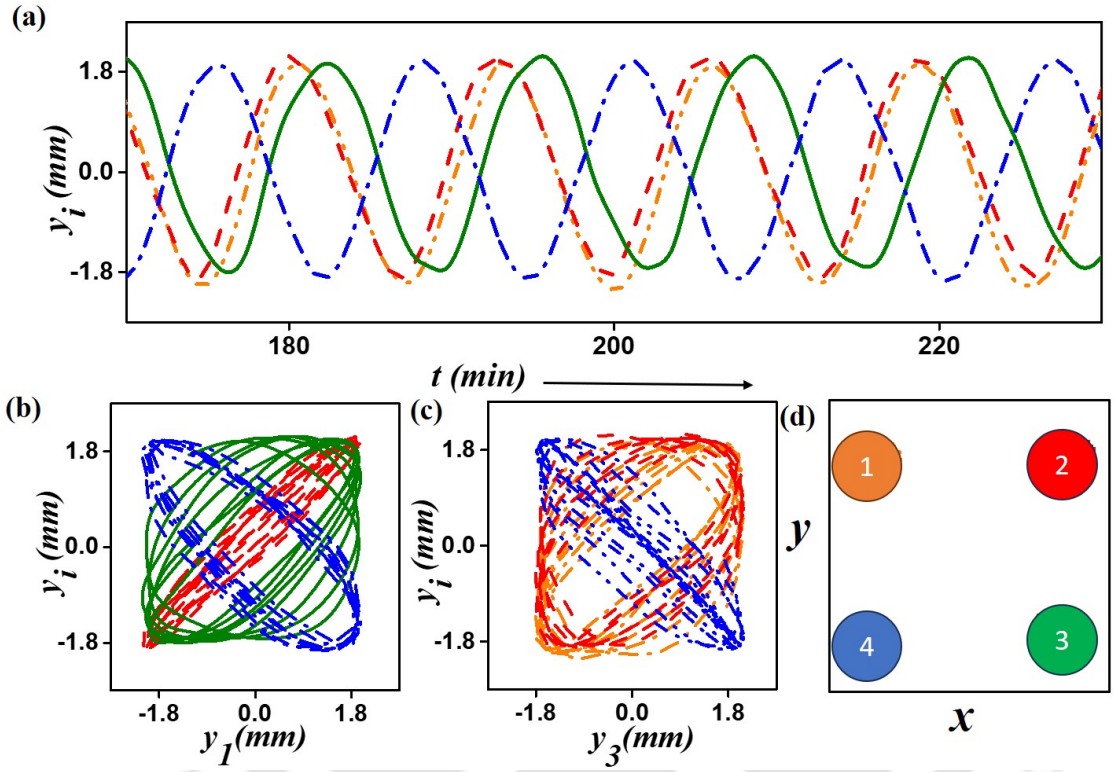

Figure 6.3: Experimentally observed chimera states in a network of four identical rotors for $l = 14$ mm. (a) Temporal evolution of the $y$position of rotors during the later part of the reaction: y_1(orange dash-dot-dotted curve), y_2(dashed red curve), y_3(solid olive curve) and y_4(dash-dotted blue curve). Phase portraits with respect to (b) y_1 and (c) y_3. (d) Illustration depicting final synchronization of the rotors: Rotor 1 and 2 form a in-phase synchronized cluster, rotor 3 and rotor 4 are asynchronized.

6.3.2 Chimera Dynamics

An example of a chimera phenomenon is demonstrated in Fig. 6.3. The system evolves over time and stabilizes in a dynamics where the rotors 1 and 2 move in sync, while the rotor-4 is almost anti-phase to this pair. The time series of the system [Fig. 6.3(a)] hints at this. The rotor-3 seems to be out of sync to the rest of the rotors, as its position is drifting across the cycles. The phase diagram with respect to rotor-1 [Fig. 6.3(b)], makes the dynamics even more explicit. While the rotor-2 shows in-phase synchronization with rotor-1; rotor-4 shows some amount of asynchrony, and rotor-3 fills the entire region of space, which points at its complete lack of phase synchronization with the other rotors. Figure 3(c) supports the same observation. This kind of a behavior of the population of rotors, showing simultaneous synchronization (rotors 1 and 2) and asynchronization (rotors 3 and 4) is typical of classic chimera.

6.4 Numerical Methods

The governing equations of the system can be written as:

$$\frac{\partial \theta_i}{\partial t} = \omega_i(t) \tag{6.1}$$

$$\frac{\partial \omega_i}{\partial t} = F_i(t) r_i - c\left(\omega_i(t) - \Omega_i\right) \tag{6.2}$$

where, Ω_i is the natural frequency of the rotor i and the term $c(\omega_i(t) - \Omega_i)$ signifies the tendency of the rotor to achieve its autonomous or natural frequency, Ω_i [142]. F_i is the tangential component of the forces on the ith particle due to its neighbors. It has been assumed here that the radial component of the force is balanced by the constraint arising from the pinning of the spirals onto the circle. F_i is given by:

$\mathrm{F}_i(t) = \sum_{j=1, j\neq 1}^{n} [\mathrm{c}_1 e^{(-k_1 r_{ij})}(1 + k_1 r_{ij}) - c_2 e^{(-k_2 r_{ij})}(1 + k_2 r_{ij})] \times [\sin(\theta_i - \theta_j) - \Delta C_x \sin\theta_i - \Delta C_y \cos\theta_i]/r_{ij}^3$

Here θ_i, θ_j and r_{ij} are function of time. For a Yukawa potential $P = e^{-k_1 r_{ij}(t)}/r_{ij}(t)$, the force has taken the form $e^{-k_1 r_{ij}(t)}(1 + k_1 r_{ij}(t))/r_{ij}(t)^2$. $r_{ij}(t)$ being the instanta-

neous distance between the two point rotors i and j. The Eqs. 6.1 and 6.2 are solved using the fourth-order Runge-Kutta method with a time interval of 10^{-4}. It requires the system a finite amount of time (around 5000 time units) to evolve and reach a stable state. We analyze the synchronization pattern at a much later time. This pattern is stable, and remains so for thousands of rotations. We carry out several simulations by varying the distance l.

6.5 Numerical Results

To further understand the mechanism of formation of cluster and chimera states in this square network of pinned spirals, we invoke a set of coupled differential equations, inspired by the Kuramoto model [143]. The rotors are considered as point particles, having an instantaneous frequency of ω_i and an angular position of θ_i, rotating around circles of radii $r_i = 1.0$, for $i = 1$ to 4. Since the rotors are identical, all circles are considered to have the same size, with their centers placed at the vertices of the square having length l, as shown in Fig. 6.1(b). The rotors are globally coupled, each experiencing a potential from the others. The force of interaction experienced by a particle due to a neighbor is considered to be a difference of two Yukawa potentials. This is because, the interaction between free spirals are known to depend on the distance between their cores [26]. The interaction is attractive till a particular distance, beyond which it becomes repulsive. When they are further apart, at a distance nearly equal to their wavelength, the spirals do not seem to influence each other. Similar behavior was also observed in three dimensional scroll waves [144], and the trend could be fitted quite well using the difference of two Yukawa potentials. Earlier theoretical studies [145] also used similar potentials, that could describe both the attractive and repulsive behaviors, as a function of the distance of separation.

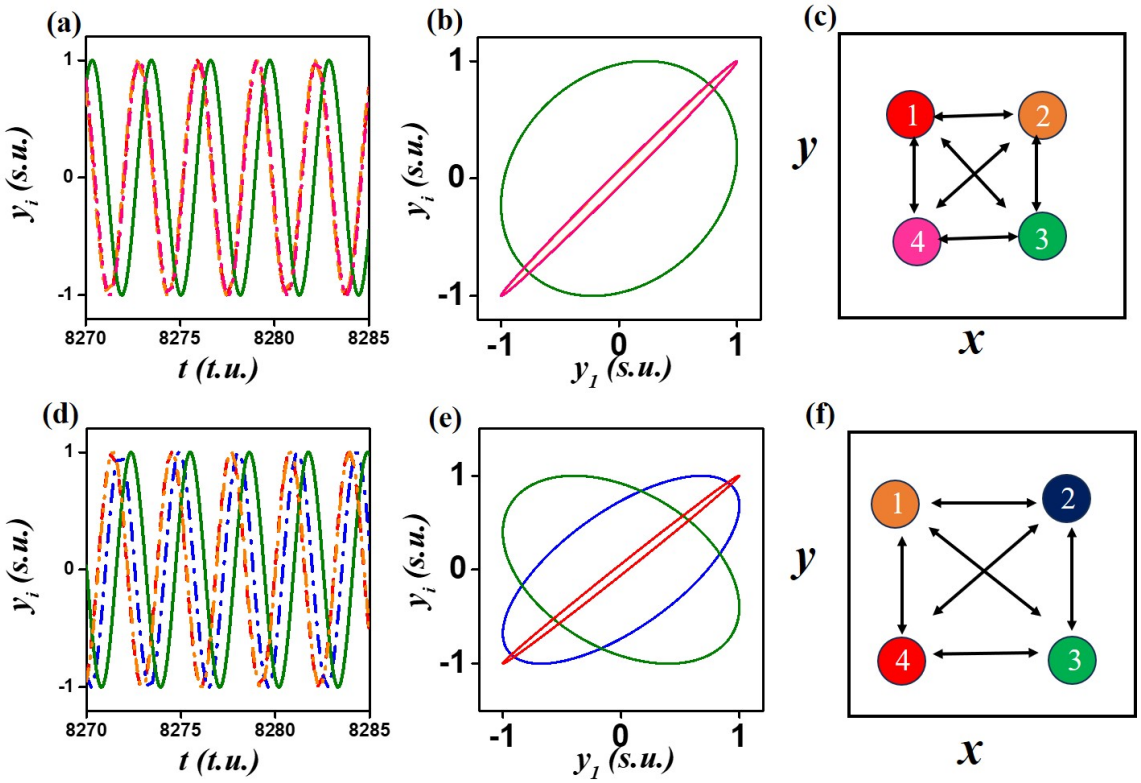

Figure 6.4: Clustering of a four-rotor model system, coupled according to Eqs. 1 and 2 . (a)-(c) Triplet-singlet system showing clustering for $l = 3.17$ units. (d)-(f) Doublet-singlet-singlet phase-clustering for $l = 4.01$ units. (a) and (d) show the time evolution of the four rotors long after synchronization has been reached. (b) and (e) are phase diagrams that display the nature of clustering with respect to y_1. (c) and (f) are illustrations of the corresponding system, color coordinated to show final synchronization.

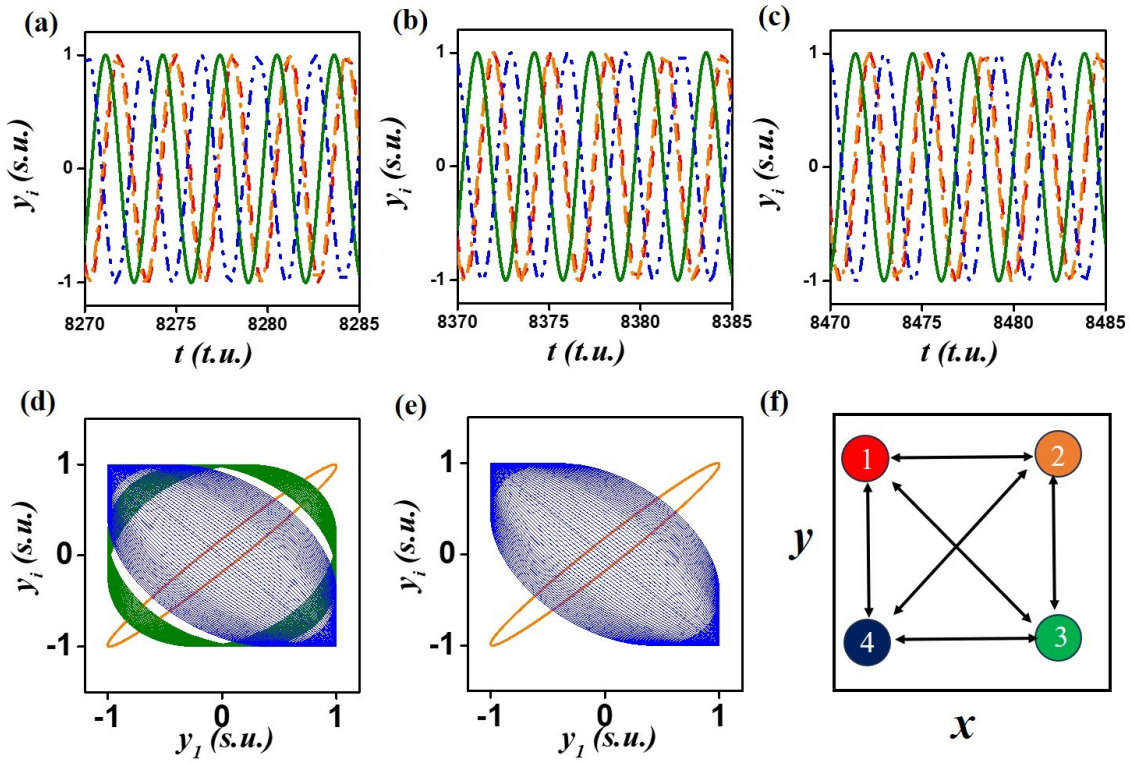

Figure 6.5: Chimera state observed in a four-rotor model system for $l = 2.57$ units. (a)-(b) Shows temporal evolution of the $y$coordinates across two different periods of time that clearly illustrates the asynchronous dynamics of the blue (dash-dot-dotted line) and olive (solid line) rotor. (c) and (d) are phase diagrams with respect to rotor1 and 3, respectively, showing the space-filling chiral dynamics of rotor 4, and a slow asynchrony of rotor 3, as rotors 1 and 2 synchronize in-phase to form a cluster. (f) is the color-coordinated illustrations of the rotors.

6.5.1 Cluster states

Figure 6.4 shows two results where the system exhibits clustering phenomena. A doublet-singlet-singlet state is observed for $l = 4.01$, where rotors 2 and 3 have synchronized in phase, and rotors 1 and 4 are lag synchronized, as is evident from the time-evolution and phase portrait [Fig 6.4(d) and (e)]. The lower panel of Fig. 6.4 demonstrates a triplet-singlet system for $l = 3.17$ space units. The phase portrait here clearly shows the in-phase synchronization of the three rotors 2, 3, and 4 [Fig. 6.4(a and b)]. For oscillators having exactly identical natural frequencies, cluster states are found over an appreciable range of l values. A phase diagram of the dynamical states with variation of l is explained below.

6.5.2 Chimera Dynamics

We introduced a tiny mismatch (<0.1%) in the value of the natural frequencies of the rotors, Ω_i. This could reflect the inherent heterogeneity of the experimental system, that could arise out of local noise or fluctuation. Considering this slight mismatch in the natural frequencies of the oscillators led to the observation of the elusive chimera dynamics, with a doublet cluster, albeit over a very narrow range of l-values. An example of a chimera state is given in Fig. 6.5. The time series of the four rotors show the prominent drift of the blue rotor-4. The rotors 1 and 2 are phase-locked, as is evident from Fig. 6.5(c), while rotor-3 displays an appreciable amount of asynchrony. The phase diagrams [Figs. 6.5(c) and 6.5(d)] bear testimony to the strikingly asynchronous dynamics of rotors 3 and 4, with respect to the synchronized pair, and each other. This coexistence of coherent and incoherent behavior is the signature of a chimera state.

6.5.3 Other dynamical states

Varying l for a large range is not possible for the experimental set-up, whereas in numerical simulation, it is possible. We explored dynamical states other than phase cluster and chimera. Fig. 6.6 shows two such phenomena. The phase portrait in

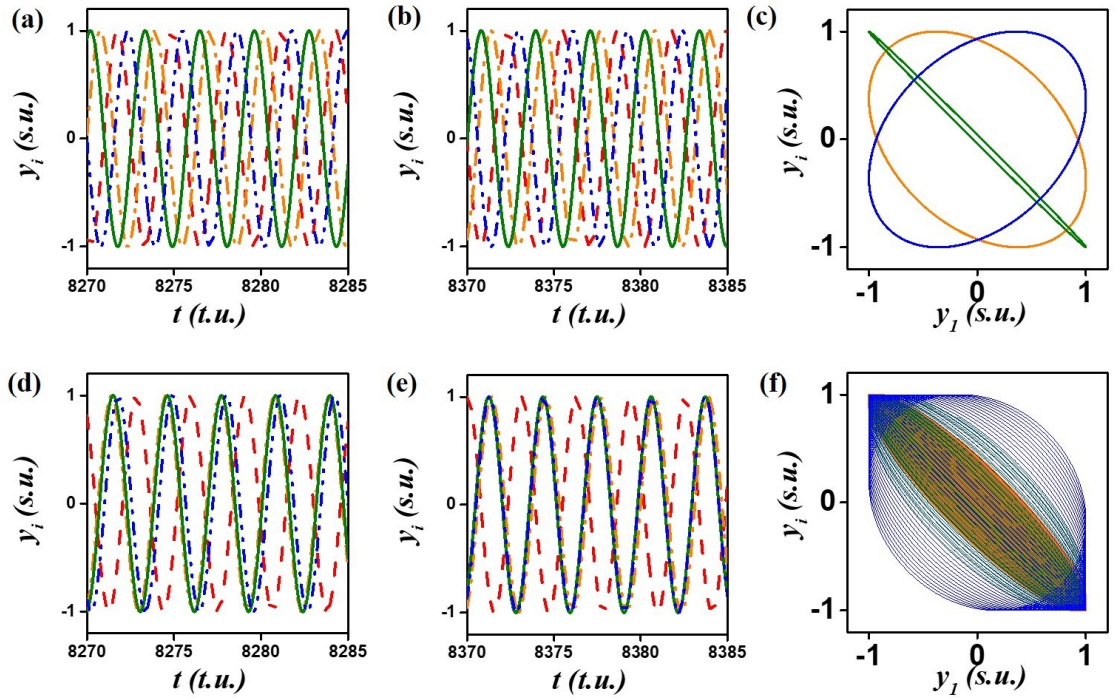

Figure 6.6: Phase lock cluster and complete asynchrony. Complete phase lock asynchronization at $l = 2.45$ of the unperturbed system (a to c). (a and b) are time series at two different stages, much after synchronization has been reached. Phase portraits at (c) show the absence of asynchrony in the system. (d, e, f) show the complete asynchrony at $l = 3.15$ for system with slightly perturbed natural frequency. Phase plot at (f) show the complete asynchronous behavior.

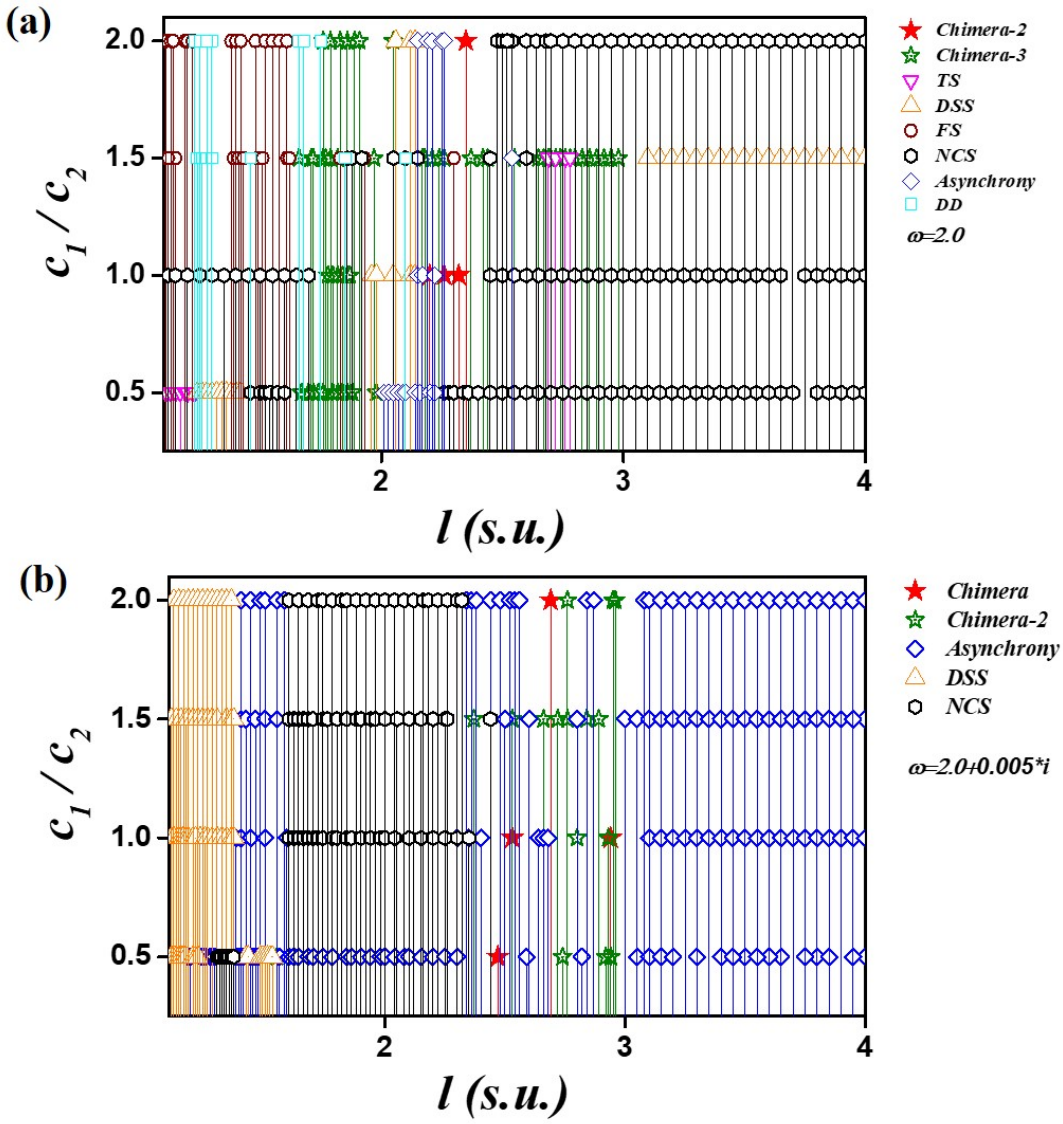

Figure 6.7: Phase diagram showing the variation of synchronization behavior with increasing l, for (a) unperturbed system ($\Omega_i = 2.0$) and (b) perturbed system (noise in Ω). Unique symbols have been used to depict a particular kind of synchronization and cluster formation. chimera-2 and chimera-3 are chimera like dynamics, but not exact chimera what we described in fig. 6.5, complete filling of the asynchronous oscillator is not observed in case of chimera-2 and chimera-3. TS, DSS, FS, NCS, DD represents Triplet-Singlet, Dublet-Singlet-Single, Full Synchonization or complete synchronization, No cluster synchronization or phase lock cluster, Doulet-Doublet states respectively. It can be seen that asynchrony is more prominant feature for a perturbed system than the unperturbed.

6.6(c) shows that all the oscillators are in sync with others, maintaining a definite lag. We call it a phase lock cluster. We also observed complete asynchrony of the rotors for certain l values when the initial frequency is slightly perturbed. One of those situation can be seen at 6.6(d,e,f). Complete filling of space in 6.6(f) represents the asynchronous dynamics. Figure 6.7 demonstrate the obseration of a range of different dynamical states.

6.6 Discussion and Conclusion

The coupling strength between any two particles depends upon their mutual force of interaction, which is a complex function of the inter-particle distance (r) and falls off with increasing r . Even when the spiral rotors are identical in their frequencies and placements, there exists an intrinsic heterogeneity in the interactive force experienced by each rotor, and hence the coupling strength, as the instantaneous distances of one rotor from all other rotors are determined by their mutual phase.

In conclusion, we have experimentally shown how a square network of pinned spirals in the BZ reaction-diffusion system, can be a candidate for the study of synchronization behavior of homogeneously coupled spiral rotors. Over and above general lag synchronization, and complete asynchrony, we have observed that spiral rotors can also form phase-clusters. In our experiments we came across two distinct types of cluster states, the doublet-singlet-singlet clusters and triplet-singlet clusters. We were also able to observe the state of coexisting synchronous and asynchronous behavior, or the chimera. Our mathematical model is able to shed some light on the emergence of the asymmetry in the otherwise symmetric system. One may merely envisage to what extent the interaction of multiple spirals (or scrolls) would alter the dynamics of an intricate system, such as the heart, were they to form partially synchronized states. It would be interesting to explore if such partial synchronization patterns are responsible for the cardiac death ensuing ventricular fibrillation. In networks of coupled oscillators, chimera has been known to lead to amplitude death [146]. Future studies of interacting spirals could focus on the possible death of

oscillations in excitable systems.

Summary

- Clustering and chimera dynamics is observed in a square network of four pinned spiral rotors.
- Chimera is the state where both synchronization and asynchronization takes place simultaneously in the same medium.
- Numerical study is being carried out with a modified Kuramoto based model.
- In experiment, the change of dynamics from a Triplet-Singlet cluster to Doublet-Singlet-Singlet cluster to chimera occurred with cahnge in size of the square.
- In numerical simulations, we found a rich dynamics over and above the above three states.

Chapter 7

Synchronization through signal transmission

7.1 Introduction

We went into detail about the synchronization phenomenon in the introductions of Chapters 5 and 6. We have demonstrated the synchronization of a pair of pinned counter-rotating spiral waves anchored to heterogeneities of different diameters [25] as well as synchronization pinned corotating spirals[147]. We observed cluster and chimera dynamics in a network of pinned spiral rotors in the previous chapter. Then we wondered how communication could play an important role in synchronization.

Huygen's pendulums show synchronization behavior when they are connected through a common wall [148]. The information from one clock to another clock was passed through the common base. This transformation of information leading to synchronization, gives a very basic idea that a communicator is required for oscillators to synchronize. So, the synchronization process can also be studied in terms of signal transmission. One of the very first signal transmission studies with BZ reaction was performed by Showalter *et al.* in 1994 [149]. However, in our knowledge, there is no such study with the spirals in the BZ reaction to date.

In earlier studies, it was observed that the pinned spirals anchored to heterogene-

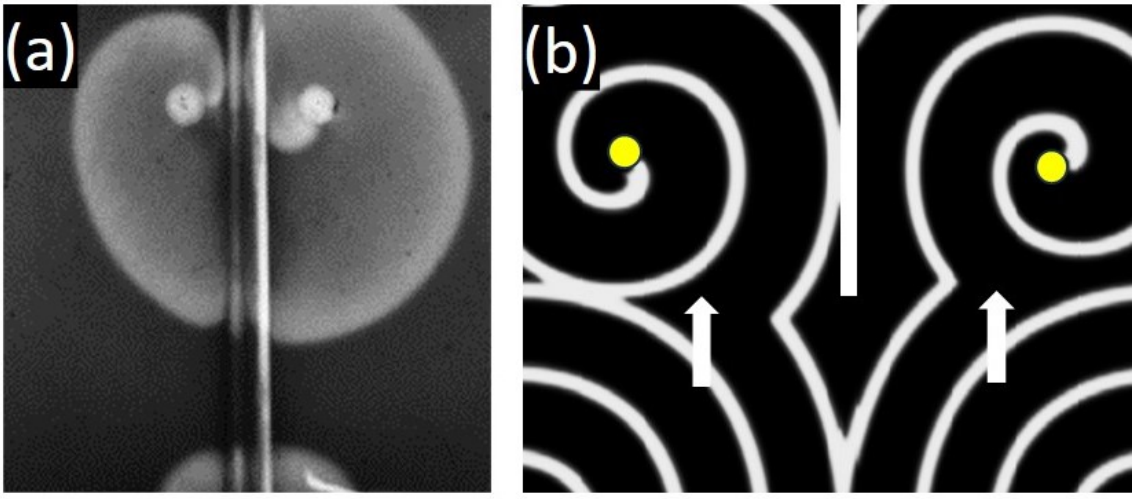

Figure 7.1: The system of study. Snapshot of an (a)experimental system (1.8 cm × 1.8 cm) and a (b) numerical simulation. The counter-rotating spirals are pinned to two circular regions, which are pinning heterogeneities of diameter 1.4 mm for the experimental system, and 24.5 s.u. for numerical simulation. A separating boundary separates the two spiral waves. The messenger wave near from the boundary grow towards the separated waves.

ity are unpinned and finally terminated when encountered with a wave train [150]. Here in this study, we investigated two pinned spirals, separated by a boundary. These individual pinned spirals are allowed to communicate with another wave, here we call a messenger wave. We report the occurrence of complete synchronization of the individual oscillators by the communication of this messenger. We also performed the numerical simulations on similar system and and encountered similar results.

7.2 Experimental methods

The basic experimental ingredients and procedure is same as described in chapter-6. Here we used thin boundary to separate the pinned spiral rotors, as shown in Fig 7.1(a). Thereafter a free spiral wave was generated from below. The free spiral has a faster frequency and is allowed to interact with the separated waves. Experimental

snapshots at 2s interval were recorded with a CCD camera placed on the top. Images were saved on a personal computer and analyzed with a MATLAB code. 7.1(a) demonstrates the experimental system under observation.

7.3 Numerical methods

The experimental scheme was mimicked in our numerical system. We carried out our numerical simulations with Barkley's reaction-diffusion model. The model loosely explains the BZ reaction-diffusion system has the form,

$$\epsilon \frac{\partial u}{\partial t} = \left[u(1-u)(u - \frac{v+b}{a}) \right] + D_u \nabla^2 u \tag{7.1}$$

$$\frac{\partial v}{\partial t} = u - v + D_v \nabla^2 v \tag{7.2}$$

Here, $\nabla^2 u = \frac{\partial^2 u}{\partial x^2} + \frac{\partial^2 u}{\partial y^2}$, $\nabla^2 v = \frac{\partial^2 v}{\partial x^2} + \frac{\partial^2 v}{\partial y^2}$; where, u is an activator, and v an inhibitor. A specific set of parameter values were able to generate spiral patterns. The parameter values were as follows: $a = 0.85$, $b = 0.07$, $\epsilon = 0.02$. Diffusion coefficient values D_u and D_v are considered equal (1.0). The numerical integration was solved using Euler's method to generate sustainable spirals in our 500×500 space grid system. The time step was taken as 0.01, and the space step size was taken as 0.35. We checked different values for choosing the space-step and time-step and selected the best values that produce good numerical accuracy and yields a stable pair of counter-rotating spirals in our system with zero flux boundary conditions. To separate the spirals we introduce a rectangular area setting u and v zero inside that area and also setting a zero flux boundary (at the separating-boundary). To observe the influence of a messenger wave, the separating-boundary was set up to a desired distance(s.u.) as shown in Fig. 7.1(b). Spirals under our observation were anchored to a circular heterogeneity of diameter of 24.5 s.u. They were pinned with a time lag so that a phase difference remain at the initial stage.

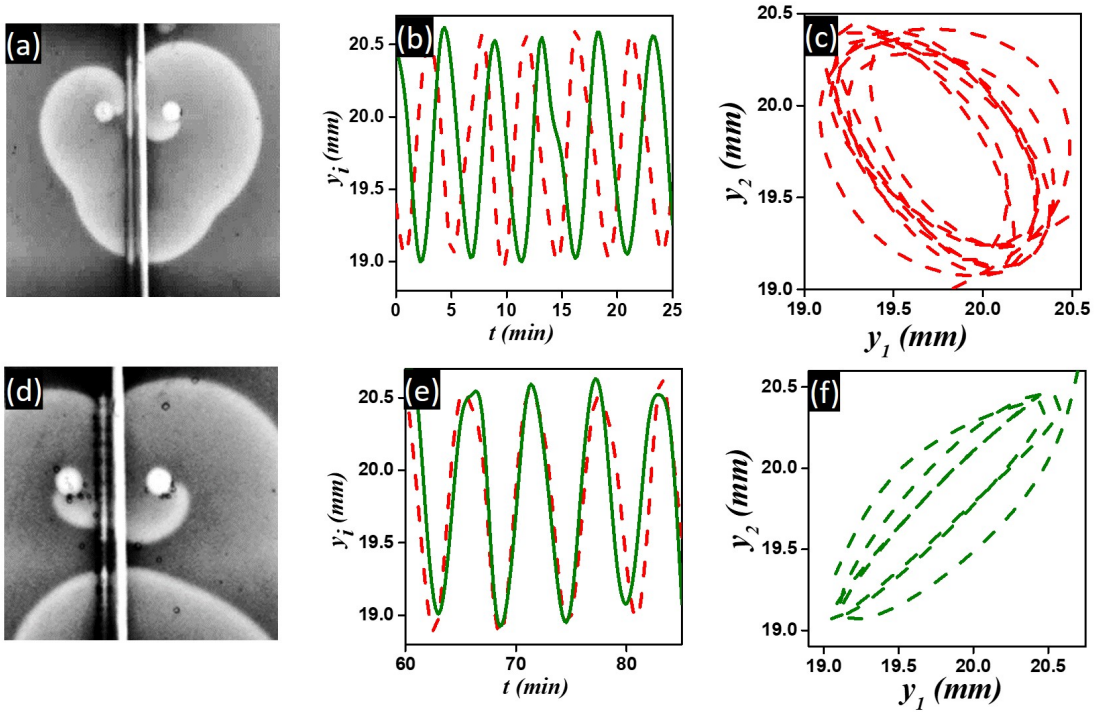

Figure 7.2: Experimental results for symmetrical system with respect to physical boundary. Snapshots - a (2 cm × 2 cm) and d (1.5 cm × 1.5 cm) are at the begining (1^{st} rotation) and after the synchronization is achieved (11^{th} rotation). (b) and (e) depicts the initial and final time series, (c) and (f) show the corresponding phase plots. The top pannel (a,b, and c) show the intial dynamics and (d,e, and f) show the final dynamics after synchronization.

7.4 Results

7.4.1 Experimental Findings

We first separated two counterrotating spiral waves with a thin boundary and then pinned them with a circular heterogeneity of diameter of 1.4 mm. One arm of each spiral was attached to that thin boundary. For analysis, we observed the trajectories of both the pinned spiral rotors. A time series analysis of the y-coordinates and phase plots of both spiral rotors is efficient in explaining the change of dynamics

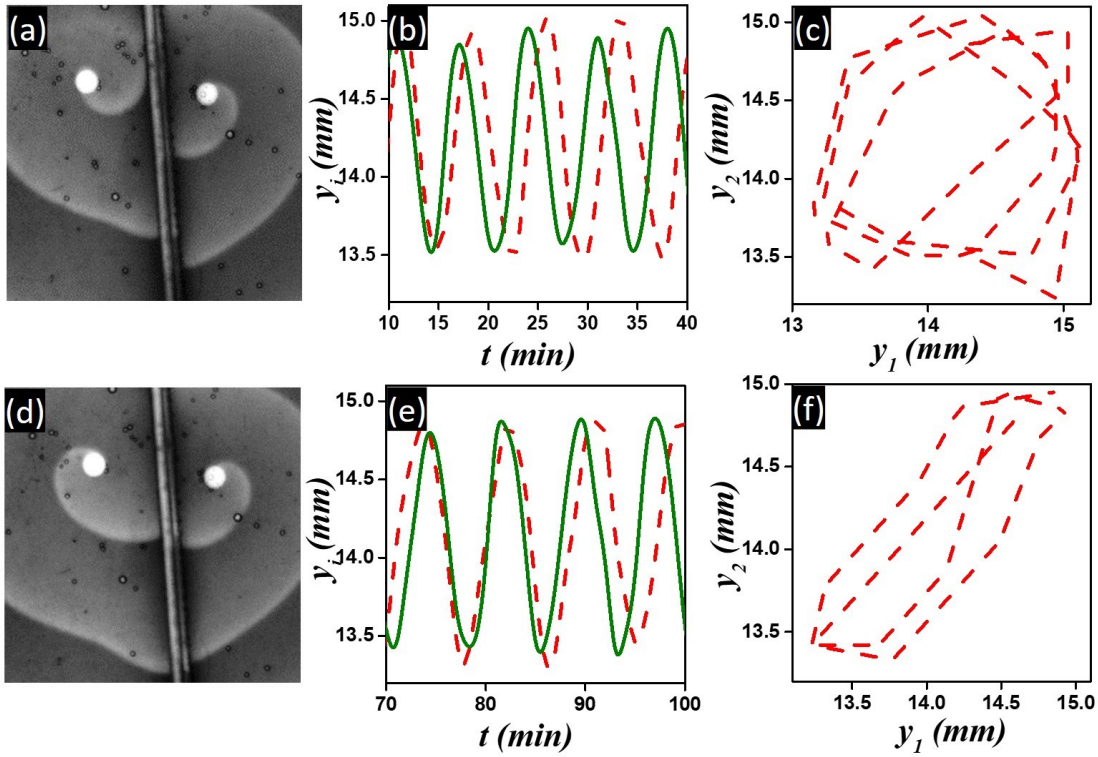

Figure 7.3: Experimental results for assymmetric system with respect to physical boundary. (a and d) are the snapshots (2 cm × 2 cm) at the begining and after the synchronization is achieved . (b) and (e) demonstrate the initial and final time evolution plots, (c) and (f) show the corresponding phase plots. The top pannel (a,b, and c) show the intial dynamics and (d,e, and f) show the final dynamics after synchronization.

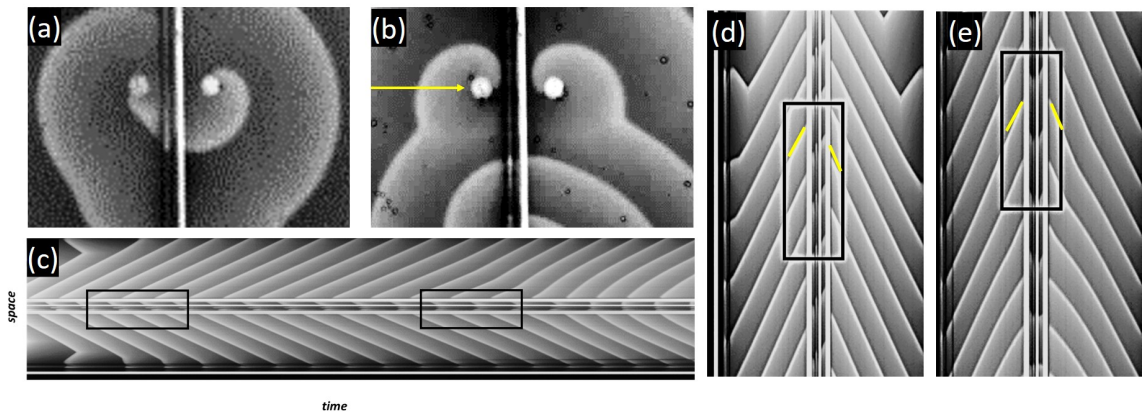

Figure 7.4: Illustrates the phase synchronization with snapshots and a time-space plot. (a) show the snapshot (1.5 cm × 2.2 cm) at 7 min after the beginning of the reaction. (b) show a snapshot (1.5 cm × 2.2 cm) at 72 min after the beginning of the reaction. (c) show a time-space plot of around 100 minutes. The yellow arrow at (b) show the line along which the time-space plot is recorded. The tip position of the rotors 1 (left) and 2(right) at (a) clearly shows the phase difference, whereas, in (b) the rotors have zero phase difference. The time-space plot also describes the phase change scenario. The black boxes in (c) show how the phase difference between the spirals decreases with time. A zoomed view of the space-time plot is depicted in (d) for intial and in (e) for final stage of the reaction.

before and after the interaction with the free messenger wave. y_i is the instantaneous y-coordinate of the $i-th$ spiral under our observation.

The experiments are performed in two categories. (1) When pinned spiral rotors are placed symmetrically from the thin separating boundary and (2) when they are in asymmetric position with respect to the boundary. Fig. 7.2 demonstrates the first case. Two individual pinned spirals were not in synchrony at the initial stages. This can be seen from the time evolution plot at Fig. 7.2(b). The phase plot at Fig. 7.2(c) also confirms the observation. Fig. 7.2(c) show the y_2 coordinate is spread over the whole space when plotted against y_1 and confirms that the two spirals are out of sync. The Fig. 7.2(e) shows the time series for a later stage of the experiment, and the corresponding phase plot at Fig. 7.2(f) demonstrates the achievement of synchronization. This synchronization through the forcing of the messenger wave can also be observed in Fig. 7.4. The initial snapshot (Fig. 7.4(a)) and the final snapshot (Fig. 7.4(b)) show the decrease of phase difference. The time-space plot at Fig. 7.4(c,d,e) also confirms the same phenomena.

The Fig. 7.3 demonstrates a different scenario, when the pinned spirals are asymmetrically placed with respect to the separating boundary. The time evoluation plots at Fig. 7.3 (b) show the initial asynchrony, whereas Fig.7.3(e) at the later stage show the synchronized dynamics. The phase plots at 7.3(c and f) also replicate the same behaviors.

7.4.2 Numerical Findings

We establish a similar situation in our numerical simulations. Three different situations are created- 1) when two pinned spirals are symmetric with respect to separating boundary in presence of messenger wave, 2) when two pinned spirals are asymmetric with respect to the separating boundary and 3) When there is no messenger wave. We looked at the tip positions and plotted the y-coordinate positions with respect to time. A phase plot of the initial and the final state also describes the dynamical change.

For case-1 and 2, when pinned spirals under our observation are arranged in

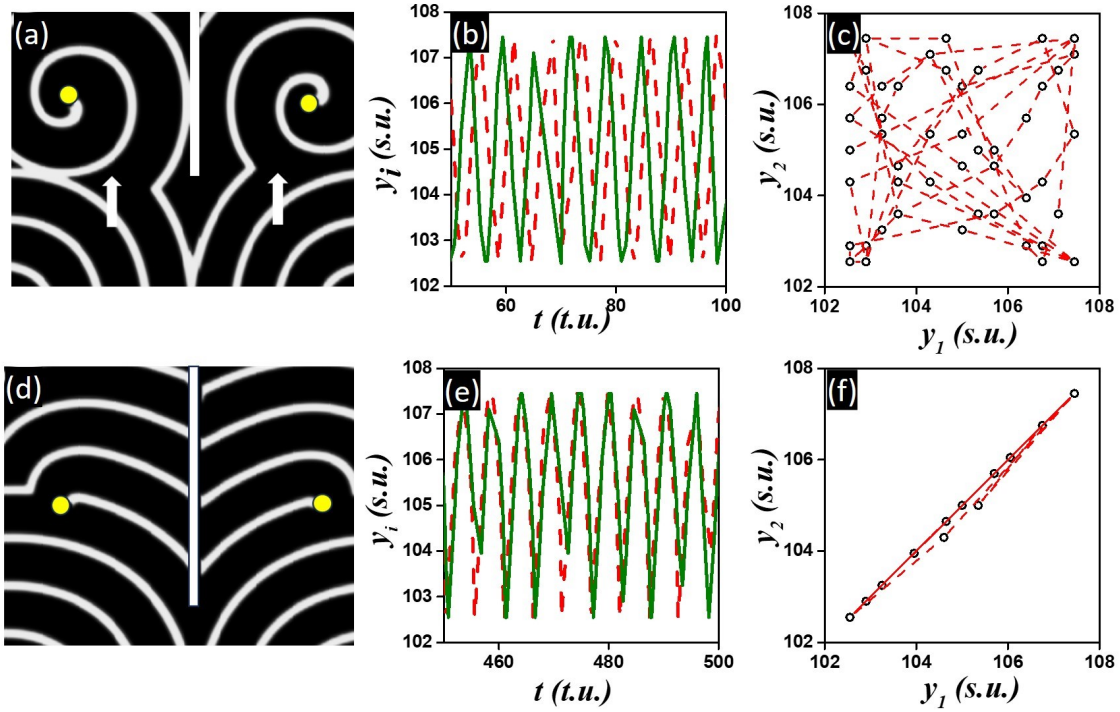

Figure 7.5: Illustration of simulation results for a symmetrical system. (a) and (d) are the snapshots ((116.6 s.u. × 145.8 s.u)) of 100 t.u. and 500 t.u. for a numerical simulation where the separation boundary is up to a particular length, and a messenger wave is communicating from the below. The direction of propagation of the communicating wave is described with the upward arrow in (a). (b, e) show the time series and (c, f) are corresponding phase plots. (e,f) demonstrate the final synchronization states.

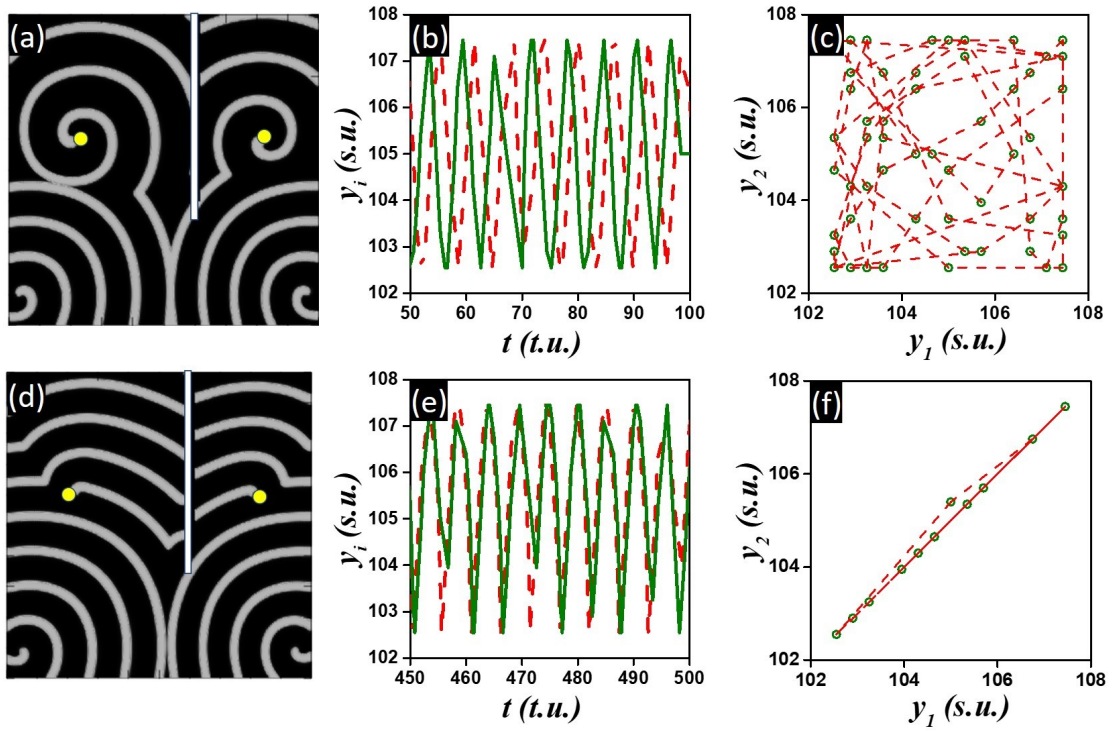

Figure 7.6: Illustration of simulation results for a assymmetric system. (a) and (d) are the snapshots ((175.0 s.u. $\times$ 175.0 s.u)) of 100 t.u. and 700 t.u. (b and e) show the time series and (c, f) are the corresponding phase plots. (e,f) demonstrate the final synchronization states.

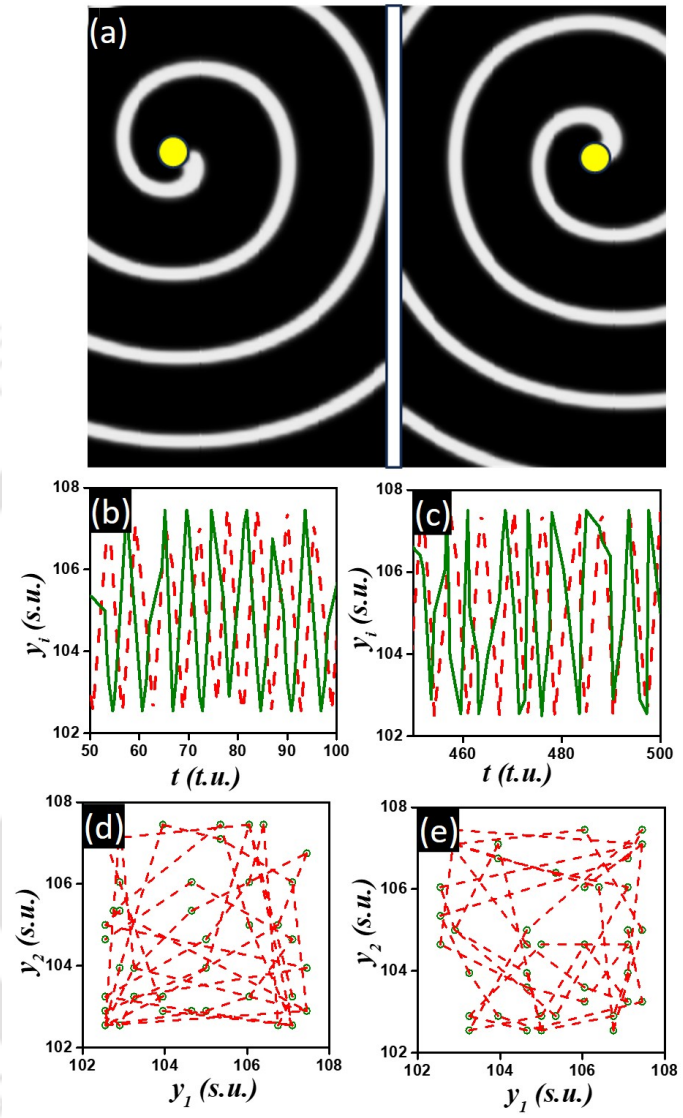

Figure 7.7: The simulation time series and phase plots for a system with two completely separated pinned spirals in the absence of messenger wave. (a) Snapshot of the system, (b) and (c) are the initial and final time evolution plots describing no change in the collective behavior. (d) and (e) are the corresponding phase plots for the time series plots at (b) and (c), respectively. The phase plots at the initial and final times show the absence of any synchronization phenomena.

symmetric and asymmetric fashion with respect to the separating boundary, we noticed the synchronization phenomena is spotted finally. Fig. 7.5(b and c) show the initial dynamics for a symmetrical system and indicate the presence of asynchrony at the initial stage. This is same for asymmetric system as shown in Fig. 7.6(b and c). The final state is a synchronized state in both the cases for symmetrical as well as for asymmetrical and can be perceived from Fig. 7.5(e and f) and from Fig. 7.6(e and f) when a third messenger wave is forcing from below. For the case-3, when there is no messenger wave, synchronization is not achieved as illustrated in Fig. 7.7. The time series plot describes the asynchrony at initial and final states. The phase plots also show the spreading of y_2 over the whole space with respect to y_1.

7.5 Discussion and conclusion

We report the phase synchronization of two spiral rotors under the influence of a third (messenger) wave. The final complete synchronization is actually complete antiphase synchronization as our rotors are counterrotating. We did not make the rotors unidirectional during our calculation as our intention was to notice the effect of the messenger wave only. Complete (phase/antiphase) synchronization behavior in presence of the messenger wave show the decrease of the phase difference.

Our experiment showed that complete synchronization occurs if there is some communication. If no communication is present, a complete phase synchronization state will not occur. In chapter-5, We discussed if two counterrotating spirals were pinned in a BZ medium, they completely synchronize if the pinning heterogeneity is of the same diameter, and synchronized with a lag if they are of different diameters. Here we cut off the initial communication between the counterrotating pinned spiral rotors so that they behave like individual spiral rotors. We establish that those individual waves do not synchronize until the communicating messenger wave communicates with them. Our numerical simulation also supports the results obtained in the experiments. As the nature of any wave is to communicate information, here also we found the information sharing of messenger waves leads to complete synchronization. This synchronization of the pinned rotors by the signal transmission of the

messenger wave in the BZ chemical system is being reported for the first time. It establishes Huygen's observation of pendulum sympathy in chemical systems. Waves are capable of sending information and here they determine the fate of the other two which were under our observation. Our messenger spirals can also be compared with wave trains. A study by Pumir *et al.* [150] showed that loosely anchored spirals can be unpinned with wave trains. In our study we found this wave train can help in synchronizing.

A broad range of work can be found on synchronization induced by noise, optical feedback etc. Here we described the synchronization induced by another wave. One can further work by applying chemical noise to the system of two separated pinned spiral waves. Future work can also be done by manyfold compartmentalizing our present system and observing the collective nature. As signal transmission is a very important process in terms of our communication system as well as our neuronal system, this work may shed light on those systems.

Finally, we conclude our discussion by explaining the relation with our cardiac system. As scar tissues are present in our heart, broken cardiac waves may get attached to those. The presence of both free and multiple pinned spirals in our heart and their mutual communication leading to synchronization may lead to fatal situation. Thus, the study of this kind is necessary.

Summary

- Synchronization occurs through communication or coupling.
- Two individual pinned spirals separated through a boundary is studied.
- Another wave (messenger) forced to phase-synchronize two individual waves.
- Numerical results show synchronization of separated spirals will not take place if there is absence of the messenger wave.

- Relative position of the pinned spirals from the separating boundary (Symmetric/Asymmetric) does not affect the final outcome.

Chapter 8

Conclusions

In this thesis we began with a free individual spiral and attempted to control it with a mild concentration gradient. Then, we moved to a pair of pinned spiral waves and looked at their synchronization. We then investigated pinned spirals in a network. Our findings es-tablish that mild gradients can control the dynamics of spirals in a BZ reaction but are un-able to unpin them from heterogeneities. We report the synchronization in a pair of spirals and clustering and chimera dynamics in a network of four spirals placed in square geome-try. We hope this work, motivated by the cardiac system, will enrich the literature and con-tribute to understanding the mechanism of ventricular fibrillation and defibrillation tech-niques in a better way. We have been able to answer a few questions and the outcomes have also generated some new questions to work on.

8.1 Answered and Unanswered Questions

The major contributions and original works in this thesis will be summarised in this section.

8.1.1 Spiral Breakup

We explored **(chapter 3)** in our numerical simulations of a modified Oregonator model developed from FKN mechanism that a spontaneous spiral breakup leading to chaos is possible and that it can be brought about by a change in the concentration of hydrogen ion in the system. Although, as of now, we do not have any experimental evidence from our experiments with the BZ system, which depicts this phenomena inside a Petri Dish.

8.1.2 Spiral drift with mild gradient

In **chapter 4**, we have shown how a mild concentration gradient can drift rigidly rotating spirals. We showed that the drift is controllable by varying the gradient strength, i.e. by modifying the source of the concentration gradient; in our case a proton exchange resin.

Anamolous drift of spiral tips

In our experiments for spiral drift in presence of a mild concentration gradient we observed some chaotic movements of the spiral tips at a later stage of the experiment (after 120 min from the addition of the beads). This can be seen in Fig. 8.1. The reason of this anamolous drift is still unknown to us.

8.1.3 Synchronization and Chimera dynamics

The cardiac system is more heterogeneous than our experimental system that is largely homogeneous. Hence, incorporating heterogeneity in the medium will take it closer to the cardiac system. For the first time, we have shown in our experiments, as well as in our numerical simulation, that pinned spiral rotors synchronize in frequency as well as in phase **(chapter 5 and 6)**. We have also reported a plethora of dynamical states including chimera and clusters for identical spiral rotors arranged in a square geometry **(chapter 6)**.

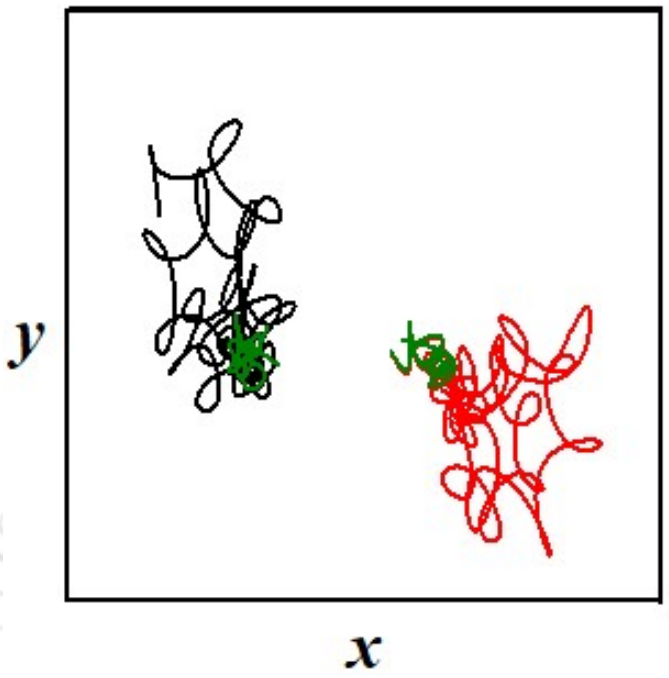

Figure 8.1: Anamolous drift of spiral tips. Full trajectory of right(red) and left(black) spiral tips. The Olive colour show the intial trajectory (0-30 min) after the addition of the resin beads for our typical experiment.

Extended Eight Rotor System

From a square geometry of four rotors we extended our system to a regular octagonal network. As the number of oscillators increased, the complexity of the system also increased. One can expect the outcome of chimera dynamics is more feasable in a bigger network. In our experiment with eight rotors we observed a clustering dynamics. Figure 8.2 show one such example of TTSS (Triplet-Triplet-Singlet-Singlet) cluster. It may be possible to have chimera dynamics depending upon the size of the octagon or other coupling parameters, which needs further study and analysis.

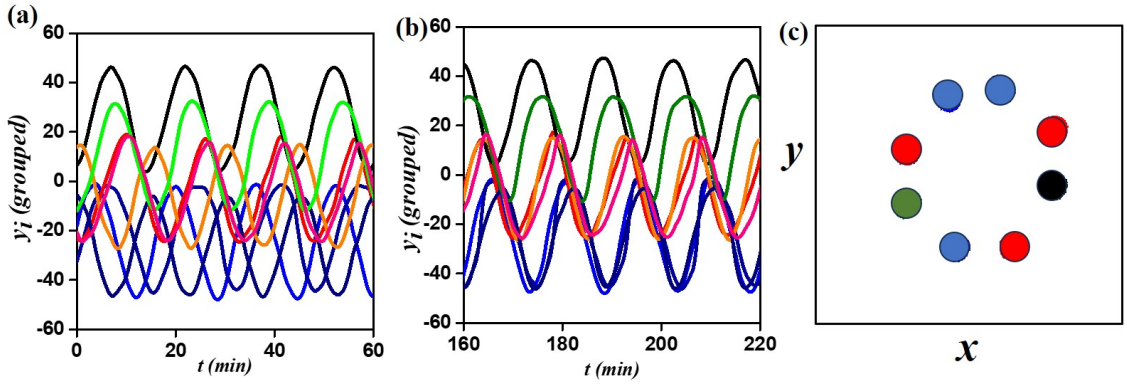

Figure 8.2: Clustering in an eight rotor experimental system. (a) and (b) depict the initial and final time-evaluation plots of the rotors. The rotors are grouped according to their clustering pattern. Color coordinated (c) shows the Triplet-Triplet-Singlet-Singlet dynamical state.

8.1.4 Synchronization through a messenger wave

In **chapter 7**, we reproduced the Huygen's observation of pendulam sympathy in our chemical reaction-diffusion system where a wave or messenger transfers its information to other two individual spirals and controll their collective nature.

8.2 Limitations

1. There is a limitation in the production of spirals at such concentrations of hydrogen ions in our experimental system, so as to achive a spiral breakup phenomena.
2. Making a perfect corotating spiral in our experimental system is still a challenge for us.

8.3 Future Directions

We studied spiral waves with a motivation of understanding the human cardiac system. Spirals in the BZ system are the two dimensional counterparts of scroll

waves, which are three dimensional in nature. While we could not unpin the pinned spirals with our mild concentration gradient, future works can be carried out to study the unpinng of a pinned scroll wave with such mild gradients. The synchronization we observed for pinned spirals, can be extended to pinned scrolls in the future. We achived synchronization of two separated spirals through information transmition by another wave. Information transmission properties of spiral waves can be explored in details in the future. Besides these, as we studied the collective behavior of pinned rotors in a network, one can extend this work for more complex higher order networks. These are some possible future works but should not be limited to this.

Publications

- H. Kalita, **P. Khan**, and S. Dutta, Rotational synchronization of pinned spiral waves, *Phys. Rev. E*, 106, 034201(2022).
- Synchronization of corotating spirals anchored to heterogeneities in a chemical system, **P. Khan**, and S. Dutta, *Eur. Phys. J. Spec. Top.* 233, 787-795(2024).
- Controlling spiral wave dynamics in the BZ-system: drift, suppression and turbulence, **P. Khan**, and S. Dutta (Under review)
  (arXiv version: https://doi.org/10.48550/arXiv.2403.15731).
- Effect of concentration gradient on spiral wave dynamics, **P. Khan**, and S. Dutta (Under review).
- Complete synchronization of two spirals by a messenger wave in a reaction-diffusion system, **P. Khan**, and S. Dutta, *CHAOS* 34, 091103(2024).
- Chimera and cluster states in a network of pinned spiral rotors. **P. Khan**, H.Kalita, and S. Dutta (Communicated).
- A journey into the world of scroll waves: perspectives from a chemical laboratory (Book Chapter), S. Dutta, D. Mahanta, **P. Khan** (Communicated).

Selected Conference Presentation

- Presented a poster at CTTC-2022, A national level conference held at BARC,Mumbai, India.
- Presented a poster at RAC-TCA-2022, A national level conference held at NEHU, Shilong, India. (**Awarded with best poster)**.
- Presented a poster at FICS-2022, An international conference held at IIT Guwahati, India.
- Presented a poster at PNLD-2023, An international conference held at IIT Madras, India. (**Awarded with best poster)**.
- Presented an oral presentation at CNSA-2024, An international conference held at IIT Bhubaneswar, India.
- Presented an oral presentation at CDSA-2024, An international conference held at Digha, West Bengal, India.

Bibliography

[1] Steven H Strogatz. *Nonlinear dynamics and chaos: with applications to physics, biology, chemistry, and engineering*. CRC press, 2018.

[2] Irving R Epstein and Kenneth Showalter. Nonlinear chemical dynamics: oscillations, patterns, and chaos. *The Journal of Physical Chemistry*, 100(31):13132–13147, 1996.

[3] Francesc Sagués and Irving R Epstein. Nonlinear chemical dynamics. *Dalton transactions*, (7):1201–1217, 2003.

[4] Vladimir Sergeevich Zykov. *Simulation of wave processes in excitable media*. Manchester University Press, 1987.

[5] Marek Orlik. Self-organization in nonlinear dynamical systems and its relation to the materials science. *Journal of Solid State Electrochemistry*, 13:245–261, 2009.

[6] Shigeru Kondo and Takashi Miura. Reaction-diffusion model as a framework for understanding biological pattern formation. *science*, 329(5999):1616–1620, 2010.

[7] Alan Mathison Turing. The chemical basis of morphogenesis. *Bulletin of mathematical biology*, 52:153–197, 1990.

[8] Irving R Epstein and John A Pojman. *An introduction to nonlinear chemical dynamics: oscillations, waves, patterns, and chaos*. Oxford university press, 1998.

[9] Patrick De Kepper, Irving R Epstein, and Kenneth Kustin. A systematically designed homogeneous oscillating reaction: the arsenite-iodate-chlorite system. *Journal of the American Chemical Society*, 103(8):2133–2134, 1981.

[10] Stephen K Scott. *Chemical chaos*. Number 24. Oxford University Press, 1993.

[11] José Jalife. Introduction to the series on computational approaches to cardiac arrhythmias: Translation into diagnostics and therapy. *Circulation Research*, 112(5):831–833, 2013.

[12] Simon Stewart, Carole L Hart, David J Hole, and John JV McMurray. A population-based study of the long-term risks associated with atrial fibrillation: 20-year follow-up of the renfrew/paisley study. *The American journal of medicine*, 113(5):359–364, 2002.

[13] Srijoy Mahapatra, Damien J LaPar, Castigliano M Bhamidipati, George McDaniel, Sandeep Kamath, T Jared Bunch, and Gorav Ailawadi. Incidence, risk factors, and consequences of new-onset atrial fibrillation following epicardial ablation for ventricular tachycardia. *Europace*, 13(4):548–554, 2011.

[14] Akikazu Fujita, Hiroshi Hibino, and Yoshihisa Kurachi. Regulation of ion channels by membrane proteins and cytoskeleton. In *Cell Physiology Source Book*, pages 601–622. Elsevier, 2001.

[15] Sergio Alonso, Markus Bär, and Blas Echebarria. Nonlinear physics of electrical wave propagation in the heart: a review. *Reports on Progress in Physics*, 79(9):096601, 2016.

[16] José Jalife, Mario Delmar, Justus Anumonwo, Omer Berenfeld, and Jerome Kalifa. *Basic cardiac electrophysiology for the clinician*. John Wiley & Sons, 2011.

[17] Thomas E Applegate. Atrial arrhythmias. *Primary Care: Clinics in Office Practice*, 27(3):677–708, 2000.

[18] AT Winfree. Electrical turbulence in three-dimensional heart muscle. *Science*, 266(5187):1003–1006, 1994.

[19] José Jalife, Richard A Gray, Gregory E Morley, and Jorge M Davidenko. Self-organization and the dynamical nature of ventricular fibrillation. *Chaos: An Interdisciplinary Journal of Nonlinear Science*, 8(1):79–93, 1998.

[20] KI Agladze and P De Kepper. Influence of electric field on rotating spiral waves in the belousov-zhabotinskii reaction. *The Journal of Physical Chemistry*, 96(13):5239–5242, 1992.

[21] O Steinbock, J Schütze, and SC Müller. Electric-field-induced drift and deformation of spiral waves in an excitable medium. *Physical review letters*, 68(2):248, 1992.

[22] Parisa Sadeghi and Harm H Rotermund. Gradient induced spiral drift in heterogeneous excitable media. *Chaos: An Interdisciplinary Journal of Nonlinear Science*, 21(1), 2011.

[23] Faridon Amdjadi, Mark Carter, and Jaganathan Gomatam. The eikonal equation and meandering of spiral waves: A geometrical approach. *Applied Mathematics and Computation*, 225:1–6, 2013.

[24] IV Biktasheva and VN Biktashev. Wave-particle dualism of spiral waves dynamics. *Physical Review E*, 67(2):026221, 2003.

[25] Hrishikesh Kalita, Parvej Khan, and Sumana Dutta. Rotational synchronization of pinned spiral waves. *Physical Review E*, 106(3):034201, 2022.

[26] Hrishikesh Kalita and Sumana Dutta. Interaction of multiple spiral rotors in a reaction-diffusion system. *Physical Review E*, 105(5):054213, 2022.

[27] Arkady Pikovsky, Michael Rosenblum, Jürgen Kurths, and A Synchronization. A universal concept in nonlinear sciences. *Self*, 2:3, 2001.

[28] Fatemeh Parastesh, Sajad Jafari, Hamed Azarnoush, Zahra Shahriari, Zhen Wang, Stefano Boccaletti, and Matjaž Perc. Chimeras. *Physics Reports*, 898:1–114, 2021.

[29] Richard J Field, Endre Koros, and Richard M Noyes. Oscillations in chemical systems. ii. thorough analysis of temporal oscillation in the bromate-cerium-malonic acid system. *Journal of the American Chemical Society*, 94(25):8649–8664, 1972.

[30] AM Turing. The chemical basis of morphogenesis. *Phil. Trans. R. Soc. Lond. B*, 237:37–72, 1952.

[31] Elizabeth M Cherry and Flavio H Fenton. Visualization of spiral and scroll waves in simulated and experimental cardiac tissue. *New Journal of Physics*, 10(12):125016, 2008.

[32] Xiaoying Huang, Weifeng Xu, Jianmin Liang, Kentaroh Takagaki, Xin Gao, and Jian-young Wu. Spiral wave dynamics in neocortex. *Neuron*, 68(5):978–990, 2010.

[33] Eiríkur Pálsson, Kyoung J Lee, Raymond E Goldstein, Jakob Franke, Richard H Kessin, and Edward C Cox. Selection for spiral waves in the social amoebae dictyostelium. *Proceedings of the National Academy of Sciences*, 94(25):13719–13723, 1997.

[34] Stephen K Scott. *Chemical chaos*. Number 24. Oxford University Press, 1993.

[35] Irving R Epstein and John A Pojman. *An introduction to nonlinear chemical dynamics: oscillations, waves, patterns, and chaos*. Oxford university press, 1998.

[36] Anatol M Zhabotinsky. A history of chemical oscillations and waves. *Chaos: An Interdisciplinary Journal of Nonlinear Science*, 1(4):379–386, 1991.

[37] Arthur T Winfree. Rotating chemical reactions. *Scientific American*, 230(6):82–95, 1974.

[38] James D Murray and James D Murray. Epidemic models and the dynamics of infectious diseases. *Mathematical biology*, pages 610–650, 1993.

[39] Richard M Noyes, Richard Field, and Endre Koros. Oscillations in chemical systems. i. detailed mechanism in a system showing temporal oscillations. *Journal of the American Chemical Society*, 94(4):1394–1395, 1972.

[40] Richard J Field and Richard M Noyes. Oscillations in chemical systems. iv. limit cycle behavior in a model of a real chemical reaction. *The Journal of Chemical Physics*, 60(5):1877–1884, 1974.

[41] Alfred Gierer and Hans Meinhardt. A theory of biological pattern formation. *Kybernetik*, 12:30–39, 1972.

[42] Myles J Fisher, Idupulapati M Rao, Miguel Angel Ayarza, CE Lascano, JI Sanz, Richard J Thomas, and Raúl R Vera. Carbon storage by introduced deep-rooted grasses in the south american savannas. *Nature*, 371(6494):236–238, 1994.

[43] Dwight Barkley. Euclidean symmetry and the dynamics of rotating spiral waves. *Physical Review Letters*, 72(1):164, 1994.

[44] Gavin R Armstrong, Annette F Taylor, Stephen K Scott, and Vilmos Gáspár. Modelling wave propagation across a series of gaps. *Physical Chemistry Chemical Physics*, 6(19):4677–4681, 2004.

[45] Paul K Becker and Richard J Field. Stationary concentration patterns in the oregonator model of the belousov-zhabotinskii reaction. *The Journal of Physical Chemistry*, 89(1):118–128, 1985.

[46] Dhriti Mahanta, Nirmali Prabha Das, and Sumana Dutta. Spirals in a reaction-diffusion system: dependence of wave dynamics on excitability. *Physical Review E*, 97(2):022206, 2018.

[47] Jorge M Davidenko, Arcady V Pertsov, Remy Salomonsz, William Baxter, and José Jalife. Stationary and drifting spiral waves of excitation in isolated cardiac muscle. *Nature*, 355(6358):349–351, 1992.

[48] Alexandre V Panfilov. Spiral breakup as a model of ventricular fibrillation. *Chaos: An Interdisciplinary Journal of Nonlinear Science*, 8(1):57–64, 1998.

[49] Lu Qun Zhou and Qi Ouyang. Experimental studies on long-wavelength instability and spiral breakup in a reaction-diffusion system. *Physical Review Letters*, 85(8):1650, 2000.

[50] M Bär and M Eiswirth. Turbulence due to spiral breakup in a continuous excitable medium. *Physical Review E*, 48(3):R1635, 1993.

[51] Suparinthon Anupong, Igor Schreiber, and On-Uma Kheowan. Turbulent pattern in the 1, 4-cyclohexanedione belousov–zhabotinsky reaction. *Physical Chemistry Chemical Physics*, 22(48):28213–28221, 2020.

[52] Matthew D Eager, Marianne Santos, Milos Dolnik, Anatol M Zhabotinsky, Kenneth Kustin, and Irving R Epstein. Dependence of wave speed on acidity and initial bromate concentration in the belousov-zhabotinsky reaction-diffusion system. *The Journal of Physical Chemistry*, 98(42):10750–10755, 1994.

[53] Junzhong Yang, Fagen Xie, Zhilin Qu, and Alan Garfinkel. Mechanism for spiral wave breakup in excitable and oscillatory media. *Physical review letters*, 91(14):148302, 2003.

[54] JJ Taboada, Alberto Pérez Muñuzuri, V Pérez-Muñuzuri, M Gómez-Gesteira, and V Pérez-Villar. Spiral breakup induced by an electric current in a belousov–zhabotinsky medium. *Chaos: An Interdisciplinary Journal of Nonlinear Science*, 4(3):519–524, 1994.

[55] Hans Juergen Krug, Ludwig Pohlmann, and Lothar Kuhnert. Analysis of the modified complete oregonator accounting for oxygen sensitivity and photo-

sensitivity of belousov-zhabotinskii systems. *Journal of Physical Chemistry*, 94(12):4862–4866, 1990.

[56] Kritsana Khaothong, Jarin Osaklung, Malee Sutthiopad, Jiraporn Luengviriya, Kenneth Showalter, and Chaiya Luengviriya. Effect of excitability on partially pinned scroll waves in excitable chemical media. *Physical Review E*, 108(5):054201, 2023.

[57] W Jahnke, WE Skaggs, and Arthur T Winfree. Chemical vortex dynamics in the belousov-zhabotinskii reaction and in the two-variable oregonator model. *The Journal of Physical Chemistry*, 93(2):740–749, 1989.

[58] José Jalife, Mario Delmar, Justus Anumonwo, Omer Berenfeld, and Jerome Kalifa. *Basic cardiac electrophysiology for the clinician*. John Wiley & Sons, 2011.

[59] Francis X Witkowski, L Joshua Leon, Patricia A Penkoske, Wayne R Giles, Mark L Spano, William L Ditto, and Arthur T Winfree. Spatiotemporal evolution of ventricular fibrillation. *Nature*, 392(6671):78–82, 1998.

[60] Elizabeth M Cherry and Flavio H Fenton. Visualization of spiral and scroll waves in simulated and experimental cardiac tissue. *New Journal of Physics*, 10(12):125016, 2008.

[61] Eiríkur Pálsson, Kyoung J Lee, Raymond E Goldstein, Jakob Franke, Richard H Kessin, and Edward C Cox. Selection for spiral waves in the social amoebae dictyostelium. *Proceedings of the National Academy of Sciences*, 94(25):13719–13723, 1997.

[62] Xiaoying Huang, Weifeng Xu, Jianmin Liang, Kentaroh Takagaki, Xin Gao, and Jian-young Wu. Spiral wave dynamics in neocortex. *Neuron*, 68(5):978–990, 2010.

[63] Rajeev Singh, Jinshan Xu, Nicolas G Garnier, Alain Pumir, and Sitabhra Sinha. Self-organized transition to coherent activity in disordered media. *Physical Review Letters*, 108(6):068102, 2012.

[64] NA Gorelova and J Bureš. Spiral waves of spreading depression in the isolated chicken retina. *Journal of neurobiology*, 14(5):353–363, 1983.

[65] Arthur T Winfree. Spiral waves of chemical activity. *Science*, 175(4022):634–636, 1972.

[66] S Nettesheim, A Von Oertzen, HH Rotermund, and G Ertl. Reaction diffusion patterns in the catalytic co-oxidation on pt (110): front propagation and spiral waves. *The Journal of chemical physics*, 98(12):9977–9985, 1993.

[67] Sumana Dutta, Nirmali Prabha Das, and Dhriti Mahanta. Dynamics and control of spiral and scroll waves. *Complexity and Synergetics*, pages 155–165, 2018.

[68] Richard J Field and Richard M Noyes. Oscillations in chemical systems. iv. limit cycle behavior in a model of a real chemical reaction. *The Journal of Chemical Physics*, 60(5):1877–1884, 1974.

[69] AT Winfree. Two kinds of wave in an oscillating chemical solution. In *Faraday Symposia of the Chemical Society*, volume 9, pages 38–46. Royal Society of Chemistry, 1974.

[70] Arthur T Winfree. Scroll-shaped waves of chemical activity in three dimensions. *Science*, 181(4103):937–939, 1973.

[71] Sumana Dutta, Syed Shahed Riaz, and Deb Shankar Ray. Noise-induced instability: an approach based on higher-order moments. *Physical Review E*, 71(3):036216, 2005.

[72] Hana Sevčíková, Milos Marek, and Stefan C Müller. The reversal and splitting of waves in an excitable medium caused by an electrical field. *Science*, 257(5072):951–954, 1992.

[73] Sumana Dutta and Deb Shankar Ray. Thermodiffusion-induced instabilities in reactive systems. *Physical Review E*, 75(6):066206, 2007.

[74] Masakazu Kuze, Mari Horisaka, Nobuhiko J Suematsu, Takashi Amemiya, Oliver Steinbock, and Satoshi Nakata. Chemical wave propagation in the belousov–zhabotinsky reaction controlled by electrical potential. *The Journal of Physical Chemistry A*, 123(23):4853–4857, 2019.

[75] Michael Vinson, Sergey Mironov, Scott Mulvey, and Arkady Pertsov. Control of spatial orientation and lifetime of scroll rings in excitable media. *Nature*, 386(6624):477–480, 1997.

[76] Nirmali Prabha Das and Sumana Dutta. Controlling three-dimensional vortices using multiple and moving external fields. *Physical Review E*, 96(2):022206, 2017.

[77] Dennis Kupitz, Sergio Alonso, Markus Bär, and Marcus JB Hauser. Surfactant-induced gradients in the three-dimensional belousov-zhabotinsky reaction. *Physical Review E*, 84(5):056210, 2011.

[78] Sumana Dutta and Oliver Steinbock. Spiral defect drift in the wave fields of multiple excitation patterns. *Physical Review E*, 83(5):056213, 2011.

[79] Dhriti Mahanta, Nirmali Prabha Das, and Sumana Dutta. Spirals in a reaction-diffusion system: dependence of wave dynamics on excitability. *Physical Review E*, 97(2):022206, 2018.

[80] Theo Plesser, Stefan C Mueller, and Benno Hess. Spiral wave dynamics as a function of proton concentration in the ferroin-catalyzed belousov-zhabotinskii reaction. *Journal of Physical Chemistry*, 94(19):7501–7507, 1990.

[81] Arkady Pikovsky, Michael Rosenblum, Jürgen Kurths, and A Synchronization. A universal concept in nonlinear sciences. *Self*, 2:3, 2001.

[82] Edward S Morse. Fireflies flashing in unison. *Science*, 43(1101):169–170, 1916.

[83] Nicolas Brunel and Vincent Hakim. Fast global oscillations in networks of integrate-and-fire neurons with low firing rates. *Neural computation*, 11(7):1621–1671, 1999.

[84] Sheida Ansarinasab, Farnaz Ghassemi, Fahimeh Nazarimehr, Dibakar Ghosh, and Sajad Jafari. Phase synchronization in cryptocurrency network and its features. *International Journal of Modern Physics C (IJMPC)*, 35(02):1–21, 2024.

[85] Animesh Biswas, Dibyendu Das, and P Parmananda. Scaling dependence and synchronization of forced mercury beating heart systems. *Physical Review E*, 95(4):042202, 2017.

[86] BC Daniels, STM Dissanayake, and BR Trees. Synchronization of coupled rotators: Josephson junction ladders and the locally coupled kuramoto model. *Physical Review E*, 67(2):026216, 2003.

[87] J Schwarz-Linek, C Valeriani, A Cacciuto, ME Cates, D Marenduzzo, AN Morozov, and WCK Poon. Phase separation and rotor self-assembly in active particle suspensions. *Proceedings of the National Academy of Sciences*, 109(11):4052–4057, 2012.

[88] Roberto Di Leonardo, András Búzás, Lóránd Kelemen, Gaszton Vizsnyiczai, László Oroszi, and Pál Ormos. Hydrodynamic synchronization of light driven microrotors. *Physical review letters*, 109(3):034104, 2012.

[89] Sheida Ansarinasab, Fatemeh Parastesh, Farnaz Ghassemi, Karthikeyan Rajagopal, Sajad Jafari, and Dibakar Ghosh. Synchronization in functional brain networks of children suffering from adhd based on hindmarsh-rose neuronal model. *Computers in Biology and Medicine*, 152:106461, 2023.

[90] Florian Siegert and Cornelis J Weijer. Three-dimensional scroll waves organize dictyostelium slugs. *Proceedings of the National Academy of Sciences*, 89(14):6433–6437, 1992.

[91] Richard A Gray, Arkady M Pertsov, and José Jalife. Spatial and temporal organization during cardiac fibrillation. *Nature*, 392(6671):75–78, 1998.

[92] Gil Bub, Alvin Shrier, and Leon Glass. Spiral wave generation in heterogeneous excitable media. *Physical review letters*, 88(5):058101, 2002.

[93] James Lechleiter, Steven Girard, Ernest Peralta, and David Clapham. Spiral calcium wave propagation and annihilation in xenopus laevis oocytes. *Science*, 252(5002):123–126, 1991.

[94] Michael H Hastings and Erik D Herzog. Clock genes, oscillators, and cellular networks in the suprachiasmatic nuclei. *Journal of biological rhythms*, 19(5):400–413, 2004.

[95] Nirmali Prabha Das, Dhriti Mahanta, and Sumana Dutta. Unpinning of scroll waves under the influence of a thermal gradient. *Physical Review E*, 90(2):022916, 2014.

[96] Nirmali Prabha Das and Sumana Dutta. Controlling three-dimensional vortices using multiple and moving external fields. *Physical Review E*, 96(2):022206, 2017.

[97] Hrishikesh Kalita and Sumana Dutta. Interaction of multiple spiral rotors in a reaction-diffusion system. *Physical Review E*, 105(5):054213, 2022.

[98] Franco M Zanotto and Oliver Steinbock. Asymmetric synchronization in lattices of pinned spiral waves. *Physical Review E*, 103(2):022213, 2021.

[99] Jyoti Sharma, Ishant Tiwari, Dibyendu Das, P Parmananda, and Véronique Pimienta. Rotational synchronization of camphor ribbons in different geometries. *Physical Review E*, 101(5):052202, 2020.

[100] Chad Giusti, Robert Ghrist, and Danielle S Bassett. Two's company, three (or more) is a simplex: Algebraic-topological tools for understanding higher-order structure in neural data. *Journal of computational neuroscience*, 41:1–14, 2016.

[101] Austin R Benson, David F Gleich, and Jure Leskovec. Higher-order organization of complex networks. *Science*, 353(6295):163–166, 2016.

[102] Per Sebastian Skardal and Alex Arenas. Higher order interactions in complex networks of phase oscillators promote abrupt synchronization switching. *Communications Physics*, 3(1):218, 2020.

[103] Soumen Majhi, Matjaž Perc, and Dibakar Ghosh. Dynamics on higher-order networks: A review. *Journal of the Royal Society Interface*, 19(188):20220043, 2022.

[104] Sangita Dutta, Prosenjit Kundu, Pitambar Khanra, Chittaranjan Hens, and Pinaki Pal. Perfect synchronization in complex networks with higher-order interactions. *Physical Review E*, 108(2):024304, 2023.

[105] Yuwei Cui, Subutai Ahmad, and Jeff Hawkins. The htm spatial pooler—a neocortical algorithm for online sparse distributed coding. *Frontiers in computational neuroscience*, 11:272195, 2017.

[106] Andrei V Bukh, Eckehard Schöll, and VS Anishchenko. Synchronization of spiral wave patterns in two-layer 2d lattices of nonlocally coupled discrete oscillators. *Chaos: An Interdisciplinary Journal of Nonlinear Science*, 29(5), 2019.

[107] Palash Kumar Pal, Sourav K Bhowmick, Partha Karmakar, and Dibakar Ghosh. Mixed synchronization in multiplex networks of counter-rotating oscillators. *Chaos, Solitons & Fractals*, 176:114069, 2023.

[108] Quintino Francesco Lotito, Federico Musciotto, Alberto Montresor, and Federico Battiston. Higher-order motif analysis in hypergraphs. *Communications Physics*, 5(1):79, 2022.

[109] Dwight Barkley. A model for fast computer simulation of waves in excitable media. *Physica D: Nonlinear Phenomena*, 49(1-2):61–70, 1991.

[110] Anatol M Zhabotinsky. Belousov-zhabotinsky reaction. *Scholarpedia*, 2(9):1435, 2007.

[111] Simin Mirzaei, Mahtab Mehrabbeik, Karthikeyan Rajagopal, Sajad Jafari, and Guanrong Chen. Synchronization of a higher-order network of rulkov maps. *Chaos: An Interdisciplinary Journal of Nonlinear Science*, 32(12), 2022.

[112] Luca Gallo, Riccardo Muolo, Lucia Valentina Gambuzza, Vito Latora, Mattia Frasca, and Timoteo Carletti. Synchronization induced by directed higher-order interactions. *Communications Physics*, 5(1):263, 2022.

[113] Per Sebastian Skardal and Alex Arenas. Higher order interactions in complex networks of phase oscillators promote abrupt synchronization switching. *Communications Physics*, 3(1):218, 2020.

[114] David Mersing, Shannyn A Tyler, Benjamas Ponboonjaroenchai, Mark R Tinsley, and Kenneth Showalter. Novel modes of synchronization in star networks of coupled chemical oscillators. *Chaos: An Interdisciplinary Journal of Nonlinear Science*, 31(9), 2021.

[115] Ling Lü, Lianjun Ge, Liyu Gao, Changhui Han, and Chengren Li. Synchronization transmission of spiral wave and turbulence in uncertain time-delay neuronal networks. *Physica A: Statistical Mechanics and its Applications*, 525:64–71, 2019.

[116] Bernd Blasius, Amit Huppert, and Lewi Stone. Complex dynamics and phase synchronization in spatially extended ecological systems. *Nature*, 399(6734):354–359, 1999.

[117] Johannes Hillbrand, Dominik Auth, Marco Piccardo, Nikola Opačak, Erich Gornik, Gottfried Strasser, Federico Capasso, Stefan Breuer, and Benedikt Schwarz. In-phase and anti-phase synchronization in a laser frequency comb. *Physical review letters*, 124(2):023901, 2020.

[118] Annette F Taylor, Panagiotis Kapetanopoulos, Benjamin J Whitaker, Rita Toth, Larry Bull, and Mark R Tinsley. Clusters and switchers in globally coupled photochemical oscillators. *Physical review letters*, 100(21):214101, 2008.

[119] Martin Rohden, Andreas Sorge, Marc Timme, and Dirk Witthaut. Self-organized synchronization in decentralized power grids. *Physical review letters*, 109(6):064101, 2012.

[120] Steven Strogatz. Sync: The emerging science of spontaneous order. 2004.

[121] Arthur T Winfree. Biological rhythms and the behavior of populations of coupled oscillators. *Journal of theoretical biology*, 16(1):15–42, 1967.

[122] Yoshiki Kuramoto. International symposium on mathematical problems in theoretical physics. *Lecture notes in Physics*, 30:420, 1975.

[123] Steven H Strogatz and Ian Stewart. Coupled oscillators and biological synchronization. *Scientific american*, 269(6):102–109, 1993.

[124] John David Crawford. Amplitude expansions for instabilities in populations of globally-coupled oscillators. *Journal of statistical physics*, 74:1047–1084, 1994.

[125] Norbert Wiener. *Nonlinear problems in random theory*. 1966.

[126] Steven H Strogatz. From kuramoto to crawford: exploring the onset of synchronization in populations of coupled oscillators. *Physica D: Nonlinear Phenomena*, 143(1-4):1–20, 2000.

[127] Yoshiki Kuramoto and Dorjsuren Battogtokh. Coexistence of coherence and incoherence in nonlocally coupled phase oscillators. *arXiv preprint cond-mat/0210694*, 2002.

[128] Daniel M Abrams and Steven H Strogatz. Chimera states for coupled oscillators. *Physical review letters*, 93(17):174102, 2004.

[129] Aaron M Hagerstrom, Thomas E Murphy, Rajarshi Roy, Philipp Hövel, Iryna Omelchenko, and Eckehard Schöll. Experimental observation of chimeras in coupled-map lattices. *Nature Physics*, 8(9):658–661, 2012.

[130] Mark R Tinsley, Simbarashe Nkomo, and Kenneth Showalter. Chimera and phase-cluster states in populations of coupled chemical oscillators. *Nature Physics*, 8(9):662–665, 2012.

[131] Eckehard Schöll. Partial synchronization patterns in brain networks. *Europhysics Letters*, 136(1):18001, 2022.

[132] Soumen Majhi, Bidesh K Bera, Dibakar Ghosh, and Matjaž Perc. Chimera states in neuronal networks: A review. *Physics of life reviews*, 28:100–121, 2019.

[133] Sindre W Haugland. The changing notion of chimera states, a critical review. *Journal of Physics: Complexity*, 2(3):032001, 2021.

[134] Ido Nitsan, Stavit Drori, Yair E Lewis, Shlomi Cohen, and Shelly Tzlil. Mechanical communication in cardiac cell synchronized beating. *Nature Physics*, 12(5):472–477, 2016.

[135] Joseph D Hart, Kanika Bansal, Thomas E Murphy, and Rajarshi Roy. Experimental observation of chimera and cluster states in a minimal globally coupled network. *Chaos: an interdisciplinary journal of nonlinear science*, 26(9), 2016.

[136] Yuri Maistrenko, Serhiy Brezetsky, Patrycja Jaros, Roman Levchenko, and Tomasz Kapitaniak. Smallest chimera states. *Physical Review E*, 95(1):010203, 2017.

[137] Michael M Norton, Nathan Tompkins, Baptiste Blanc, Matthew Carl Cambria, Jesse Held, and Seth Fraden. Dynamics of reaction-diffusion oscillators in star and other networks with cyclic symmetries exhibiting multiple clusters. *Physical review letters*, 123(14):148301, 2019.

[138] Jan Frederik Totz, Julian Rode, Mark R Tinsley, Kenneth Showalter, and Harald Engel. Spiral wave chimera states in large populations of coupled chemical oscillators. *Nature Physics*, 14(3):282–285, 2018.

[139] Mahesh Wickramasinghe and István Z Kiss. Spatially organized partial synchronization through the chimera mechanism in a network of electrochemical reactions. *Physical Chemistry Chemical Physics*, 16(34):18360–18369, 2014.

[140] Malee Sutthiopad, Jiraporn Luengviriya, Porramain Porjai, Metinee Phantu, Jarin Kanchanawarin, Stefan C Müller, and Chaiya Luengviriya. Propagation of spiral waves pinned to circular and rectangular obstacles. *Physical Review E*, 91(5):052912, 2015.

[141] Hrishikesh Kalita, Parvej Khan, and Sumana Dutta. Rotational synchronization of pinned spiral waves. *Physical Review E*, 106(3):034201, 2022.

[142] Jyoti Sharma, Ishant Tiwari, Dibyendu Das, P Parmananda, VS Akella, and Véronique Pimienta. Rotational synchronization of camphor ribbons. *Physical Review E*, 99(1):012204, 2019.

[143] Juan A Acebrón, Luis L Bonilla, Conrad J Pérez Vicente, Félix Ritort, and Renato Spigler. The kuramoto model: A simple paradigm for synchronization phenomena. *Reviews of modern physics*, 77(1):137, 2005.

[144] Nirmali Prabha Das and Sumana Dutta. Interaction of scroll waves in an excitable medium: reconnection and repulsion. *Physical Review E*, 91(3):030901, 2015.

[145] Mark-Anthony Bray and John P Wikswo. Interaction dynamics of a pair of vortex filament rings. *Physical review letters*, 90(23):238303, 2003.

[146] K Premalatha, VK Chandrasekar, M Senthilvelan, and M Lakshmanan. Different kinds of chimera death states in nonlocally coupled oscillators. *Physical Review E*, 93(5):052213, 2016.

[147] Parvej Khan and Sumana Dutta. Synchronization of corotating spirals anchored to heterogeneities in a chemical system. *The European Physical Journal Special Topics*, pages 1–9, 2024.

[148] Jonatan Peña Ramirez, Luis Alberto Olvera, Henk Nijmeijer, and Joaquin Alvarez. The sympathy of two pendulum clocks: beyond huygens' observations. *Scientific reports*, 6(1):23580, 2016.

[149] Agota Toth, Vilmos Gaspar, and Kenneth Showalter. Signal transmission in chemical systems: propagation of chemical waves through capillary tubes. *The Journal of Physical Chemistry*, 98(2):522–531, 1994.

[150] Alain Pumir, Sitabhra Sinha, S Sridhar, Médéric Argentina, Marcel Hörning, Simonetta Filippi, Christian Cherubini, Stefan Luther, and Valentin Krinsky. Wave-train-induced termination of weakly anchored vortices in excitable media. *Physical Review E*, 81(1):010901, 2010.